STRATIGRAPHY, DEPOSITIONAL ENVIRONMENTS AND RESERVOIR DESCRIPTION OF THE TUSSY (DESMOINESIAN) SANDSTONES, SOUTHEAST JOINER CITY FIELD, LOVE AND CARTER COUNTIES, OKLAHOMA

By

JEFFREY M. COOK

Bachelor of Science in Geology

University of Oklahoma

Norman, Oklahoma

2010

Submitted to the Faculty of the
Graduate College of the
Oklahoma State University
in partial fulfillment of
the requirements for
the Degree of
MASTER OF SCIENCE
May, 2012

STRATIGRAPHY, DEPOSITIONAL ENVIRONMENTS

AND RESERVOIR DESCRIPTION OF THE

TUSSY (DESMOINESIAN) SANDSTONES,

SOUTHEAST JOINER CITY FIELD,

LOVE AND CARTER COUNTIES,

OKLAHOMA

Thesis Approved:

Dr. James Puckette

Thesis Adviser

Dr. Darwin Boardman

Dr. Gary Stewart

Dr. Sheryl A. Tucker

Dean of the Graduate College

TABLE OF CONTENTS

LIST OF TABLES

Table Page

LIST OF FIGURES

Figure Page

CHAPTER I

INTRODUCTION

Purpose of the Research

Pennsylvanian sandstones are important reservoirs that produce large volumes of oil and gas within the Ardmore and Marietta basins of southern Oklahoma. The purpose of this study was to acquire and interpret a data set of subsurface geology, and thereby develop a better understanding of reservoir characteristics of the Pennsylvanian Tussy sandstones in the Southeast Joiner City field of Love and Carter Counties, Oklahoma. The endeavor was initiated at the suggestion of Mid-Con Energy Operating, to aid in developmental drilling and production-enhancement operations. The purpose was to interpret the stratigraphic framework and depositional environments, relate depositional facies to reservoir quality, and deduce spatial distribution and connectivity of reservoir rocks. Describing and mapping the stratigraphic variation of these reservoirs was expected to produce these benefits: enhanced reservoir-management strategies, improved prediction of reservoir properties, increased production, and prolonged life of the field. This study will serve as an analogue for exploration and development of similar Pennsylvanian sandstone reservoirs.

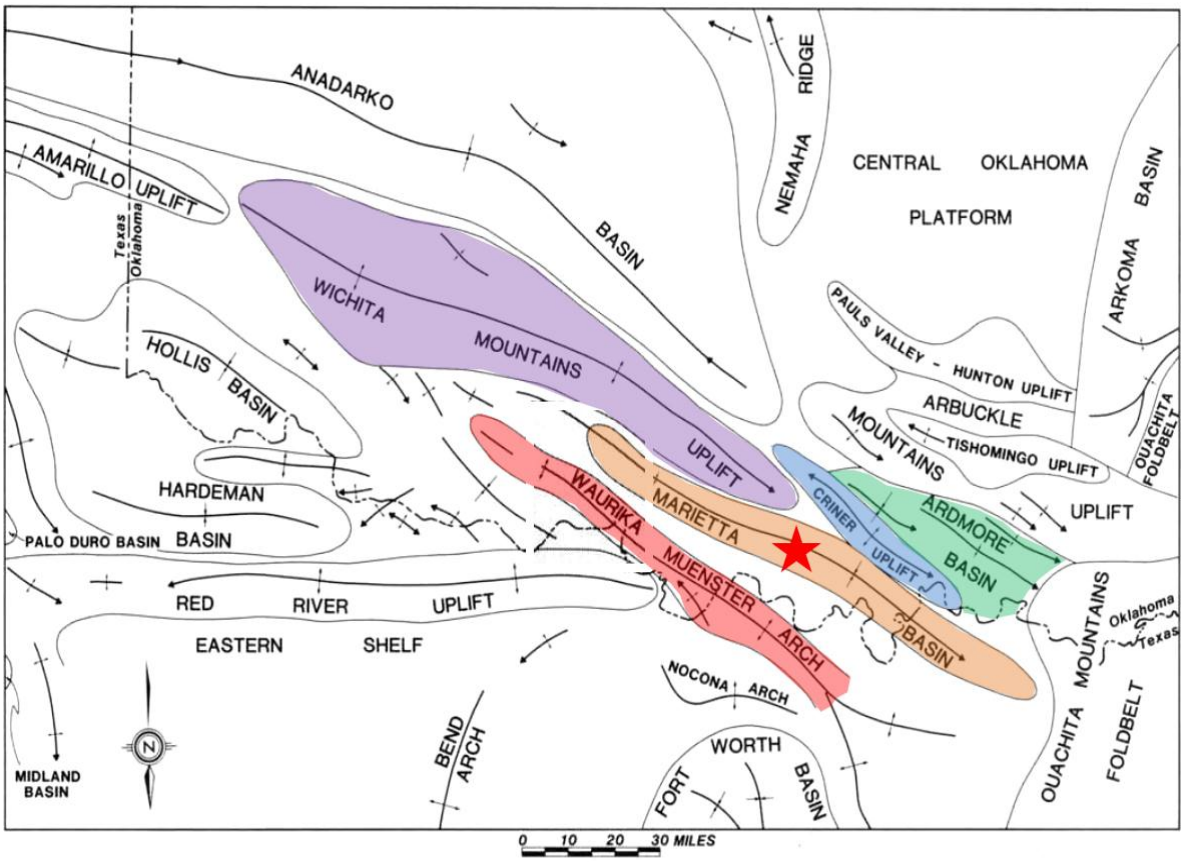

Figure 1: Map of southern Oklahoma and north Texas showing the location of the study area (red star) relative to prominent tectonic features. Marietta Basin – orange, Criner Uplift – blue, Ardmore Basin – green, Wichita Uplift – Purple, Waurika-Muenster Arch – red (modified from Al-Shaieb and others, 1980).

General Methods

To achieve the research objectives, these methods were employed:

1) Analysis of conventional wireline logs, borehole image logs, and cores, to provide information necessary interpret the stratigraphic framework and depositional environments of the Tussy sandstones in the Southeast Joiner City field,
2) Interpretation of core-derived depositional facies, relative to reservoir quality,
3) Determination of controls on reservoir quality and identification of the dominant rock constituents and porosity types, through petrographic analysis,
4) Calibration of cored lithofacies to chromatic patterns on borehole-image logs,
5) Inference of depositional facies and, thereby, influence of reservoir facies in wells where the Tussy sandstones were not cored, but were depicted on borehole-image logs,
6) Characterization of reservoir geometry, connectivity, and overall reservoir quality through stratigraphic analysis and subsurface mapping.

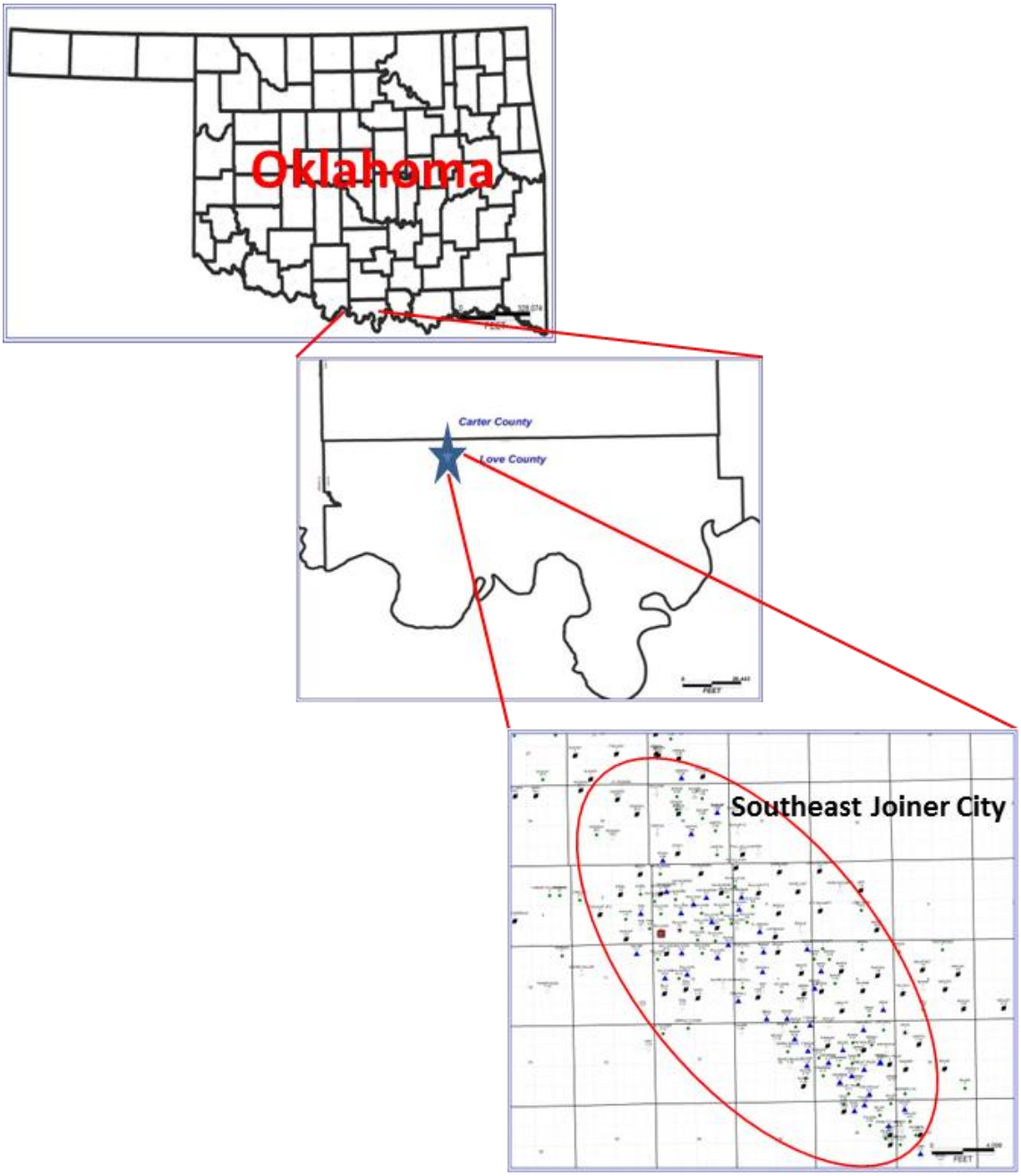

Figure 2: Map of Oklahoma showing the locations of Love and Carter Counties and of the Southeast Joiner City field.

Study Area

The Southeast Joiner City field (Figure 2) is a mature oil field in Love and Carter counties, in T. 5-6 S., R. 1-2 W., in far south-central Oklahoma, approximately 10 miles southwest of the city of Ardmore. The northernmost portion of the study area lies within the North Simon field (Figures 3 and 4). Tussy sandstones have produced approximately 5 million stock-tank barrels of oil within the study area. These sandstones under study are in the central portion of the Marietta Basin (Figure 1) and were deposited in Desmoinesian time. Within the Southeast Joiner City field the Tussy sandstones are unitized and are currently under secondary recovery production enhancement by Mid-Con Energy Operating.

The fields were chosen for this study due to the abundance of subsurface data, which consists of two cores, more than 100 wireline logs and 11 borehole-image logs. Fifteen thin-sections from one of the cores were analyzed to determine the influence of diagenesis on reservoir quality. Core-derived petrophysical properties were used to relate reservoir quality to lithofacies. Wireline logs were the principal source of information used to depict the stratigraphic framework and configuration of the local basin. These logs were rich in information for inferences about lithofacies and reservoir quality: Extended Range Micro Image (XRMI^{SM}) (Halliburton), Electrical Micro Imager (EMI^{TM}) (Halliburton), Fullbore Formation MicroImage (FMI) (Schlumberger ®) or Compact™ MicroImage (CMI) (Weatherford).

Previous Work

Deese sandstones have produced large volumes of oil and gas in the Ardmore and Marietta Basins. Published studies regarding Desmoinesian depositional environments and reservoir-scale analyses are mostly restricted to strata of the Ardmore Basin. In terms of Desmoinesian sedimentary rocks, the Marietta Basin is the subject of regional stratigraphic studies regarding correlations and mapping, reservoir geometries, oil and gas production, and

types of traps. As the result of southern Oklahoma's complex structural setting, detailed structural geologic studies have been concentrated on specific oil and gas producing fields. No information has been published on reservoir characterization of the Tussy sandstones. Previous works allow for a broad regional overview of the Lower Pennsylvanian sedimentary rocks of the Marietta Basin or else they focus on petroleum geology of specific fields.

Hoard (1954) detailed the stratigraphy and lithology of the Tussy Sandstone sequence within the "Tussy Sector" of the Tatums Field in Carter and Garvin Counties. Mullen (1954) provided a stratigraphic, lithological and structural analysis of the Hewitt Field in Carter County, approximately 10 miles north of the Southeast Joiner City study area. Neustadt (1954) analyzed the geologic history and subsurface structure of the West Hewitt Field which is also approximately 4 miles north of the study area. Reeves and Mount (1960) provided a detailed study of possible oil accumulations along the northern flank of the Marietta Basin, and proposed that Pennsylvanian sandstones as prime candidates for stratigraphic traps. Reeves and Mount (1960) proposed that the Deese sands originated as the result of erosion of the Simpson sands on the Criner Hills. Stark (1961) defined the evolution of the Marietta Basin and correlated Pennsylvanian time-stratigraphic relationships between the Fort Worth Basin, Marietta, and Criner-Hill-Ardmore Basins, to construct regional isochore and facies maps. Tomlinson and McBee (1959) observed that the abrupt differences in lithology, and the lenticular geometries of the Pennsylvanian sandstones make stratigraphic correlations difficult in the Ardmore Basin. Westheimer (1965) noted that the Lower Deese sandstones are relatively lenticular and have limited areal extents. Billingsley and others (1996) interpreted a tidal influence on lower Deese sandstones exposed in the Ardmore Basin as made evident by bi-directional flow indicators such as herringbone cross-stratification and flaser to lenticular bedding.

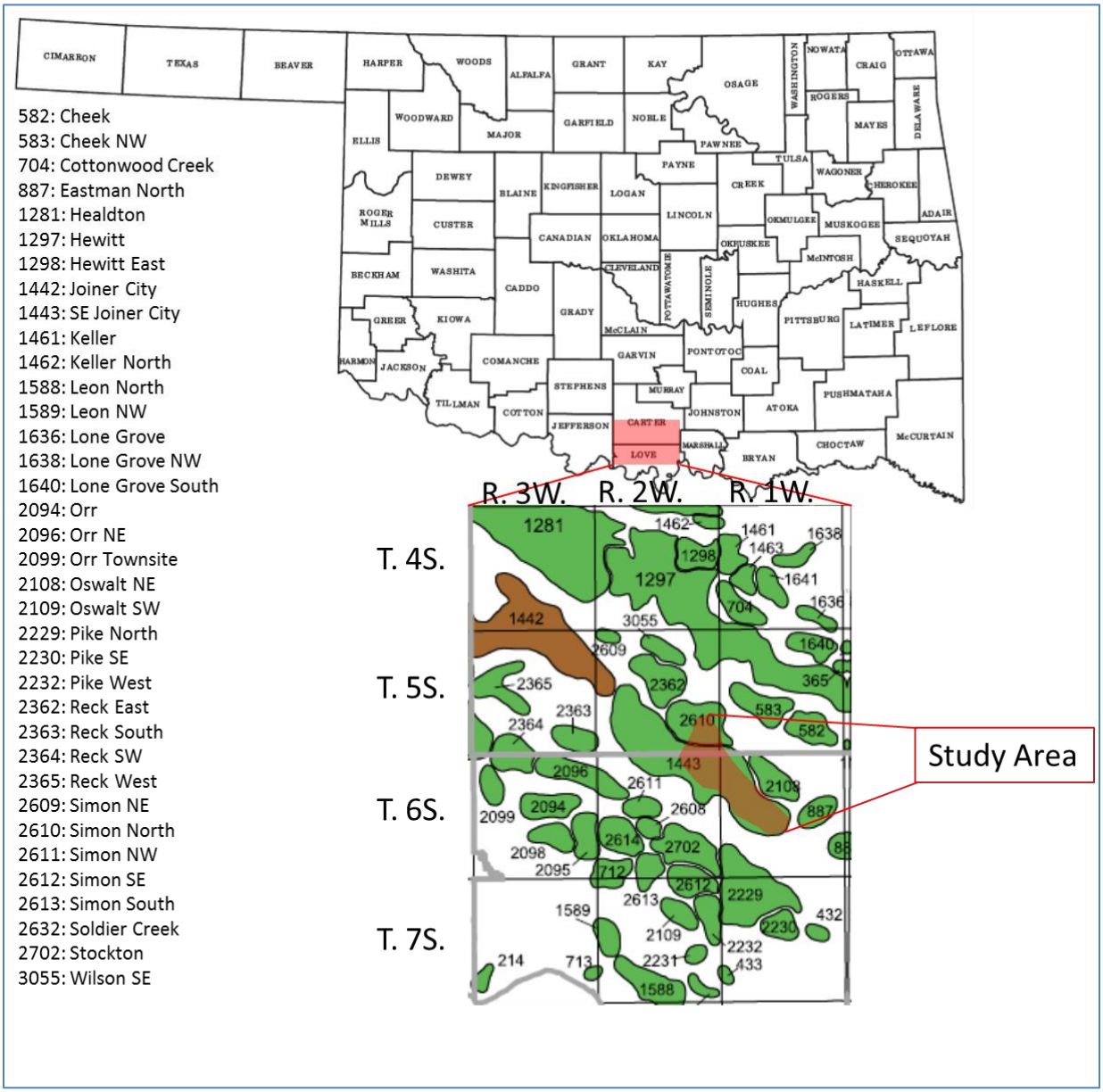

Figure 3: Map of Oklahoma showing the location of the Southeast Joiner City field and study area relative to surrounding oil fields in northern Love and southern Carter counties. Field names are shown on left side of the figure (modified from Boyd, 2002).

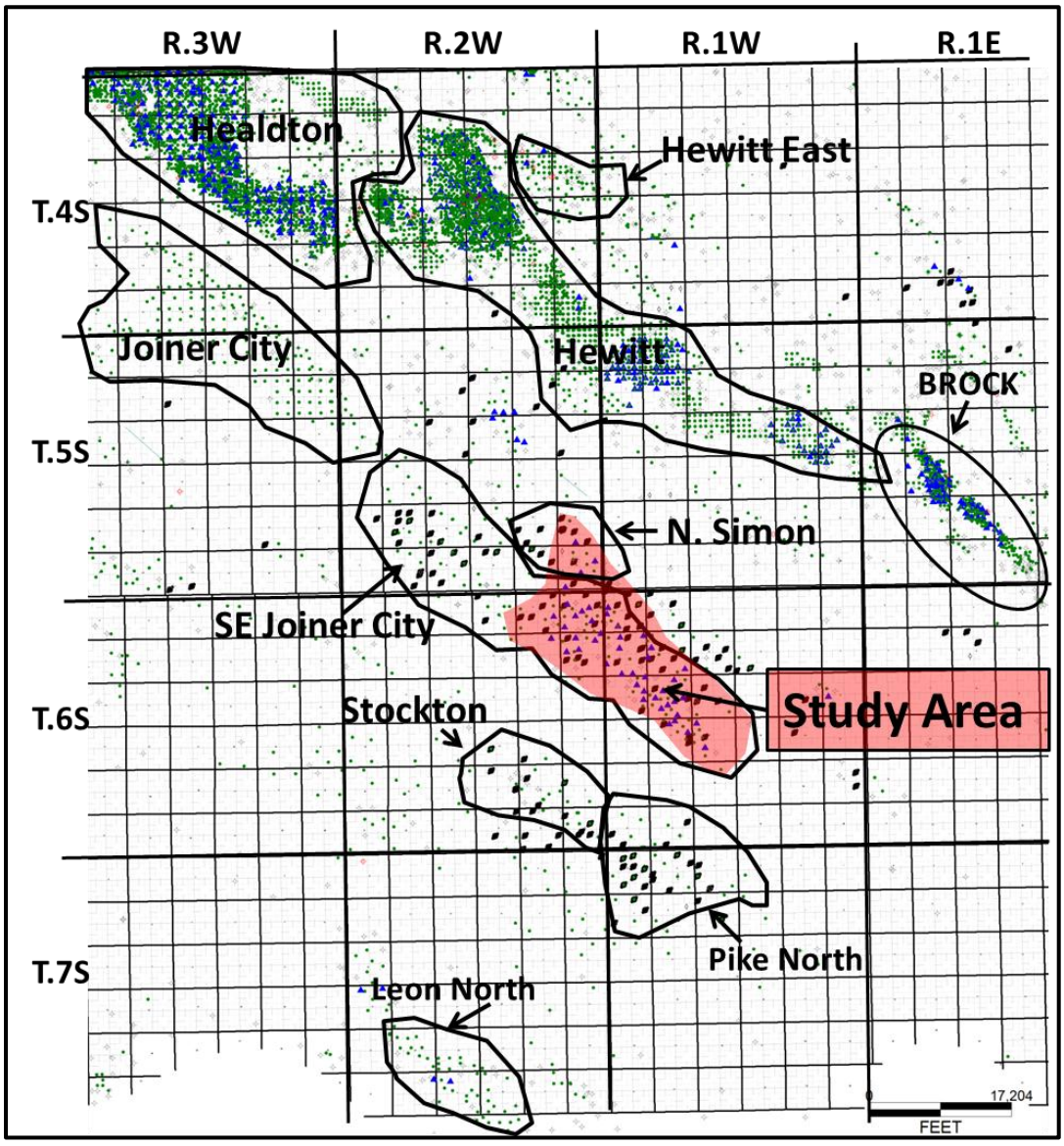

Figure 4: Map of northern Love and southern Carter counties showing the distribution wells and the location of the study area relative to prominent oil fields (oil fields are delineated by black polygons, associated field names and arrows).

CHAPTER II

GEOLOGIC SETTING

Stratigraphy

Stratigraphic nomenclature used in this study was modified from that used by the operator who discovered the field. Figure 5 displays common subsurface names used in the Marietta and Ardmore Basins and Figure 6 is a type log for the study area. The Tussy interval is defined as the set of strata between the Tussy Limestone at the top and the Atokan Upper Dornick Hills Group at the base. "This limestone is the key bed used in subsurface work of the Lower Deese formation in southern Oklahoma" (Hoard, 1954). The Tussy interval is divided informally in descending order: Tussy A, B and C (Figure 6). The top of the Tussy interval, marked by the Tussy Limestone, is easily identifiable in the subsurface on wireline logs by its distinct gamma-ray and bulk density signature. The Tussy A sandstone is fine-grained, and its gamma-ray signature is bell-shaped (Figure 6). Tussy B consists of two sandstones; the lower typically is very fine-grained sandstone that commonly is shown by a funnel-shaped gamma-ray signature, whereas the upper Tussy B sandstone has a bell-shaped gamma-ray character (Figure 6). Tussy C consists of a sandy limestone conglomerate that is almost certainly ubiquitous within the study area (Figure 6). Mudstones are between the Tussy A, B and C sandstones. The base of the Tussy interval unconformably overlies the Desmoinesian upper Dornick Hills.

System	Series	Group		Marietta Basin Subsurface Names (Price, 2012)	Ardmore Basin Surface Names (Waddell, 1966)
Pennsylvanian	Missourian	Hoxbar	Ochelata	"C"	Zuckerman Limestone
				"E" palacine loco	Daube Limestone
			Skiatook	"G" loco limestone	Anadarche Limestone
				Bayou limestone	Crinerville Limestone
					Confederate Limestone
	Desmoinesian	Deese	Marmaton	chubbee	Natsy Limestone
				norris	williams Limestone
			Cherokee	Lone grove	
				u. fusulinid	Camp Ground
				l. fusulinid	rocky point
					Arnold
				tussy	Devils Kitchen
		Upper Dornick Hills		NK	Pumpkin Creek
	?				Frensley
	Atokan				Lester
					Bostwick

Figure 5: Surface nomenclature commonly used in the Ardmore Basin (From Waddell, 1966), and subsurface nomenclature commonly used in the Marietta Basin (From Price, 2012, verbal communication). Subsurface stratigraphic nomenclature for the Marietta Basin lacks a unified naming system; it consists of locally derived names created by local operators (verbal communication with Charles Price). Future research correlating Ardmore Basin surface stratigraphy to the Marietta Basin subsurface would be of great value. NK: not known

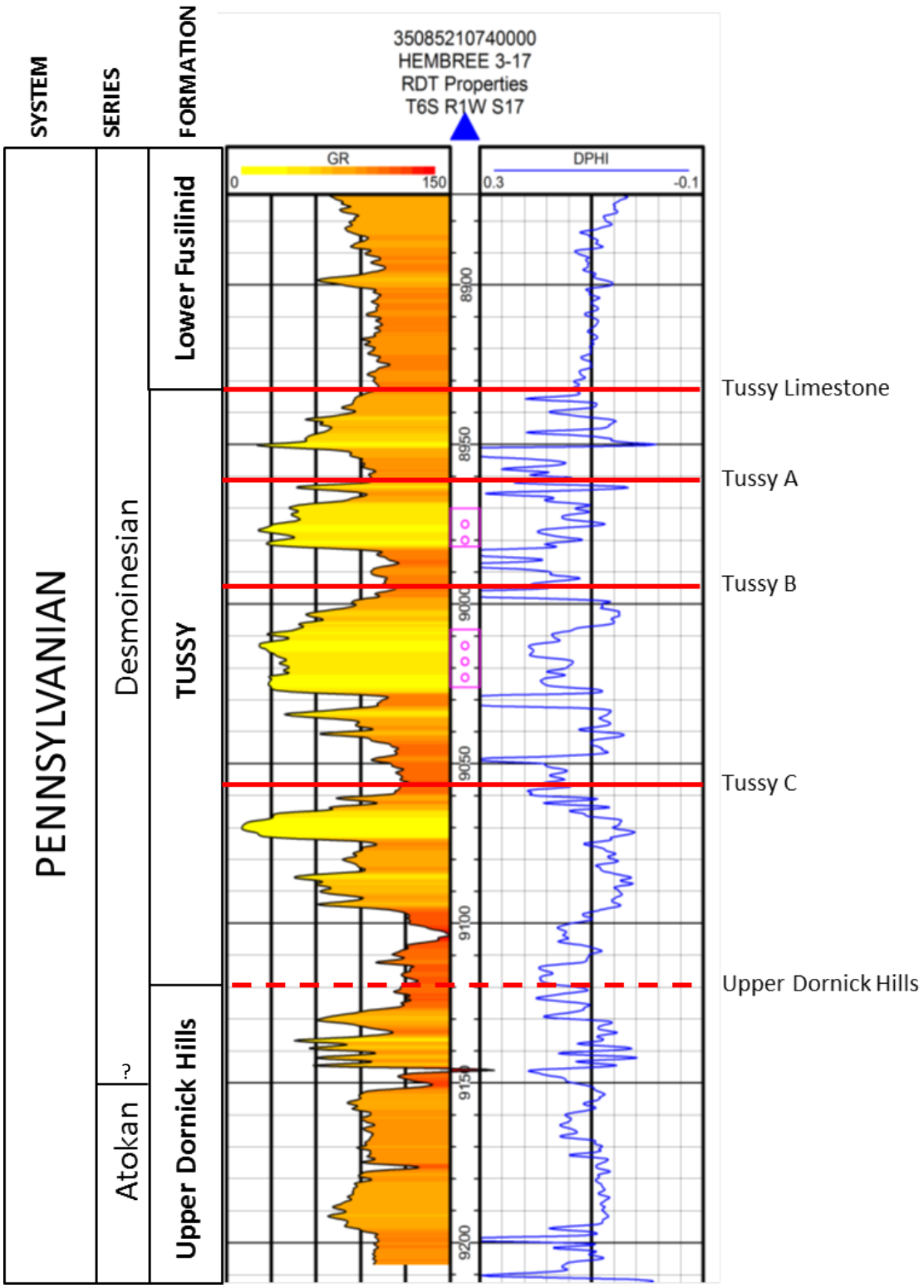

Figure 6: Type log including the Tussy interval, N.E Oswalt Field, Marietta Basin (RDT Properties, Hembree 3-17, Sec. 17, T. 6S., R.1W.). Gamma-ray (GR) values increase from yellow to orange and density porosity (DPHI) is shown in blue on the right track.

Regional Structural Setting

The Marietta Basin is a small, northwest-trending structural basin in southern Oklahoma (Figure 1). The study area is in the central portion of the basin, in northern Love and southern Carter counties. The Marietta Basin is bounded by two northwest-trending positive structural features, the Criner Arch and the Muenster Arch. Two major structural features are progressively north of the Criner Arch: the Ardmore Basin and the Arbuckle Mountains, respectively (Figure 1). The Marietta Basin becomes progressively deeper southeast of the study area; this portion of the basin is known as the Gordonville Trough, it is sub-parallel to the Red River in Love County and adjacent to Cooke and Grayson Counties, Texas (Bradfield, 1968).

The Ardmore and Marietta basins are within the southeast portion of the southern Oklahoma aulacogen. The southern Oklahoma aulacogen (Figure 7) extends from the Ouachita fold belt in southeastern Oklahoma 700 km W-NW into southwestern Oklahoma and northern Texas (Feinstein, 1981). Ham et al. (1964) believe that the southern Oklahoma aulacogen formed in three phases: rifting, subsidence and deformation. "The last stage of deformation resulted in fragmentation of the original long basin and formation of the new tectonic provinces" (Feinstein, 1981). Ham et al. (1964) theorized that the Marietta and Ardmore Basins were connected and possibly formed the southeastern portion of the much larger Anadarko Basin, prior to the final deformation stage. Feinstein (1981) noted similarities in the subsidence curves of the Marietta and Ardmore basins, which support the theory that the basins are two fragments of an original larger basin (Ham et al., 1964). Uplifts were created in Late Mississippian through Pennsylvanian time during the final deformation stage of the aulacogen are believed to have been sources of the large volume of sediment in the Ardmore and Marietta basins. Ham and others (1964) estimated downwarp of the Marietta basin relative to the Muenster Arch was approximately 15,000 ft. The Criner Hills were gained approximately 20,000 ft of relief above the surrounding basins during Desmoinesian time, (Tomlinson and McBee, 1962).

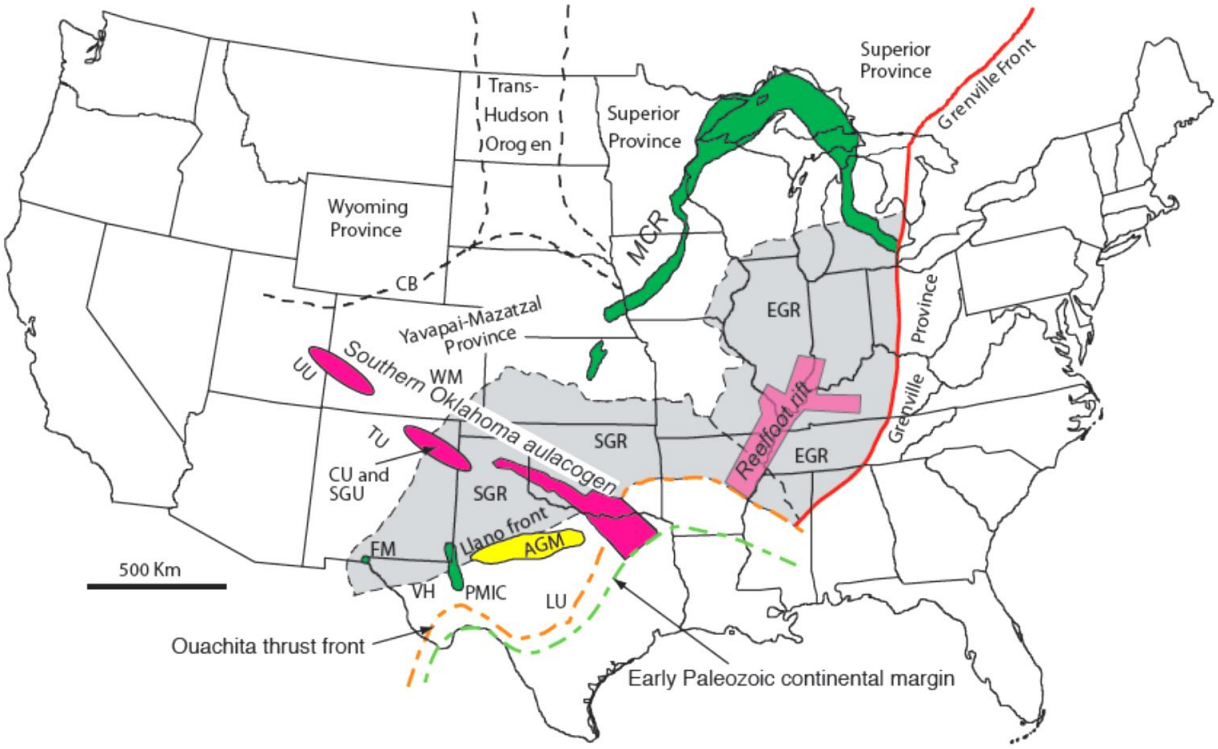

Figure 7: Regional tectonic index map of the Southern Oklahoma aulacogen. EGR: eastern granite-rhyolite province; SGR: southern granite-rhyolite province; CB: Cheyenne belt; MCR: Midcontinent rift system; PMIC: Pecos mafic intrusive complex; AGM: Abilene Gravity Minimum; LF: Llano Front; FM: Franklin Mountains; TU: Tusas uplift; WM: Wet Mountains; UU: Unconpahgre uplift; CU: Cimarron uplift; SGU: Sierra Grande uplift; VH: Van Horn area, and LU: Llano Uplift (Keller and Stephenson, 2007). Ouachita thrust front: orange dashed line, Paleozoic continental margin: green dashed line (Keller and Stephenson, 2007).

Local Structural Geologic Setting and Hydrocarbon Entrapment

Dip within the study area is southwestward, at 600 to 900 ft per mile. Figure 8 shows configuration of the Tussy Limestone, which marks the top of the Tussy interval (Figure 6). The Tussy section unconformably overlies the Desmoinesian Upper Dornick Hills Group. The Tussy interval is pinched out from south to north against the unconformity. Where the sandstones develop good porosity, they form reservoirs which stratigraphically trap hydrocarbons by up-dip pinchout against the upper Dornick Hills unconformity surface.

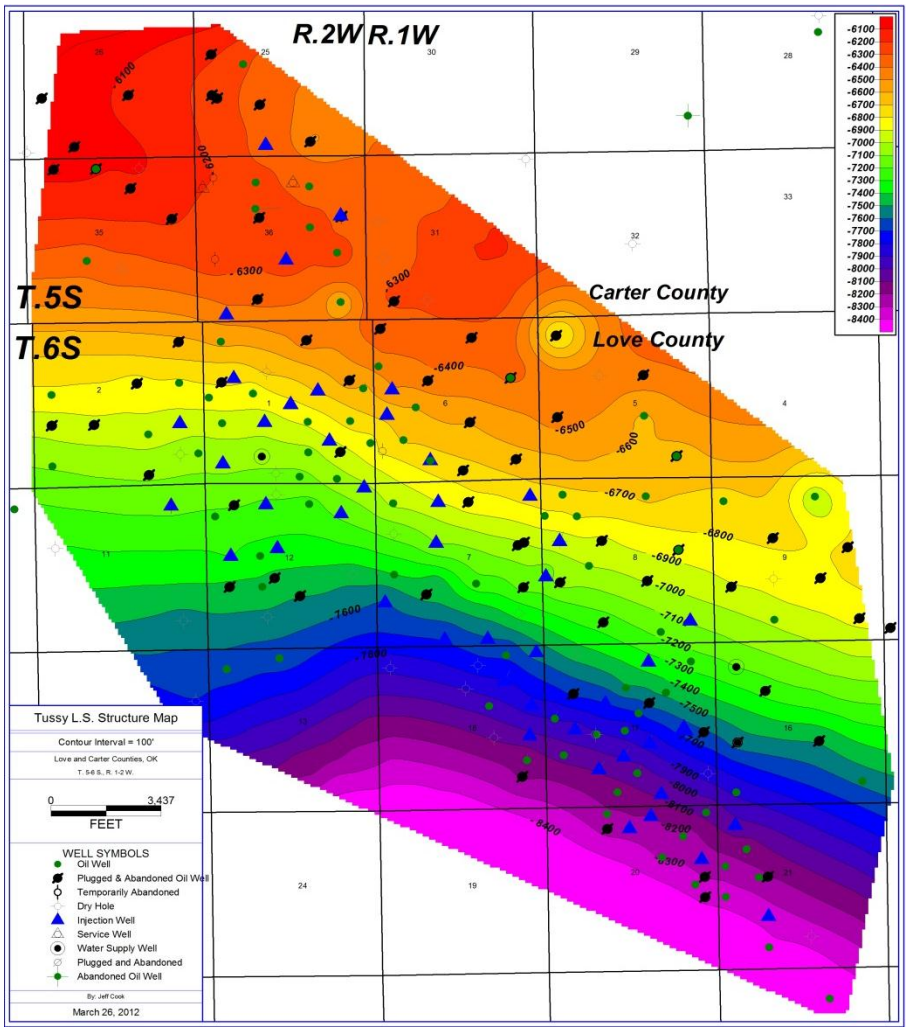

Figure 8: Southeast Joiner City Field. Structural contour map of the top of the Tussy interval within the study area, showing southerly dip associated with the S.E. Joiner City anticline. Depths relative to sea level are shown in color scale bar, upper right side of figure. On the color bar, depths range from -6400 ft (red) to -8100 ft (purple).

The pre-Pennsylvanian structure within the study area is that of a breached anticline, bounded on the northeastern and southwestern sides by normal faults, essentially an anticlinal horst that trends northwestward. Seismic reflection data would be required to determine the configurations and exact locations of these bounding faults accurately. The NW-SE anticlinal trend parallels many of the prominent regional structures previously discussed. With current well-control and without access to seismic reflection data, there is no evidence that these large scale faults offset Desmoinesian strata within the study area. Figure 9 is a Pre-Pennsylvanian subcrop map showing the breached anticlinal structure.

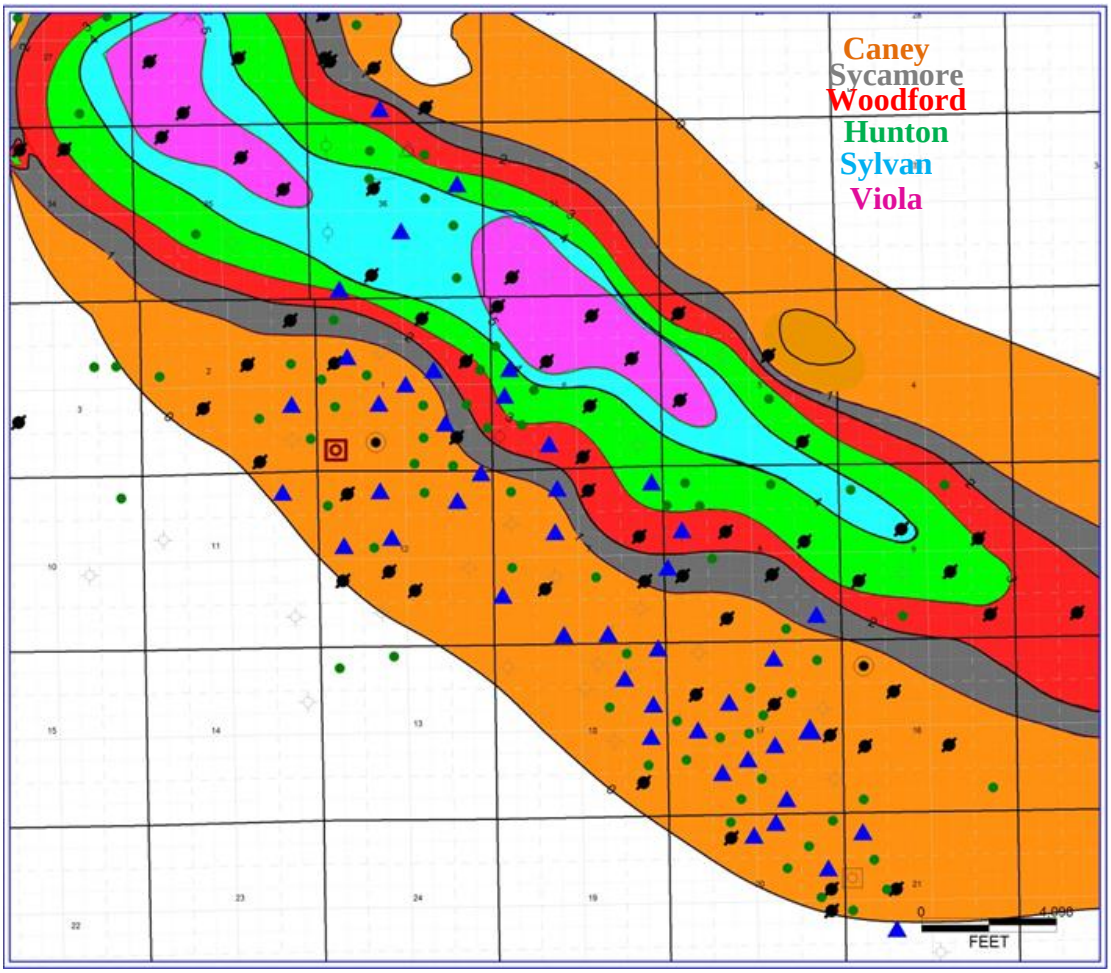

Figure 9: Paleogeologic map of pre-Pennsylvanian strata, showing evidence of a breached anticline within the study area (Abbott, 2006).

Figure 10 is composed of two rose plots of drilling-induced fracture-strike directions from the Hembree 3-17 and PD Sullivan 3-6 borehole image (BHI) logs. The wells are in the southern and northern parts of the study area, respectively. Drilling induced fractures typically form parallel or subparallel to the maximum horizontal stress direction (S_{hmax}). Analysis of BHI logs revealed a dominant northeastward strike of drilling-induced fractures. Thus, the dominant S_{hmax} direction within the study area varies between N20E and N60E within various parts of the field. The understanding of S_{hmax} is important to developmental drilling and to enhanced-recovery operations, because dominant natural fracture sets typically form parallel to subparallel to $S_{hmax.}$ Analysis of BHI logs has revealed a correlation between S_{hmax} and the orientation of natural fractures. One of the crucial components to well placement within the study area is orienting injector-producer well pairs at least 10 degrees off of the S_{hmax} within the localized area of the field. Doing so decreases the likelihood of early injection water breakthrough from injector to producer wells. Based on analysis of image logs in comparison to other highly fractured reservoirs, these reservoirs are not considered to be intensely fractured but, it is believed that fractures do have an effect on waterflood sweep efficiency and overall reservoir performance.

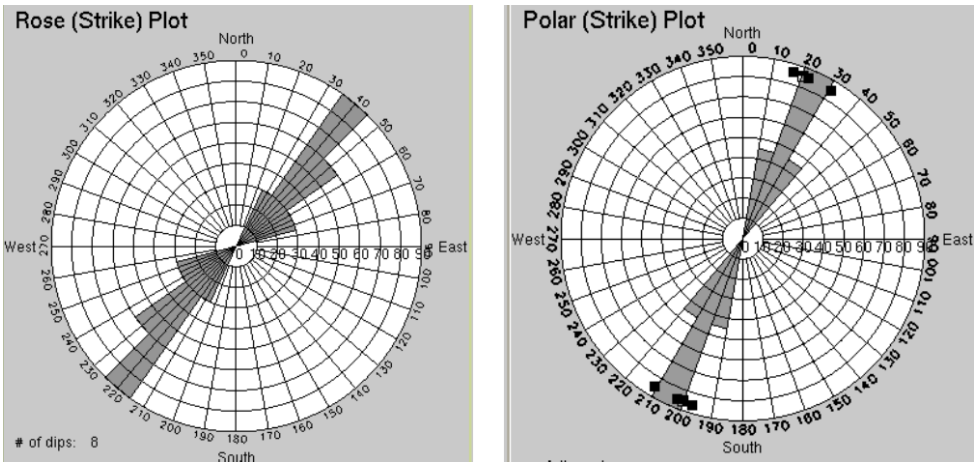

A B

Figure10: Rose plots of drilling induced fracture and maximum horizontal stress strike directions from the Hembree 3-17 (A) and PD Sullivan 3-6 (B) XRMI borehole image logs. Both sets of data were acquired by Halliburton and interpreted by R. Montalvo (Hembree 3-17) and J. Mitchell (PD Sullivan 3-6) (Halliburton borehole-image interpreters).

Paleogeography and Paleoclimate

During Middle Pennsylvanian (Desmoinesian) time, the Marietta Basin was positioned south of the Arbuckle uplift, east of the Wichita uplift, west of the Ouachita uplift and north of the Muenster Arch. Farther north on the Cherokee platform, in present-day north-central Oklahoma, Desmoinesian deltaic systems (Bartlesville, Red Fork, Skinner, Prue) were dispersing sediment from a northerly source onto the shelf. Figure 11 illustrates a model of early Desmoinesian Midcontinent paleogeography with the plotted location of the study area. Pennsylvanian paleoclimate was warm and humid as the equator was just north of present-day (Jorgenson, 1989).

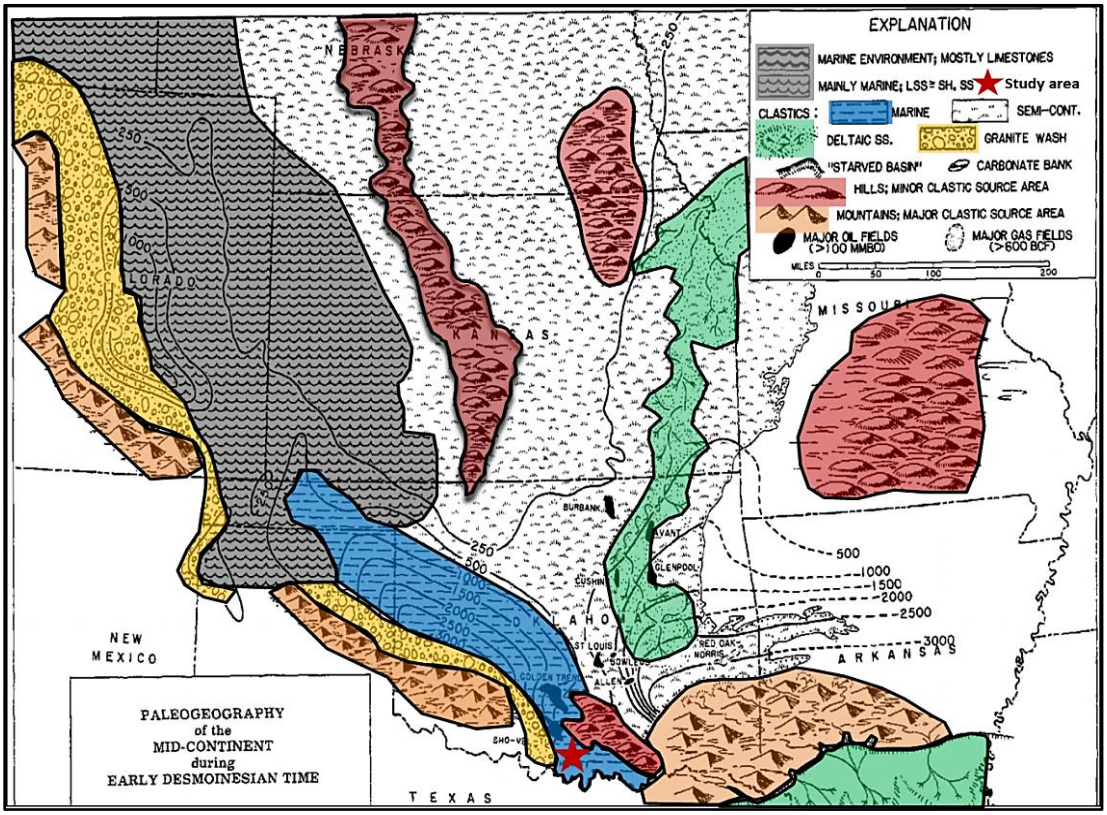

Figure 11: Paleogeography of the Mid-Continent during early Desmoinesian time, showing thickness of early Desmoinesian rocks (modified from Rascoe, B. Jr., and Adler, F.J., 1983).

CHAPTER III

STRATIGRAPHIC FRAMEWORK

Stratigraphic cross-sections were used to reconstruct the configuration of the local basin and of the stratigraphic framework. A comprehensive sequence-stratigraphic or basin-analysis study was not the intention of this research. Limitations of the data set support the reservoir-scale focus. In any reservoir characterization study, to understand the stratigraphic framework and basin configuration is important. Figure 9 is a north-to-south stratigraphic cross-section through the study area. The Tussy interval is bounded by the Tussy limestone above and unconformably by the Upper Dornick Hills below. Figure 12 shows location of cross-section. Figure 13 depicts southerly thickening of the Tussy interval, toward the Marietta Basin. Thus, the depocenter was south of the study area and represented the location of accommodation space during Tussy deposition. Rose plots of cross-bedding from two field-wide representative borehole image (BHI) logs (Figure 14) infer a dominate north-to-south sediment transport direction. Figure 15 depicts the southerly sedimentary and planar lamination dips for the Tussy A and B sandstones in the Mid-Con Operating Hembree 3-17. If this evidence is representative of Tussy sandstones in general, siliclastic sedimentary rocks within the Tussy interval in this portion of the basin probably had a northerly source. As interpreted here, Tussy stratal architecture shows evidence of three cycles of shale-sandstone-shale (Tussy A, B and C intervals).

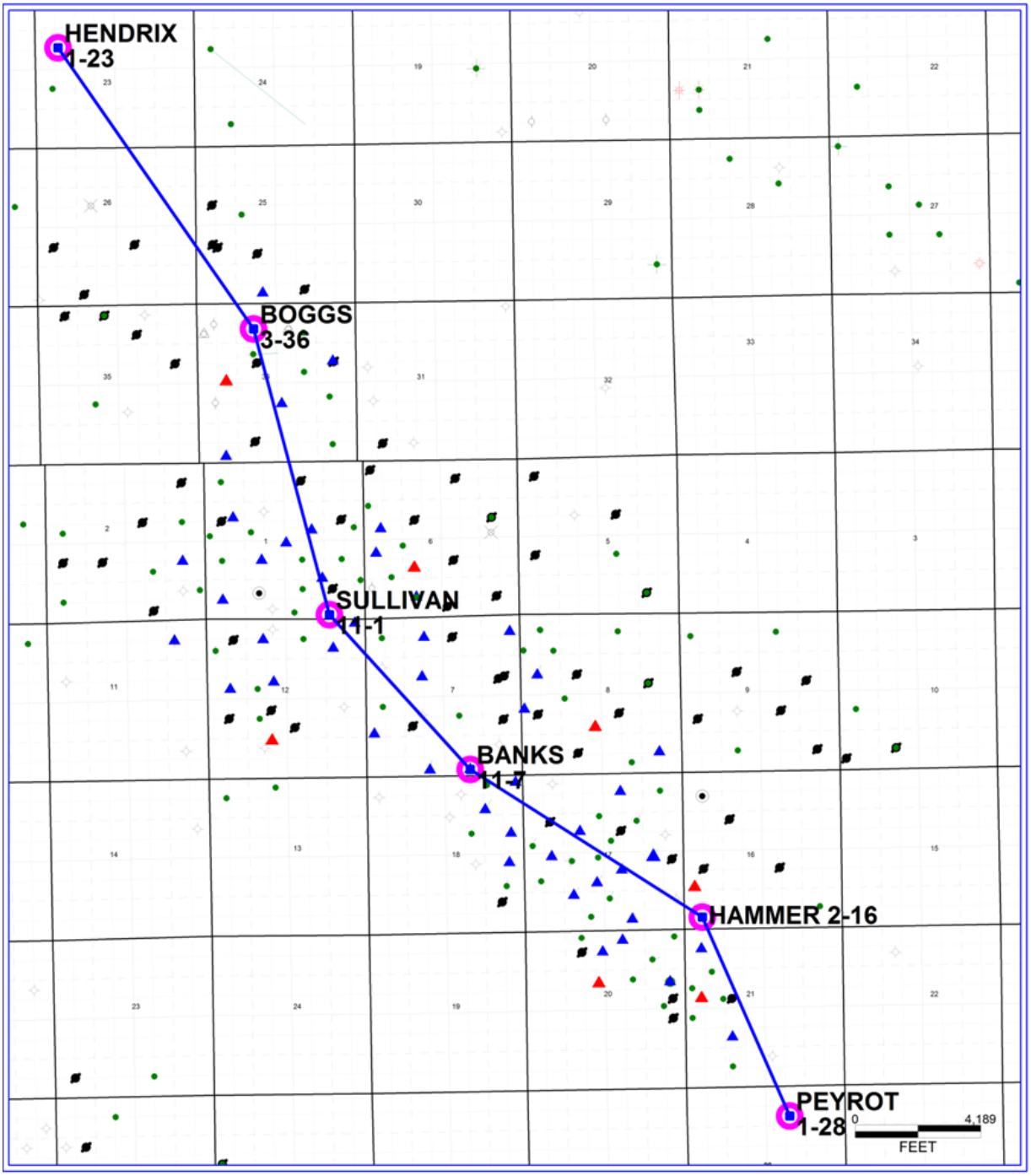

Figure 12: Map of the study area depicting the location of the north-to-south cross-section through the study area.

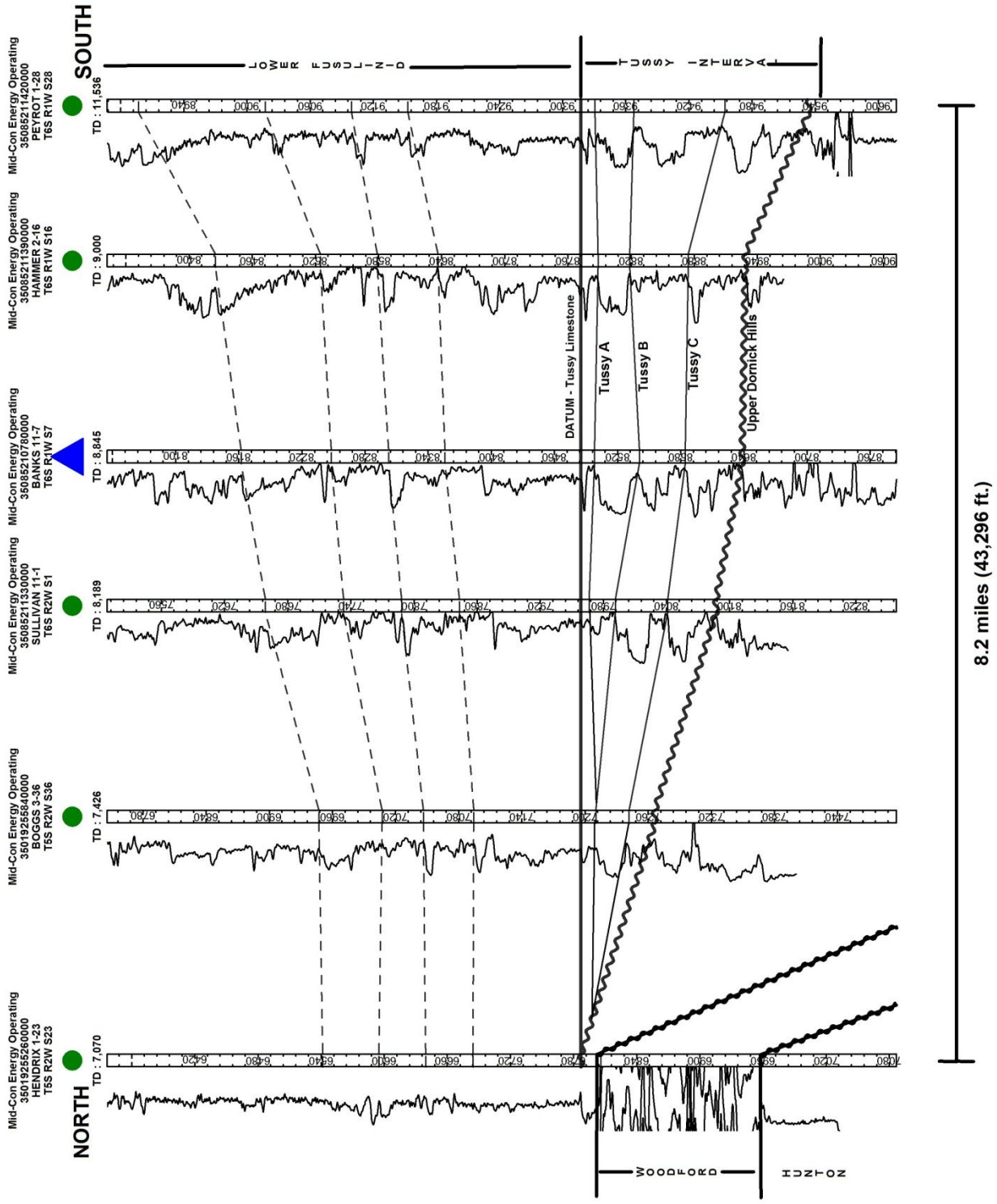

Figure 13: North-to-south gamma-ray log cross-section through the study area. The Tussy interval is bounded above by the Tussy Limestone and below by the Upper Dornick Hills Limestone. Datum is the top of the Tussy interval, marked by the Tussy Limestone. Northward from the Mid-Con Sullivan 11-1, exact stratigraphic relationships within the Tussy interval are not known. Information necessary for description of these relationships is not available.

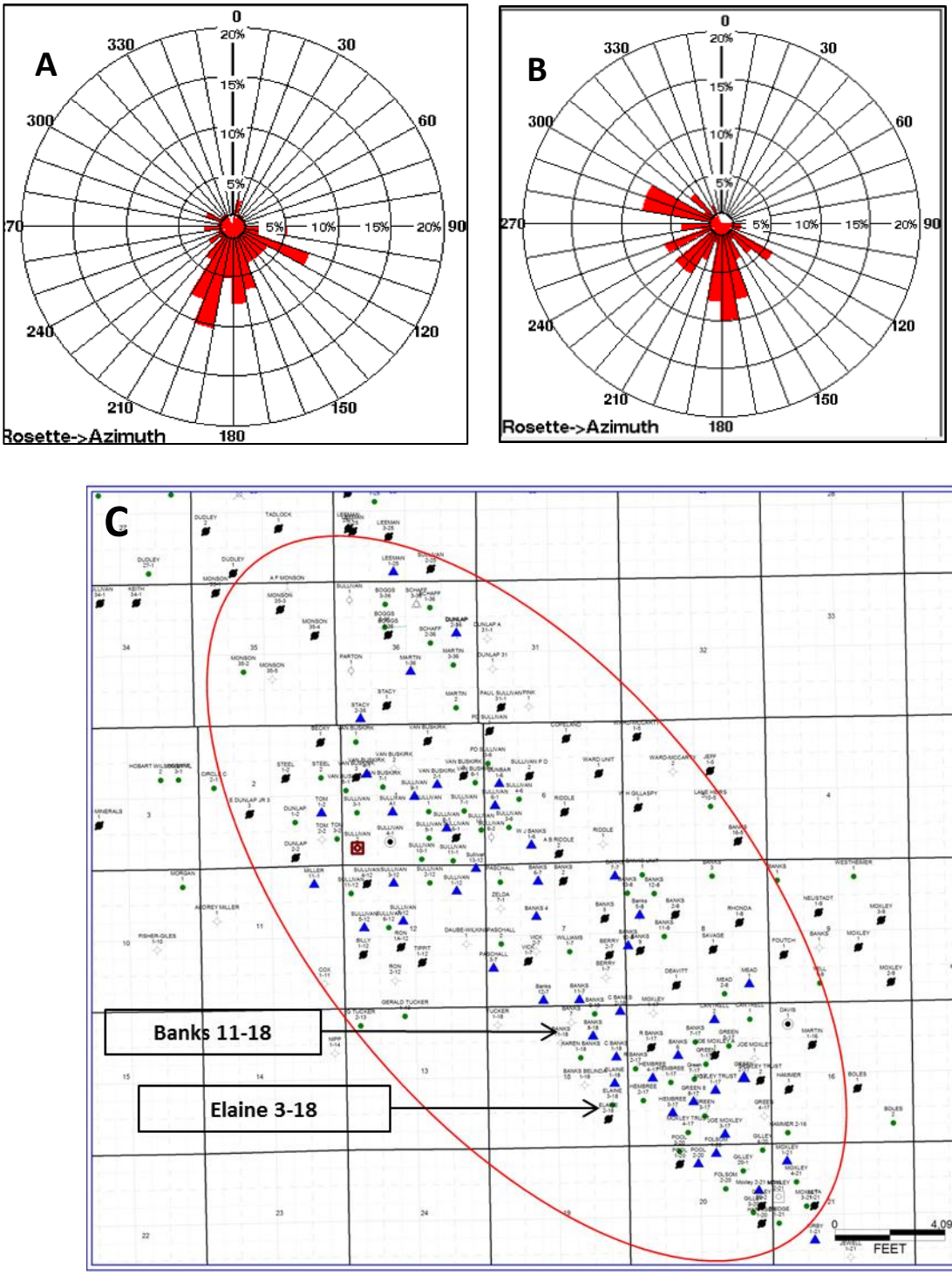

Figure 14: Rose plots of cross-bedding dips within the Tussy interval from (A) Elaine 3-18 FMI and (B) Banks 11-18 FMI. These plots show predominant north-to-south orientation of cross-beds. Both sets of data were acquired by Schlumberger and interpreted by Y. Chen (Schlumberger Borehole Geologist). (C) Location of logged wells.

Chapter IV

Petrography, Facies Analysis and Reservoir Quality

General Description of Cores

Cores of the Tussy interval are available for two wells within the study area, the Hembree 3-17 and Gilley 20-2. The Hembree 3-17 core is a sample from the Tussy A and B intervals, whereas the Gilley 20-2 core includes rocks of the Tussy A and the uppermost part of the Tussy B interval. Cores of the Tussy limestone and of the Tussy C interval were not located; therefore, these two intervals were not examined. Eleven depositional facies were described by inspection of the Tussy A and B intervals. Depositional features recognized in the cores are similar; altogether, they indicate deposition in a low-energy fluvial environment.

The Tussy A and B intervals are composed of amalgamated fining-upward sets of beds; the sets are capped by current-rippled laminae (Figures 33, 34, 35, 36). The Tussy B sandstone overlies grey silty mudstone unconformably; it consists of fine-to-medium-grained, horizontal-planar-laminated, cross-laminated, and current-rippled sandstones. The uppermost part of the Tussy B interval contains calcium carbonate, and an oxidized zone. This evidence is indicative of a surface of exposure. The Tussy A overlies variegated mudstones unconformably. It consists of fine-to-medium-grained horizontal-planar-laminated, cross-laminated, and current-rippled sandstones. The interval above the Tussy A sandstone was not cored.

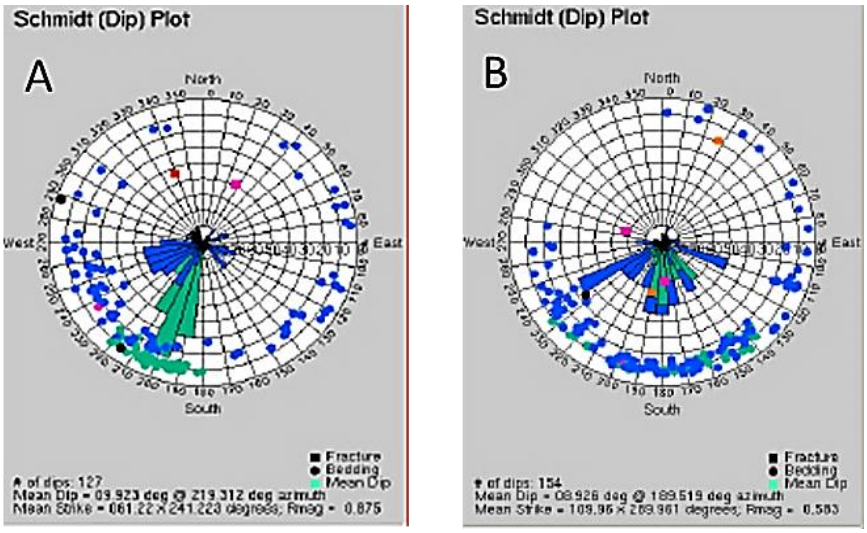

Figure 15: Rose plots from the Hembree 3-17 XRMI showing orientations of sedimentary dips (blue) and planar lamination dips (green) of the (A) Tussy A and (B) Tussy B intervals. Dips of low-energy mudstones are represented by planar laminations (green), and sedimentary structures deposited by high-energy are represented by sedimentary dips (blue). Both sets of data were acquired by Halliburton and interpreted by R. Montalvo (Halliburton borehole-image interpreter).

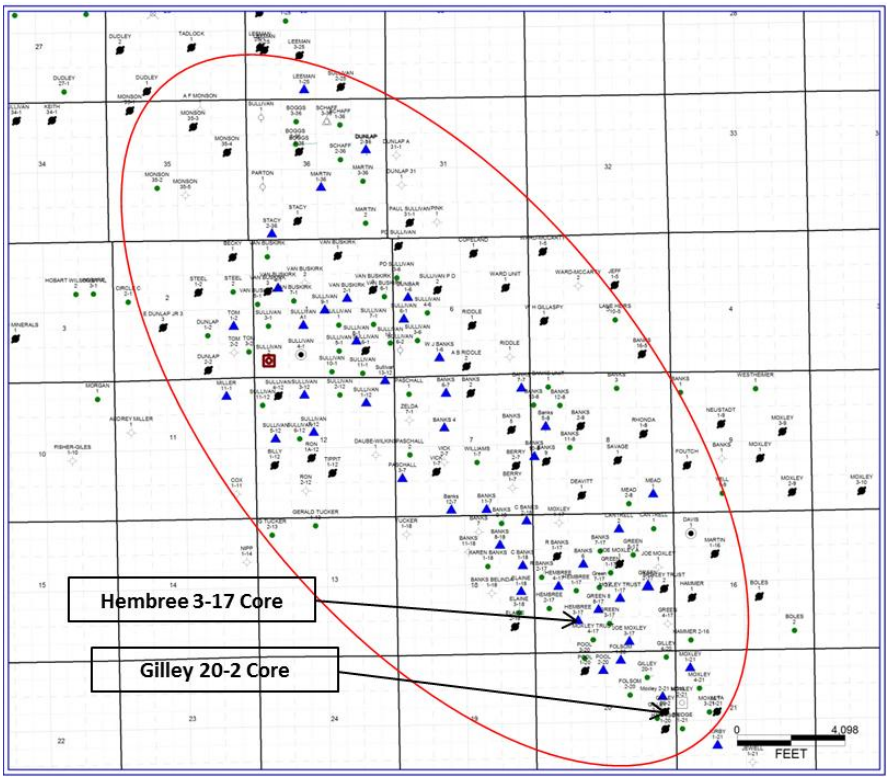

Figure 16: Map of study area showing locations of the Hembree 3-17 and Gilley 20-2 wells (black arrows), in which the Tussy and Tussy B intervals were cored.

Facies Analysis

(F1) Clay-clast Conglomeratic Sandstone

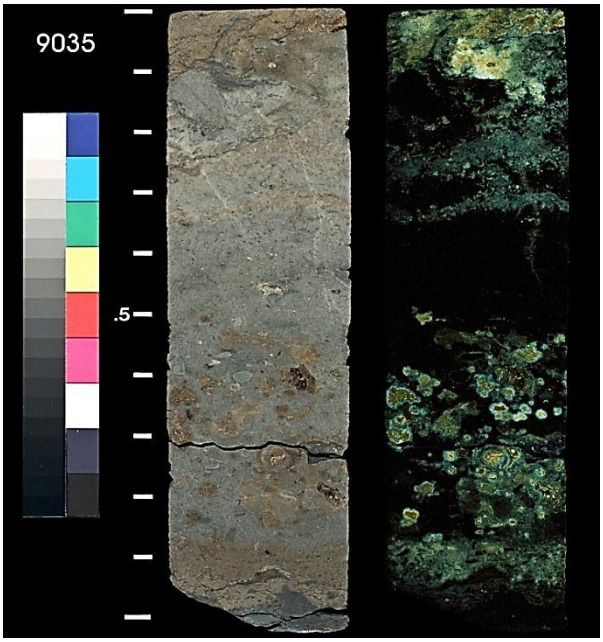

Figure 17: Core photograph of conglomeratic sandstone F1 facies. Mid-Con Energy Operating Hembree 3-17 (Sec. 17 T.6S., R.1W). Left: plain light. Right: ultraviolet light. Depth 9035 feet.

The conglomeratic sandstone facies F1 (Figure 17), is grey to brown, fine-to-medium grained conglomeratic sandstone with abundant subangular to subrounded clay clasts and dolomitized clay clasts (2-35 mm). F1 is cemented firmly by calcium carbonate. Bedding is poorly distinguishable.

The clay clasts are interpreted as rip-up clasts. They are regarded as evidence of scour and redeposition, at the base of a channel eroded into underlying clay-rich sediment. The base of this material is evidence of a local, unconformable contact between channel facies and the underlying mudstone facies. Facies F1 is at the base of channel-fill sandstones, and it overlies clay-rich mudstones directly. The channel-base-scour interpretation is supported by angularity of the rip-up clasts; this shape suggests that the clasts were deposited quickly and near their source, in a high-energy channel.

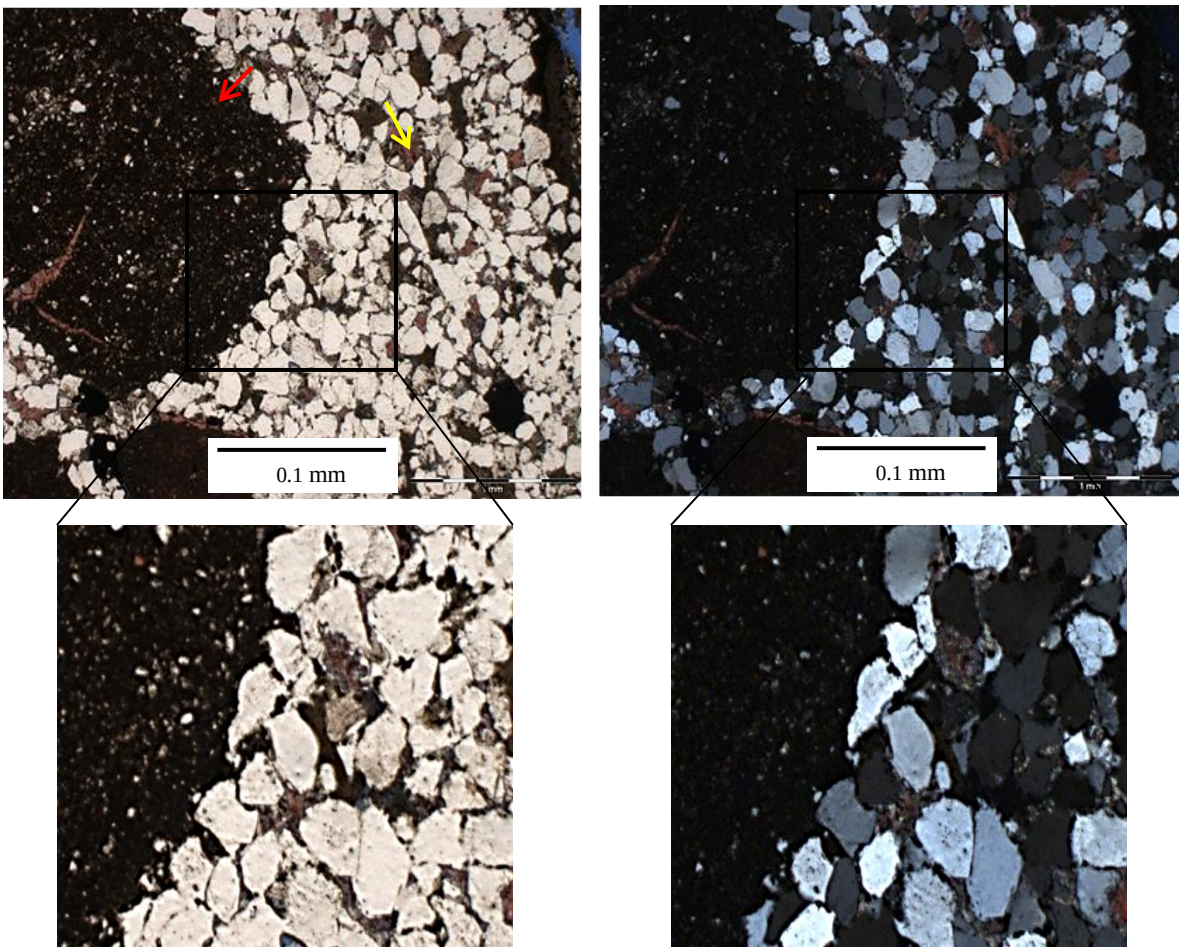

Figure 18: Photomicrographs of samples from the F1 conglomeratic facies. Dominant framework grains are quartz and dolomite. Metamorphic-rock fragments, feldspars and chert are present in lesser quantities. Calcite cement – yellow arrow. Dolomite clast – red arrow. Mid-Con Energy Hembree 3-17. Depth 9035.75 feet.

The dominant F1 facies framework grains of the F1 facies are quartz and dolomite, whereas metamorphic-rock fragments, chert and feldspars are in minor quantities (Figure 18). Quartz grains appear to be angular; this angularity is primarily the result of quartz overgrowths. Primary porosity was occluded by calcium carbonate cement and pseudomatrix; however, few secondary pores are present, and such pores that were detected originated by dissolution of feldspar and detrital clay matrix. Core-derived porosity and permeability data are not available for rocks of facies F1. However, reservoir quality is inferred to be poor, due to abundant porosity occluding calcium carbonate cement and pseudomatrix.

(F2) Horizontal Planar-laminated Sandstone

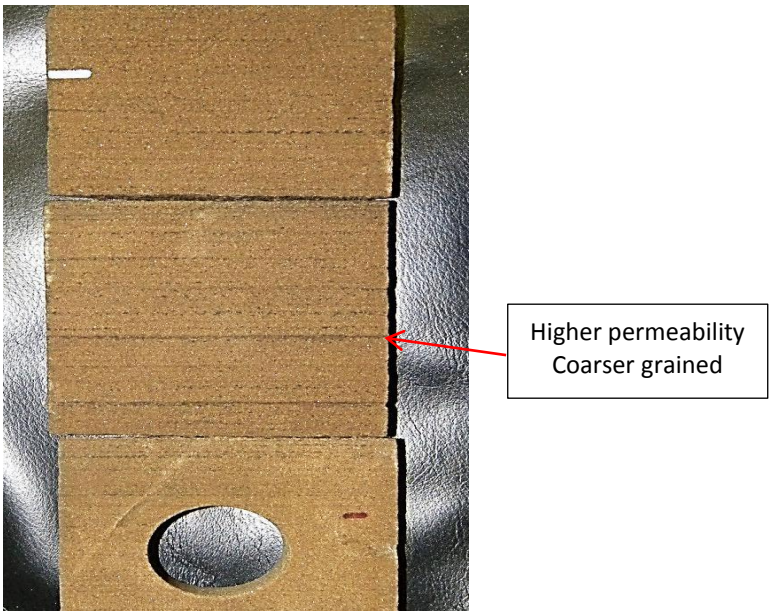

Figure 19: F2 facies from the Santa Fe Minerals Inc. Gilley 20-2 (Sec. 20 T.6S., R.1W). Planar laminations in the sandstone are conspicuous. Depth 9047 feet.

Stratigraphic unit F2 (Figure 19) is brown fine-to-medium-grained laminated sandstone with distinct thin (1-3 mm) dark brown planar laminae. The dark brown laminae are the coarser, being composed of medium-sized grains; whereas the light-brown laminae (3-10 mm thick) are fine-grained.

This planar-laminated sandstone is interpreted as the product of high-energy, sheet-like traction-flow deposition within a channel. F2 facies is interpreted as the record of fluvial deposition, unaffected by marine processes. Plane-laminated sandstones are deposited in many environments; therefore, the interpretation of them is reliant on associated facies. Facies F1 supports the interpretation. F2 facies is not present in the Hembree 3-17 cored interval. Facies F2 average core-derived permeability and porosity are 96 md and 15.5 %, respectively.

(F3) Cross-laminated Sandstone

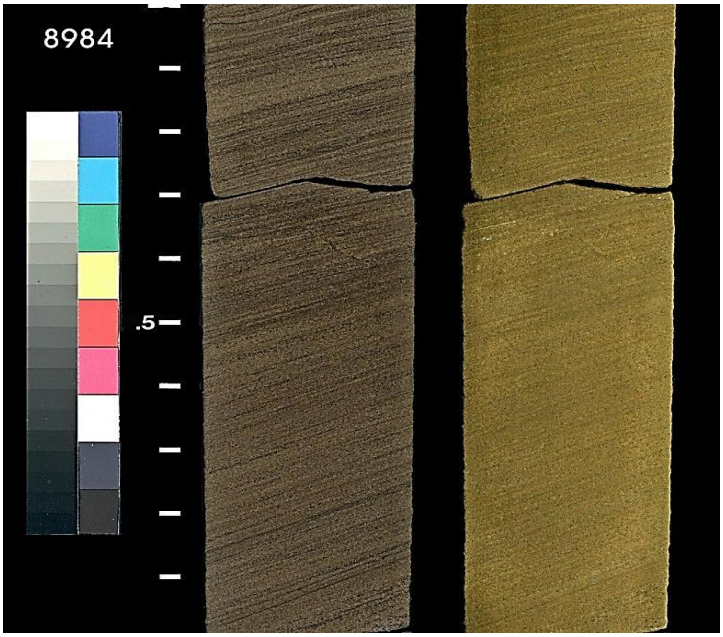

Figure 20: Facies F3 from the Mid-Con Energy Operating, Inc. Hembree 3-17 (Sec. 17 T.6S., R.1W). Cross-laminations in the sandstone are conspicuous. Depth 8984 feet.

F3 facies (Figure 20) is brown fine-to-medium-grained sandstone with dark, (1-3 mm) dipping laminae. The dark brown laminations are similar to the horizontal planar laminations in one attribute: they are of fine to medium grain-size, whereas light-brown laminations are fine-grained.

F3 facies is interpreted as the record of low-energy deposition within a sand-dominated channel; the sediment probably formed by migration of dunes. Facies F3 typically overlies F2 facies; it underlies Facies F4 at some localities, and facies F5 at others. Where facies F2 is not present, F3 directly overlies facies F1. There is no evidence of a marine influence for facies F3, as normal marine invertebrates and trace fossils were not observed. Facies F3 is interpreted as the product of deposition by fluvial processes.

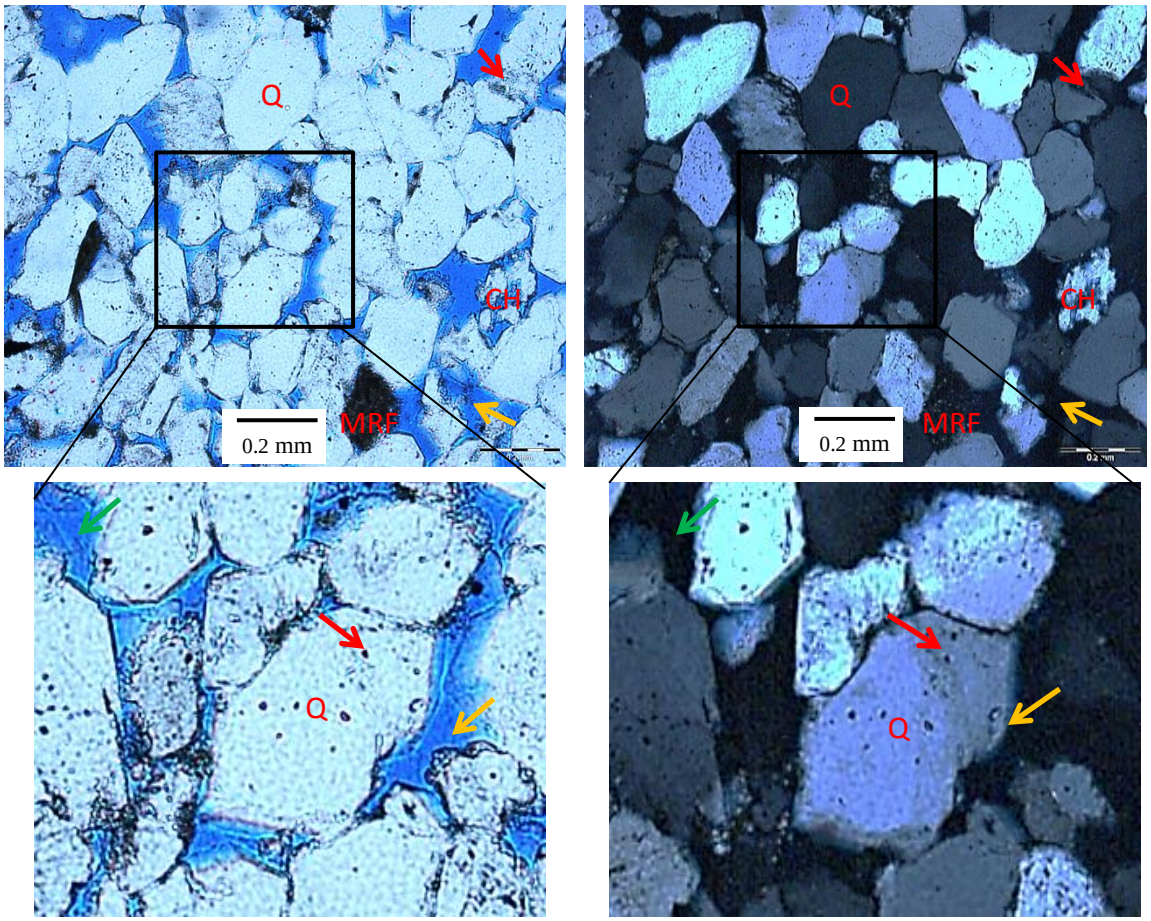

Figure 21: Photomicrographs of facies F3, showing moderately sorted sandstone. Detrital grains include: quartz (Q), chert (CH), metamorphic rock fragments (MRF) and feldspar (F). Primary porosity is identified by planar pore boundary (yellow arrows). Secondary porosity is evident by irregular pore boundary (green arrows). Quartz overgrowths are shown by red arrows. Left-hand panel: plane-polarized light. Right-hand panel: cross-polarized light. Blue epoxy shows filled pore space. Bottom images are enlarged by area in box. Mid-Con Energy Operating Hembree #3-17. Depth 8984.7 ft.

Quartz is the dominant framework grain, whereas metamorphic rock fragments, chert and feldspars compose the minor fraction (Figure 21). Quartz overgrowths and pore-lining illite are the authigenic constituents. Where present, grain-coating illite prohibits quartz overgrowths, thereby the original shape of the grain is preserved. Measured core plug (depth: 8984.7 ft.) porosity is 15.8% and permeability to air is 131 md. Primary porosity is common. Secondary porosity is also abundant. It consists of moldic and oversized pores. Secondary porosity is the result of the dissolution of metastable grains, detrital matrix, pseudomatrix and authigenic clays.

(F4) Trough Cross-laminated Sandstone

Figure 22: F4 facies from the Mid-Con Energy Operating Hembree 3-17 (Sec. 17 T.6S., R.1W). Depth 9027 feet.

Facies F4 (Figure 22) is brown very-fine- to fine-grained sandstone with foreset laminae. The laminae are curved to planar. The overall aspect of the sedimentary structures is reminiscent of trough cross bedding.

Trough cross-bedding are interpreted as evidence of deposition within a channel, under conditions of moderate energy, where sediments accumulate as migratory dunes. Trough cross-bedding also is commonly associated with point bars. At depth 9027.35 in the Hembree 3-17, F4 facies has net confining stress (NCS = 6500 psi) porosity of 13.2% and permeability to air of 0.783 md. Observations of fine-to-very-fine grain-size from facies F4 is consistent with the low permeability (<1 md) measurements for core-plug analysis.

.

(F5) Deformed Sandstone

Figure 23: F5 facies from the Mid-Con Energy Operating Hembree 3-17 (Sec. 17 T.6S., R.1W). Deformed laminae in the sandstone are conspicuous. Depth 8980 feet.

Facies F5 (Figure 23) is brown, fine-grained sandstone with deformed bedding and abundant carbonaceous debris. The deformed bedding is irregular to convoluted and contains sparse fluid escape structures.

The convolute bedding of F5 is interpreted to as the result of slumping from the instability of channel walls. Slump structures, distorted bedding, clay infills and fairly persistent layers of organic debris are commonly observed near the bases of infilled channels (Coleman and Prior, 1981). This facies could also be interpreted as the result of hydroplastic flowage caused by a flood; the plastic deformation is evident by the convoluted bedding. F5 typically is underlain by well-organized cross-bedded F3 facies and overlain by very-fine-grained current-rippled F6 facies.

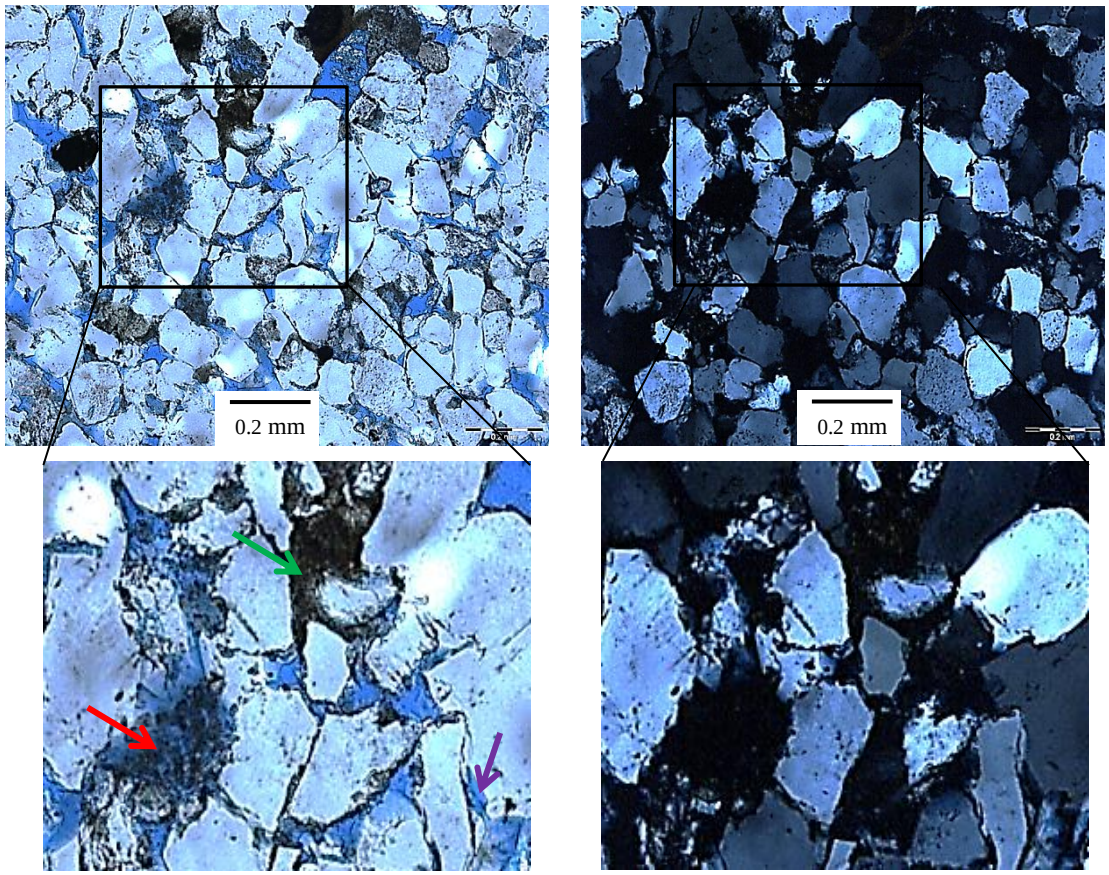

Figure 24: Photomicrographs of moderately sorted F5 facies. Red arrow shows secondary pore from dissolution of clay matrix (red arrow). Green arrow shows pseudomatrix. Primary porosity is indicated by purple arrow. Plane-polarized light (left). Cross-polarized light (right). Mid-Con Energy Hembree 3-17. Depth 8980.65 ft.

Porosity is a combination of primary intergranular porosity and secondary porosity developed by the dissolution of feldspar, rock fragments, detrital clay matrix and authigenic clays (Figure 24). Pseudomatrix formed by clay is common. Secondary pores are of intragranular, moldic and oversized. At depth of 8980.65 ft in the Hembree 3-17, F5 facies has a measured NCS (6500 psi) core-plug porosity of 14.2% and permeability to air of 2.28 millidarcies. Core-plug permeability of facies F5 (depth 8980.65 ft) (2.28 md) compared with facies F3 (depth 8984) (131 md) probably is a function of the homogenized deformed bedding in F5, because grain sizes and amounts of cement of both facies are similar.

(F6) Current-rippled Sandstone

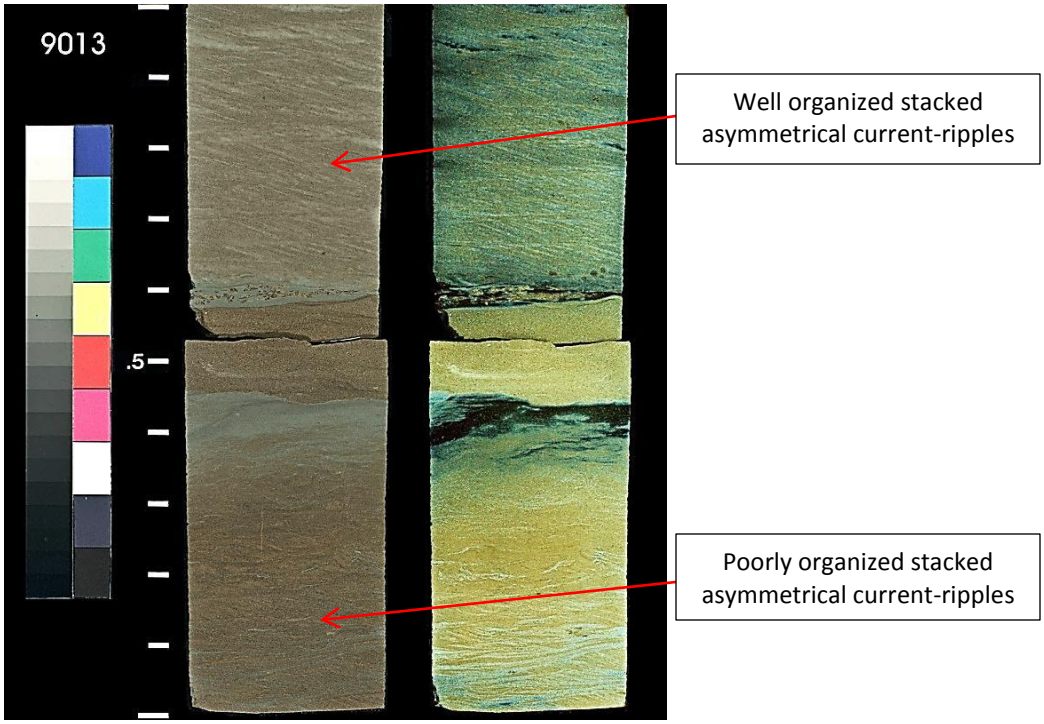

Figure 25: Facies F6 from the Mid-Con Energy Operating Hembree 3-17(Sec. 17 T.6S., R.1W).

F6 (Figure 25) is very-fine grained, brown-to-light-brown ripple-laminated sandstone. All observed ripples are asymmetrical (unidirectional), are penetrated by rare vertical burrows, and show evidence of few mud drapes. Rippled foresets are common visible (0.5 – 1cm).

F6 facies is interpreted as evidence of low-energy (lower flow regime), unidirectional current-dominated deposition within a fluvial channel system. Deposition of facies F6 is hypothesized to have been the result of decreased fluvial energy because channel abandonment, probably from a rise in base level. This low-energy fluvial process results in lower-flow-regime, unidirectional ripple bedding and decreased grain size. Evidence such as properties indicative of unidirectional flow and the lack of heterolithic rhythmic alterations of sand and mud suggest that deposition was within a fluvial channel, not directly affected by tidal processes.

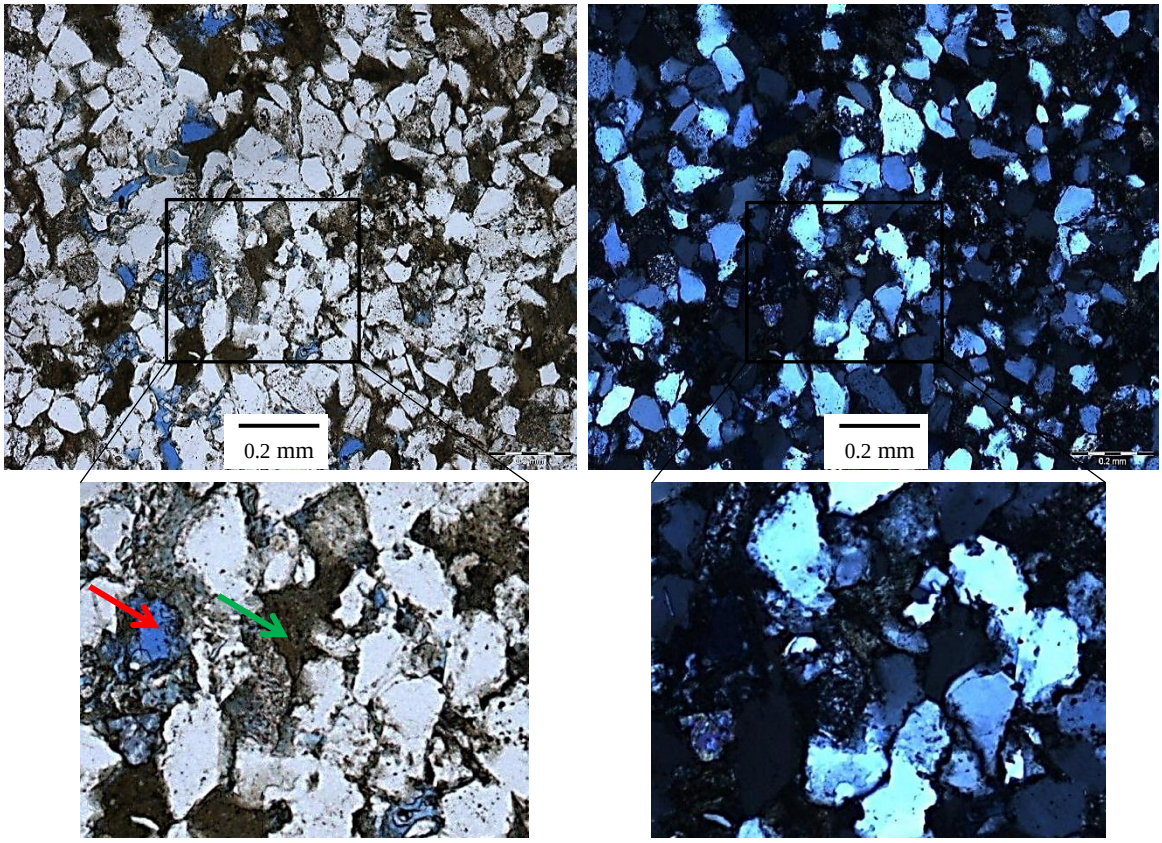

Figure 26: Photomicrographs of F6 facies, which is composed of poorly sorted, clay-rich, very-fine-grained sandstone. Secondary porosity as a result of dissolution of clay matrix is shown by red arrow. Pseudomatrix is shown by green arrow. Plane polarized light (left) and cross-polarized light (right).

Dominant framework grains of facies F6 are quartz; the minor fraction of grains is made up of feldspar, chert, metamorphic-rock fragments and sedimentary-rock fragments (Figure 26). Authigenic constituents include quartz overgrowths and grain-coating illite. Pore space was reduced by abundant pore-clogging pseudomatrix and clays. The sandstone is very fine-grained and silty. Secondary and primary porosity are evident (Figure 22). Secondary porosity is dominantly a product of dissolution of metastable grains, including feldspars and rock fragments, and dissolution of pseudomatrix. Core-plug porosity and permeability data are not available for facies E.

(E) Current-rippled siltstone

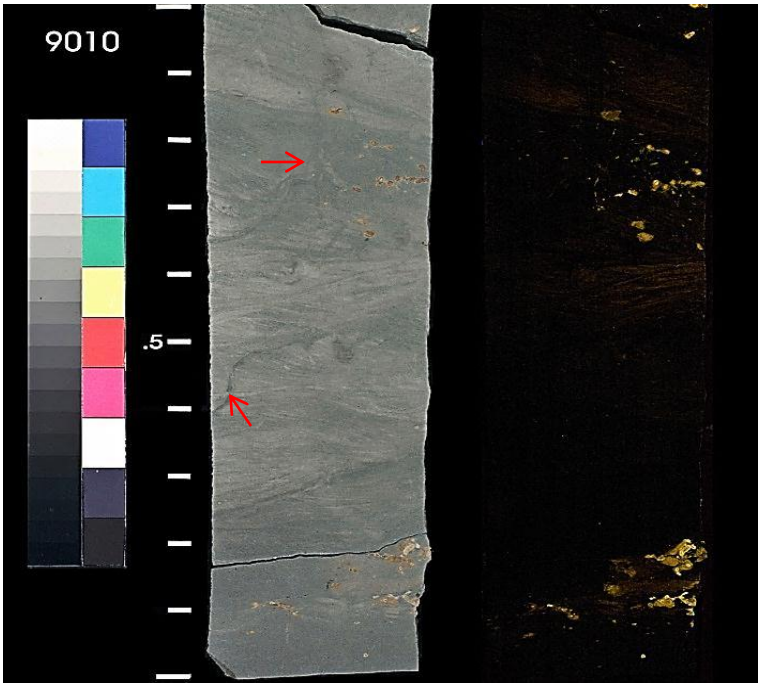

Figure 27: Facies E from the Mid-Con Energy Operating Hembree 3-17 (Sec. 17 T.6S., R.1W). Red arrows point to "vertical" burrows.

Wavy-laminated to current-rippled siltstone of facies E (Figure 27) is grey to light grey; it contains wavy laminations and current-ripples within a silt-dominated matrix. "Vertical" burrows and carbonaceous clay debris are abundant.

Facies E is interpreted as having been deposited during periods of channel flooding, initiated by rise in base level. This facies contains abundant "vertical" burrows (red arrow) (Figure 27), and carbonaceous debris (green arrow) that probably was deposited after abandonment of the channel. Abundant "vertical" burrows, very-fine-grained sand and silt grain-size and carbonaceous in debris altogether support the interpretation of rise in base level and shut down of the fluvial system by submergence. Facies E could be evidence of estuarine conditions. Facies E typically is near the top of the sandstone "package"; typically it overlies facies F6 and underlies paleosol facies P (to be described).

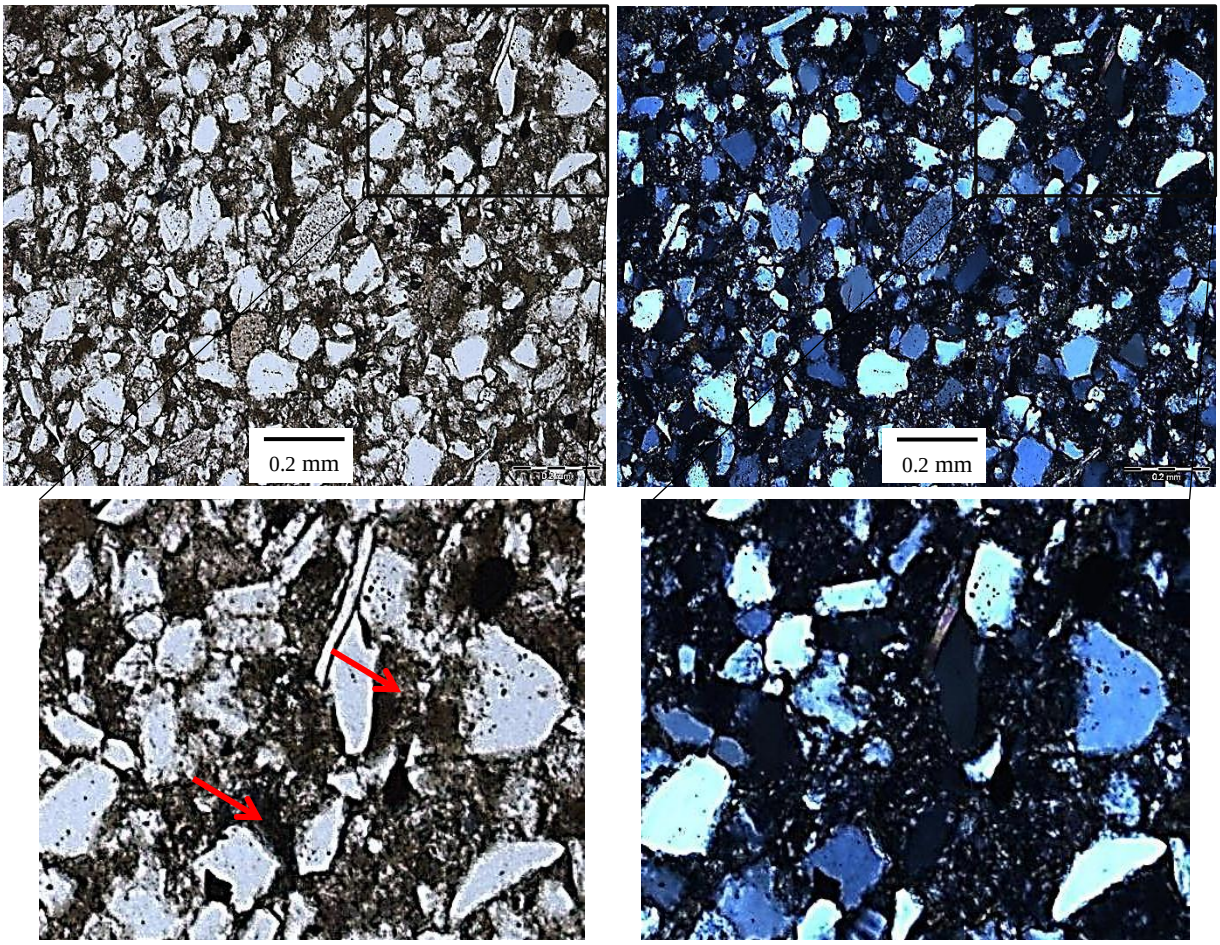

Figure 28: Photomicrographs of facies E. Poorly sorted clay-rich siltstone; the pore space of which is clogged by abundant clay matrix (red arrows). Plane-polarized light (left) and cross-polarized light (right). Mid-Con Energy Operating Hembree 3-17. Depth 9009.75 ft.

Framework grains in facies E are dominantly quartz, with smaller quantities of feldspar, chert, sedimentary-rock fragments and metamorphic-rock fragments (Figure 28). Detrital clay matrix occludes porosity. Reservoir quality is poor; the siltstone is clogged by detrital clay. Core-plug porosity and permeability data are not available for facies E.

(P) Paleosol

Figure 29: Core photograph of facies P from the Mid-Con Energy Operating Hembree 3-17(Sec. 17 T.6S., R.1W).

Facies P (Figure 29) is grey-to-dark-grey siltstone-to-very-fine-grained sandstone. Facies P has a red-to-orange crumbly oxidized character in localized nodules and vertically aligned irregular fractures – a pedogenic aspect, overall.

Facies P is crumbly, a trait that may be evidence of incipient pedogenesis associated with subaerial exposure (Figure 29). Facies P is interpreted to have formed during a decline in base level, which resulted in subaerial exposure of an underlying estuarine facies. Thus, paleosol facies is likely the subaerially exposed upper-portion of facies E. Facies P is considered to be non-reservoir, due to its clay- and silt-rich composition. Core plug data is not available for this facies, but reservoir-quality is inferred to be poor.

(FP) Variegated Mudstone

Figure 30: Facies FP from the Santa Fe Minerals, Inc. Gilley 20-2 (Sec. 20 T.6S., R.1W). FP is variegated red-green-grey and has weak structure.

Variegated mudstone facies FP (Figure 30) is crumbly, variegated grey-green-red mudstone. This facies contains sparse thin, dark grey, competent layers of shale.

Facies FP is interpreted to as the product of deposition on a floodplain, that was exposed by drop in base level. This inferred fall in base level probably was associated with activation of the Tussy A fluvial system, in which floodplain muds were deposited. Floodplain facies (FP) is overlain unconformably by the Tussy A fluvial channels. This sharp and erosional contact is evident in the Hembree 3-17 and Gilley 20-2 cored intervals; where fluvial sandstones appear to have scoured into underlying mudstone facies. Borehole-image (BHI) logs throughout the study also portray this contact to be abrupt, by these attributes: rip-up-clasts near the channel bases, and apparent sharp-contacts between channel sandstone facies and underlying mudstone facies.

(M1) Silty Mudstone

Figure 31: Oxidized zones in the M1 facies from the Mid-Con Energy Operating Hembree 3-17 (Sec. 17 T.6S., R.1W).

Facies M1 (Figure 31) is grey silty mudstone with siderite concretions. The concretions are interbedded with thin, wispy to inclined, lenticular-bedded to rippled very-fine-grained sandstone. Figure 31 illustrates the silty mudstone portion of facies M1 but does not include the thin, interbedded very-fine-grained sandstone.

Facies M1 is interpreted as having been deposited as delta-front, its gamma-ray signature diminishes upward, which implies upward increase in grain-size. The interbedded sandstones are interpreted as the record of pulses of sediment discharge from the delta mouth. The Tussy B interval in the Hembree 3-17 BHI contains M1 facies that is overlain unconformably by F1 channel facies.

(M2) Mudstone

Figure 32: M2 facies from the Mid-Con Energy Operating Hembree 3-17 (Sec. 17 T.6S., R.1W) with carbonized plant debris (green arrows).

Facies M2 (Figure 32) is dark grey, poorly indurated crumbly mudstone with few siderite concretions (3.5-5cm in thickness) and abundant carbonaceous plant debris. The siderite is sub-parallel to bedding. Facies M2 was observed only in the Tussy B cored interval in the Hembree 3-17. The Tussy A intervals in the Hembree 3-17 and Gilley 20-2 do not contain this facies.

Facies M2 probably was deposited in the distal subaqueous delta plain. Perhaps this rock is evidence of the most seaward extent of the lower delta plain, for typically sediments of the finest-grain size are transported to the most seaward position in the subaqueous lower delta plain (Boggs, 2006). Depositional facies are summarized in Table 1. Photographs of the facies are in Figures 33, 34, 35 and 36.

Facies Code	Facies Name	Grain Size	Dominant Features	Depositional Processes
Fluvial (F)				
F1	Carbonaceous clay-clast conglomeratic sandstone	Matrix-supported paraconglomeratic	1 – 5 cm diameter mud clasts, poorly sorted	Scour and fill
F2	Horizontal planar laminated sandstone	Fine to upper fine	Horizontal laminations	Unidirectional traction flow
F3	Cross-laminated sandstone	Fine to upper fine	Low-angle laminations	Alternating between bedload and suspension
F4	Trough-cross stratified sandstone	Very fine to fine	Trough-cross-laminae	"Unidirectional" to traction flow
F5	Deformed sandstone	Very fine to upper fine	Deformed/convoluted beds, flow structures	Channel fill slumping
F6	Current-rippled sandstone	Very fine	Asymmetrical climbing-ripple laminations, few burrows	Current-dominated, traction flow
Estuarine (E)				
E	Current-rippled to wavy laminated siltstone	Fine	Current-rippled to wavy laminae, heavily burrowed	Mixed fluvial-marine Estuarine processes
Paleosol (P)				
P	Paleosol	Very fine	Crumbly, oxidized material	Subaerially exposed estuarine facies
Floodplain (FP)				
FP	Variegated Mudstone	Mudstone	Variegated material (red-green-grey)	Exposed floodplain
Marine (M)				
M1	Interbedded silty mudstone and sandstone	Silty mudstone	Silty mudstone interbedded with wavy to discontinuous thin beds (1-3 cm) of siltstone to very-fine sandstone	Marginal-marine, delta-front
M2	Mudstone	Mudstone	Dark grey mudstone with carbonaceous plant debris	Marine, Pro-delta

Table 1: Summary of depositional facies designations, characteristic features and interpreted depositional processes of eleven facies described from cores, Hembree 3-17 and Gilley 20-2 wells.

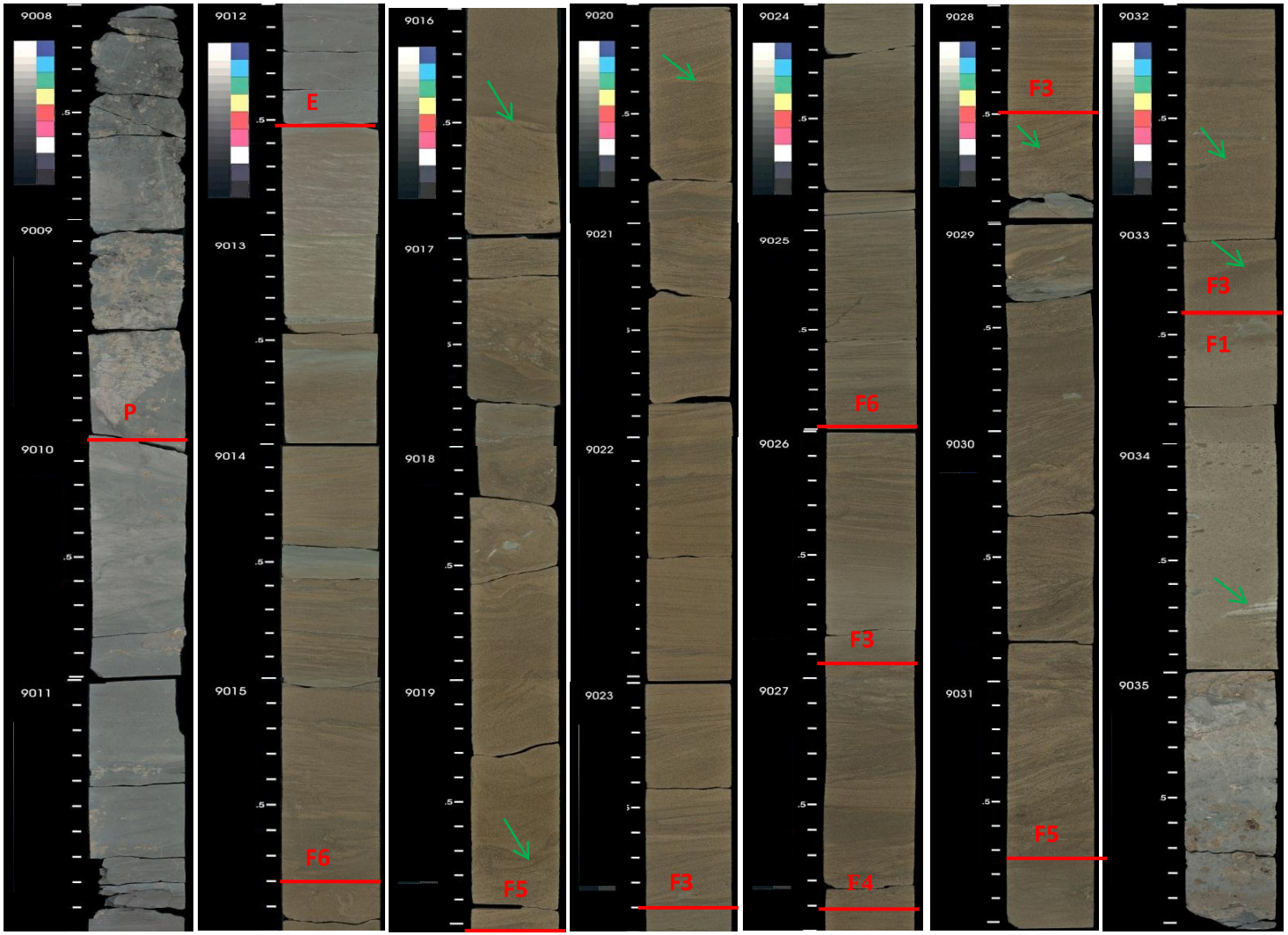

Figure 33: Tussy B sandstone, Mid-Con Operating Hembree 3-17 (Sec. 17 T.6S., R.1W), showing lithofacies, indicated in red (see Table 1 for codes of facies). Green arrows point to prominent channel reactivation surfaces.

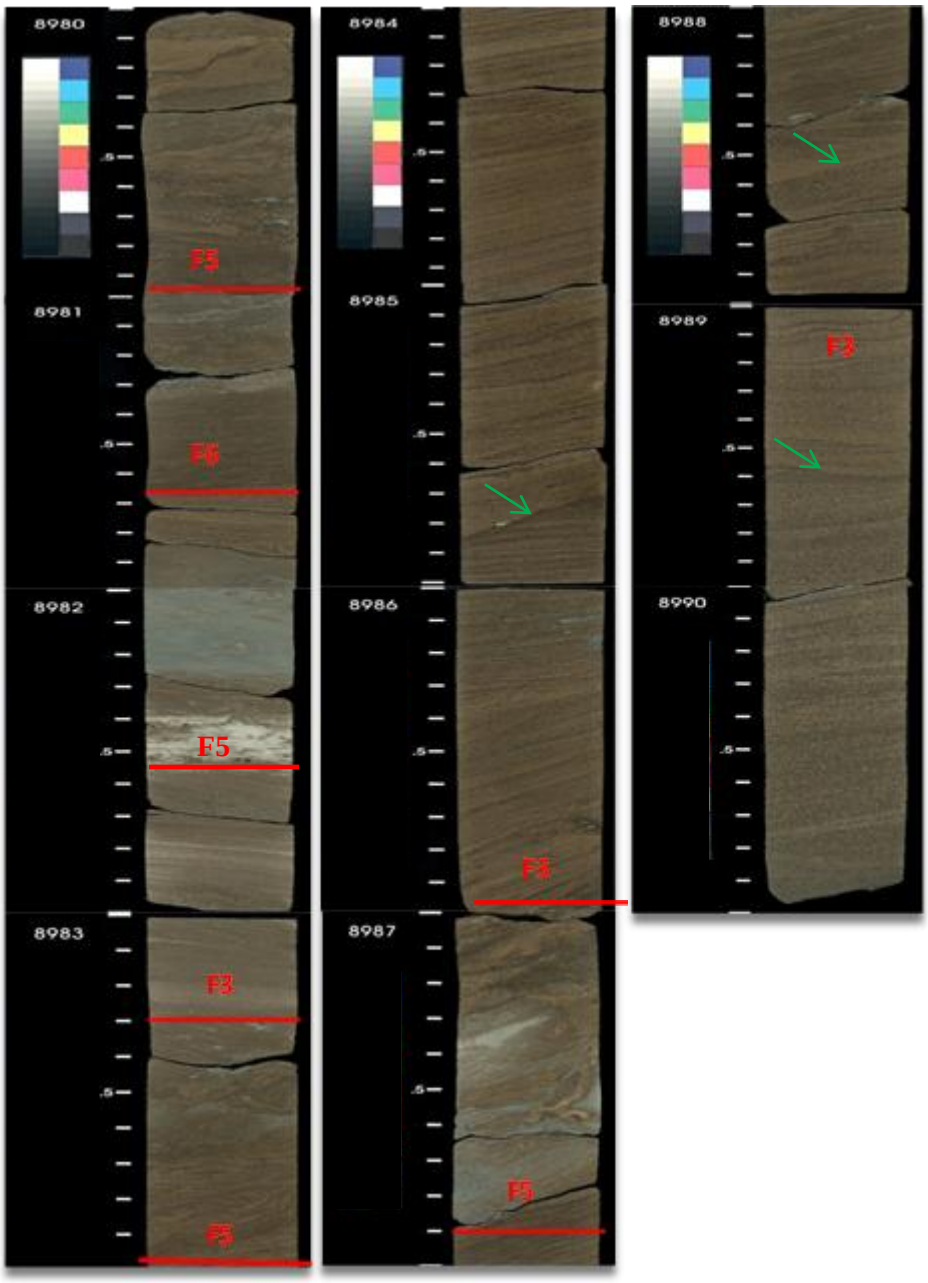

Figure 34: Tussy A sandstone, Mid-Con Operating Hembree 3-17 (Sec. 17 T.6S., R.1W), showing lithofacies, indicated in red. Green arrows point to prominent channel reactivation surfaces. See Table 1 for codes of facies.

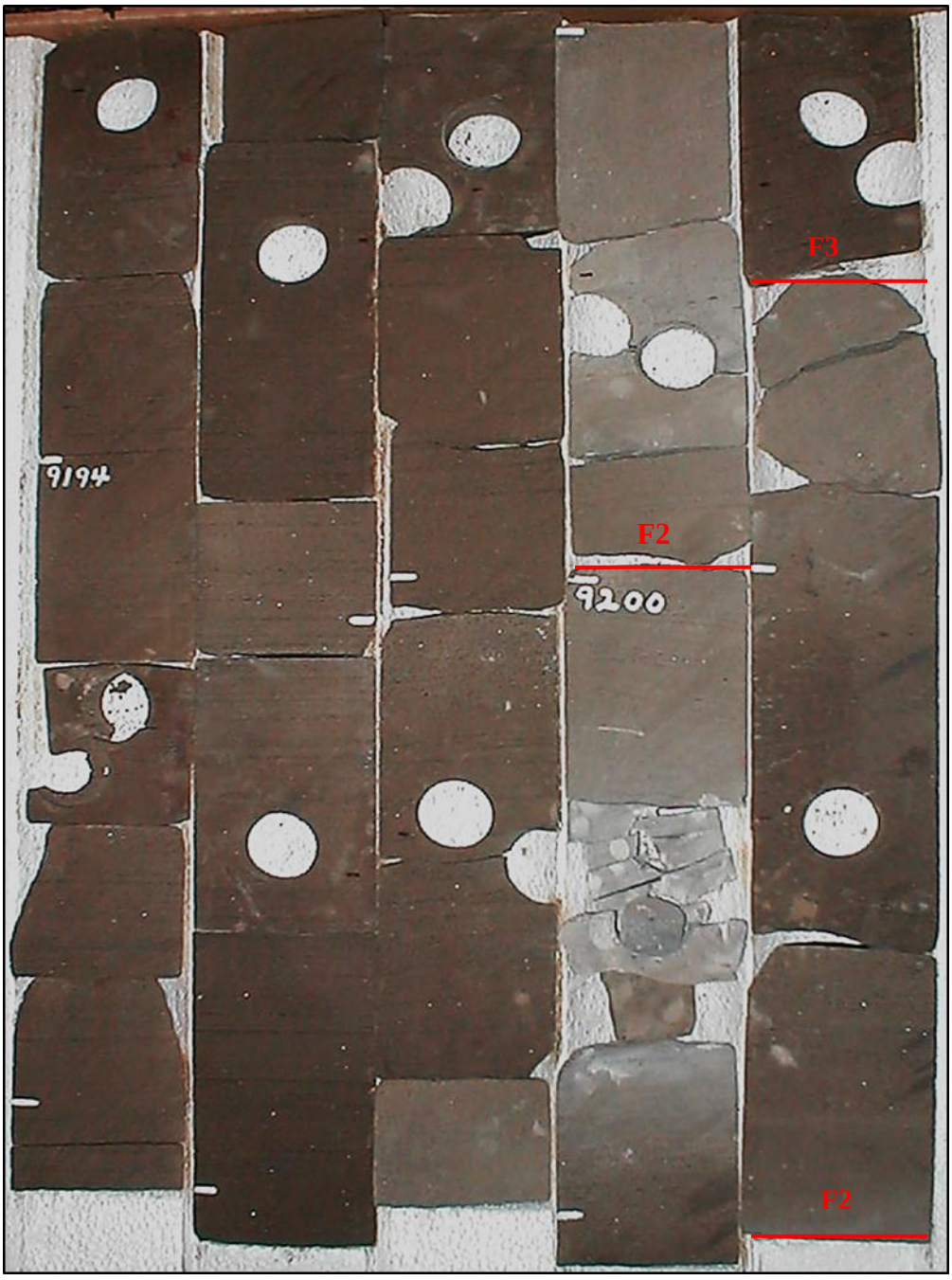

Figure 35: Tussy A sandstone, Gilley 20-2 (Sec. 20 T.6S., R.1W), showing lithofacies, coded in red. See Table 1 for codes of facies.

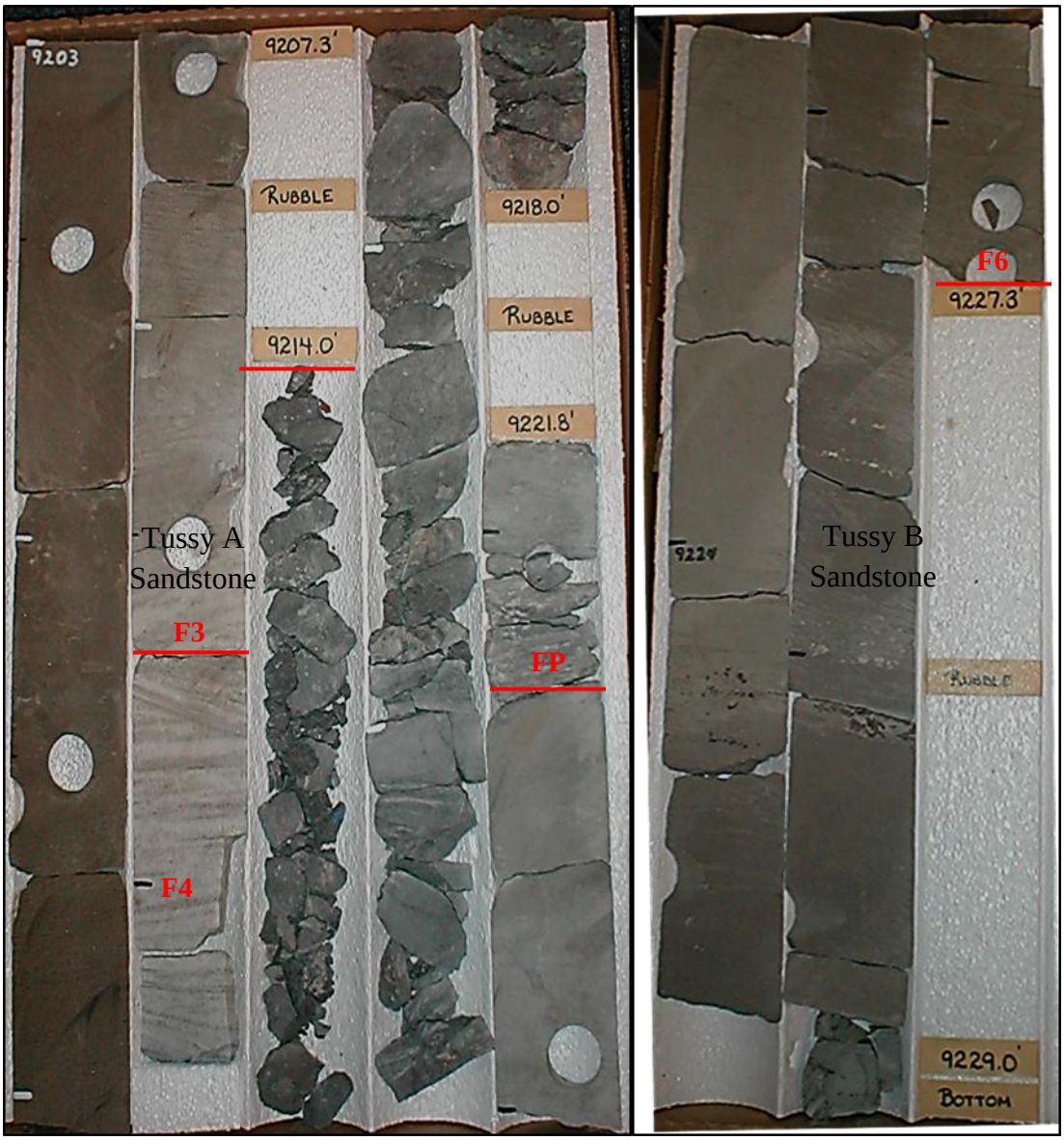

Figure 36: Basal part of Tussy A sandstone, mudstone below Tussy A sandstone and uppermost portion of Tussy B sandstone from the Gilley 20-2 (Sec. 20 T.6S., R.1W). Lithofacies indicated in red. See Table 1 for codes of facies.

Summary of Facies Analysis

Eleven depositional facies within the Tussy A and B stratigraphic intervals were described from the Hembree 3-17 and Gilley 20-2 cores; these are summarized in Table 1. The Hembree 3-17 core is composed of fluvial facies (F1, F3, F4, F5 and F6), paleosol facies (P) and marine facies (M1 and M2). Of the Hembree 3-17 core, facies boundaries of the Tussy B and A intervals are shown in Figures 33 and 34. For the Hembree 3-17, core-plug porosity and permeabilities correlated to cored-facies and static BHI are in Appendix A. The Gilley 20-2 core (Figures 35 and 36) comprises fluvial facies (F2, F3, F4, F5 and F6) and floodplain facies (FP). Facies boundaries of Tussy A and B intervals are labeled in Figures 33, 34, 35 and 36. Sandstones of the Tussy A and B intervals are litharenite (Figure 37).

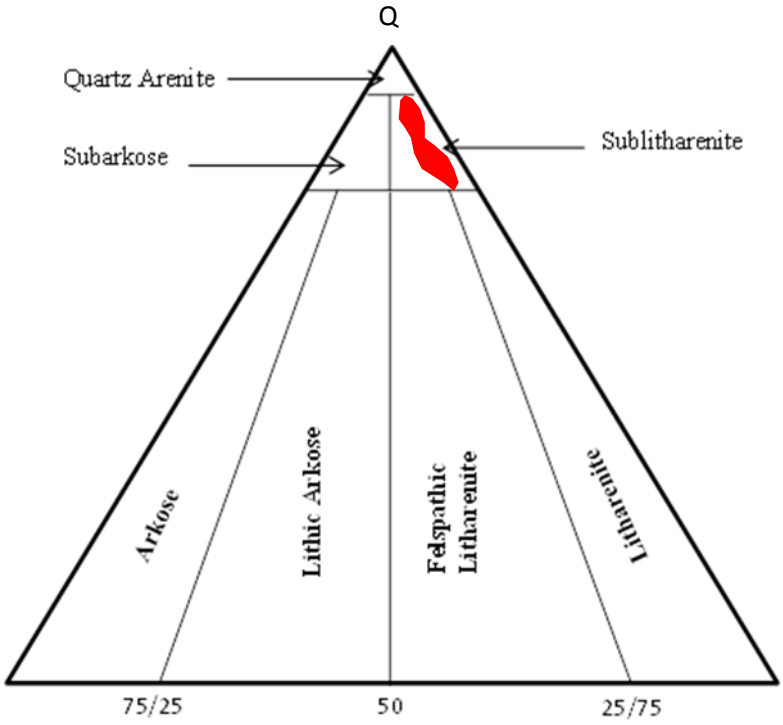

Figure 37: QFR classification scheme of the Tussy A and B sandstone reservoir facies, from point counts of thin-sections. Depicted above are the normalized percentages (adjusted to exclude percentage of pore-space) of quartz (Q), feldspar (F) and rock fragments (R).

Facies Associations

Floodplain

The floodplain association consists of variegated grey-green-red mudstone. Floodplain facies was observed in the Hembree 3-17 and Gilley 20-2 cored intervals above the Tussy B sandstone (Figures 30 and 36). This facies seems to have been exposed subaerially on a floodplain; it is interpreted to be the result of a lowered base level, which rejuvenated the Tussy A fluvial system. The floodplain facies overlies estuarine facies, and is overlain unconformably by Tussy A fluvial sandstones.

Estuarine

The estuarine facies association consists of facies E (Figure 27), a heavily burrowed, current-to-wavy-rippled dark grey, very fine grained sandstone and siltstone that overlies fluvial facies F6 (Figure 25). Estuarine facies are records of drowning of the channel belt from rise in base-level, the elevation which resulted in an estuarine environment of the estuarine facies, the chief evidence of which is burrowed rock. The uppermost portion of the estuarine facies is an exposure surface of oxidized material, associated with pedogenic processes. This surface of exposure probably is evidence of lowered base level, and consequent exposure of the estuarine facies. This association is evident in the Hembree 3-17 core (Figures 29 and 33).

Fluvial Channel

The fluvial channel facies association comprises reservoir units in the Tussy interval. It is an overall fining-upward succession of facies, including all fluvial (F) facies. Strata of channel-fill origin are multistoried (each increment 5-30 ft thick) successions of amalgamated fining-upward sequences. Fining-upward sequences have basal erosional surfaces. The internal amalgamated cross-laminated sandstones and scour surfaces are regarded as the record of stacked

lateral-accretionary point-bar deposits. They justify the inference of movement of a meandering channel within a channel belt. Bases of fluvial channels show abrupt contacts with underlying mudstone (erosional unconformities) characterized in the lower part by carbonaceous clay-clast conglomeratic sandstone (Figure 17). The sandstones fill channels scoured into mudstones. Reservoir facies are horizontal planar laminated, low-angle to wavy laminated and distorted-bedded sandstones; they are within the lower to middle portions of fluvial channels. Distorted beds that contain clay clasts are abundant within the channel body. Fluvial channel-fill deposits are capped by wavy-laminated to unidirectional-rippled siltstone. This wavy-to-unidirectional-rippled burrowed facies contains vertical burrows; the burrows indicate the onset of base level rise and the beginning of estuarine depositional processes. There is evidence, such as depositional facies and their associated stacking patterns, which support the interpretation that the Tussy A and B sandstones were deposited within fluvial channels which were inundated.

Marine

The marine facies association is dark grey mudstone with siderite concretions and carbonaceous plant debris (Figure 32), overlain by grey to dark grey silty mudstone (Figure 31). The mudstone grades upward into thin, interbedded, wispy parallel-to-inclined siltstone and rippled, very fine grained sandstone with few vertical burrows and siderite concretions. In typical modern settings, the delta front is just seaward of the lower delta plain; it forms the uppermost portion of the subaqueous delta plain. Seaward from the delta front is pro delta submarine terrane (Boggs, 2006). The delta front association was observed only directly below the Tussy B channel facies in the Hembree 3-17 core. Features in this facies association could form in many environments such as a flood plain or tidal flat – but data compiled from cores seems to indicate that a subaqueous delta-front or prodelta is plausible.

Electrofacies

The previously described facies associations are evident in distinct wireline-log signatures, particularly those observed from gamma-ray curves. Gamma-ray logs detect the combined natural radioactivity, sourced by uranium, potassium and thorium (Asquith and Krygowski, 2004). These data are normalized to API (American Petroleum Institute) units. The Tussy A and B fluvial facies are the main focus of this discussion.

Figure 38 illustrates the interpreted gamma-ray electrofacies from the Hembree 3-17. As interpreted, the channel facies in core is depicted on gamma-ray logs as sharp-based, fining upward, bell-shaped gamma-ray curves, which generally are less than 45 API units in the lower and middle portions of the sandstone body; in the fining-upward sequence gamma-ray deflection is in the range of 75-90 API, near the top. Channel facies gamma-ray signatures are aggregates of stacked internal fining-upward gamma-ray sequences; these successions of fining-upward gamma-ray signatures represent the stacked fining-upward sequences observed in core. The uppermost portion of the sandstone body is channel abandonment/estuarine facies and typically has low density porosity (4-6%) and relatively high GR values (75-90 API).

Marine facies lie below the Tussy B channel facies, coarsen upward, and are funnel-shaped (Figure 38). Gamma-ray deflection decreases from 105 API units near the base of the mudstone/siltstone sequence to 45 API near the top. Floodplain facies overlie the Tussy B channel-fill facies and underlie Tussy A channel-fill facies. The floodplain facies has gamma-ray deflection of 95-110 API units.

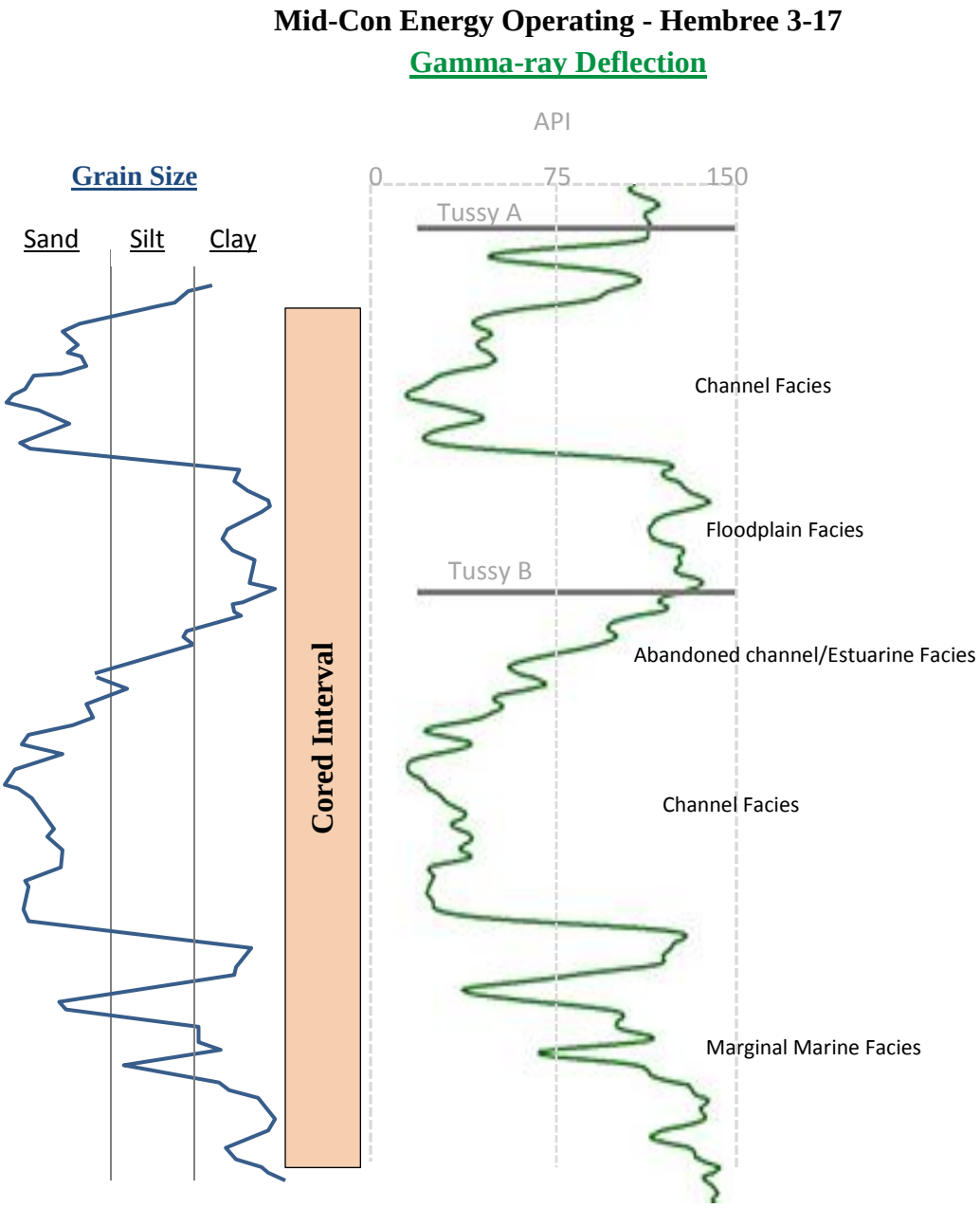

Figure 38: Field-wide representative gamma-ray (green) electrofacies signatures and generalized grain-size scale of the Tussy A and B cored intervals: Marine facies, channel facies, estuarine facies and floodplain-paleosol facies. Mid-Con Energy Operating Hembree 3-17(Sec. 17 T.6S., R.1W) .

Controls on Reservoir Quality

As discussed above, rocks of relatively high porosity and permeability are in the channel facies. Characteristics of these lithotypes from analyses of core, thin-sections and core-derived porosity and permeability data reveal that grain size, degree of cementation and clay content are the major controls on reservoir quality. The best reservoir facies are of coarse grain-size, are poorly cemented, and have small amounts of pore-clogging clays. Cross-plots of core-derived permeability and porosity (Figures 39 and 40) showed that depositional facies are another dominant control on reservoir quality. The hypothesis is that rocks of the highest permeability are the laminated sandstone facies F2 and F3. The highest recorded core-derived permeability and porosity, 148 md permeability and 17.7 % porosity, was from the cross-laminated facies F3 in the Gilley 20-2. As described in the previous facies-analysis section, dark laminae in facies F2 and F3 are slightly coarser-grained sandstone, which results in relatively high permeability values. Facies F2 and F3 have the highest measured porosity and permeability values; they are the best reservoir rock observed in the Tussy interval.

MID-CON ENERGY OPERATING
HEMBREE 3-17

PERMEABILITY VS. POROSITY

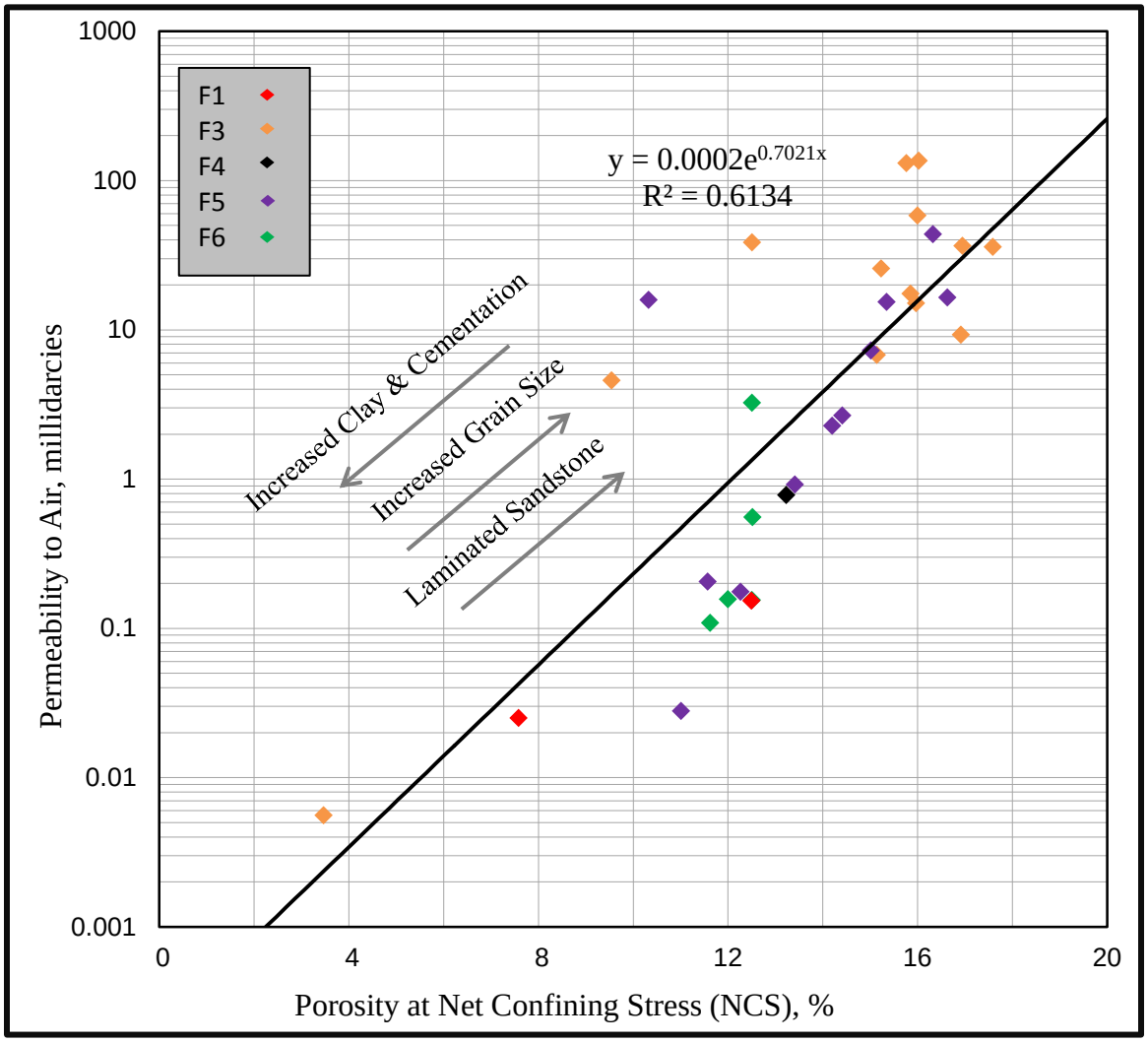

Figure 39: Cross-plot of core derived permeability (to air) versus porosity (6500 psi, net confining stress: NCS) from the Hembree 3-17 core. Data points are color coded to identify lithofacies. Color coded lithofacies designations in the upper left hand corner include F1-F6. F1: conglomeratic sandstone, F3: cross-laminated sandstone, F4: trough-cross laminated sandstone, F5: deformed sandstone, F6: current-rippled sandstone.

SANTA FE MINERALS
GILLEY 20-2

PERMEABILITY VS. POROSITY

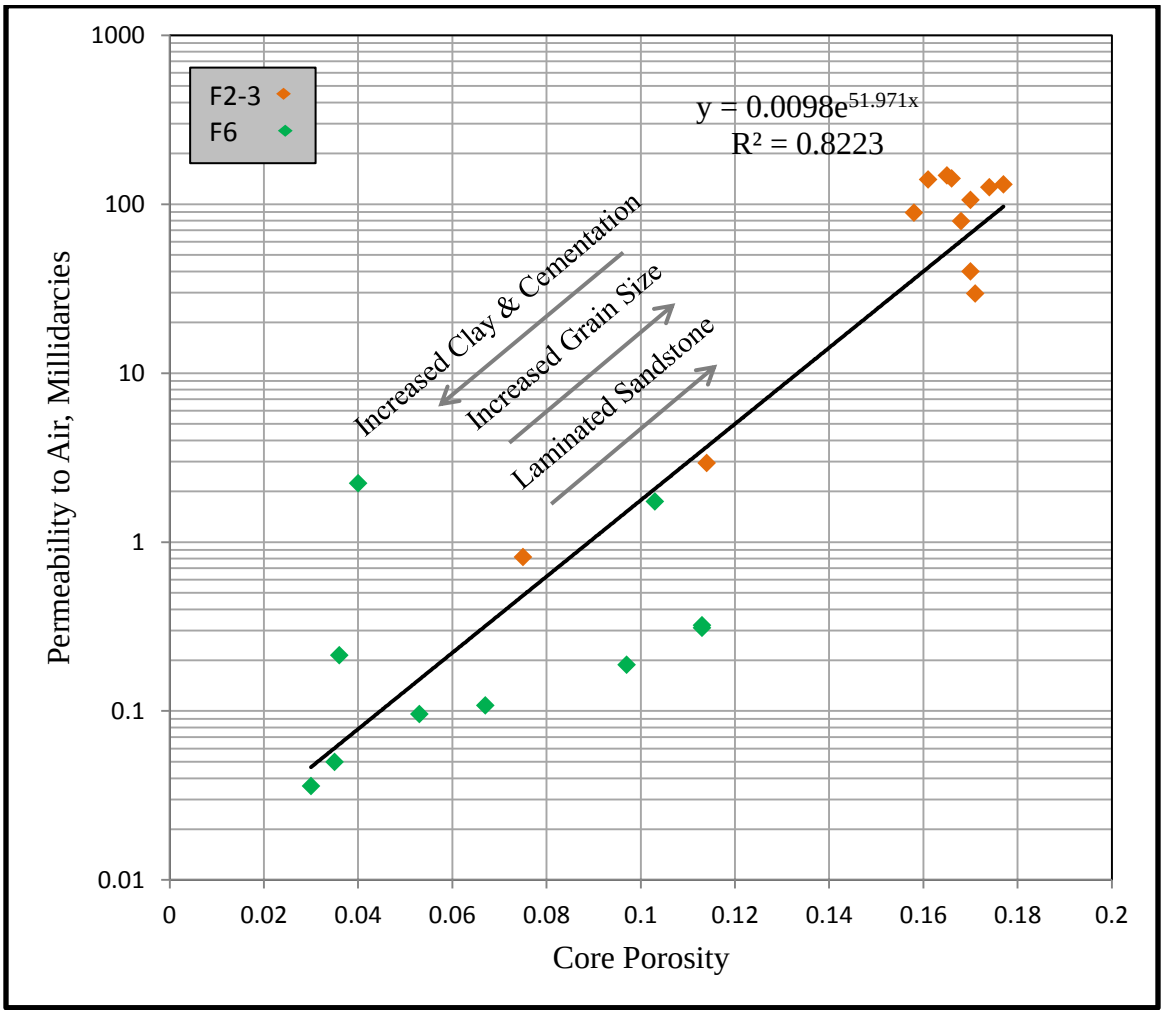

Figure 40: Cross-plot of core derived permeability (to air) versus porosity from the Gilley 20-2 core. Data points are color coded by lithofacies to represent their relative reservoir qualities. Color coded lithofacies designations in the upper left hand corner include F2-3 and F6. F2-3: cross-laminated and horizontal-laminated sandstone, F6: current-rippled sandstone.

Summary

The Tussy A and B cored intervals are rocks that were deposited in marine, fluvial, floodplain and estuarine environments; they show evidence of sea-level cyclicity. Eleven core-derived facies were interpreted, each with distinct sedimentary structures and reservoir quality. Tussy A and B sandstones are interpreted to have been deposited in fluvial-channels; these fluvial-channels consist of successions of amalgamated fining upward sequences.

Tussy B fluvial processes seem to have thrived during a relative base level lowstand. This lowstand is evidenced by the unconformable contact between the Tussy B channel base and underlying marine sediments. As base-level rose, channel abandonment occurred due to decreased fluvial energy. As base-level continued to rise, the fluvial system shut-down to form an estuary with increased biotic activity, evidenced by heavily burrowed siltstone facies. When base-level began to fall, previously deposited estuarine facies were subaeirally exposed. This base-level fall is evidenced by a paleosol above Tussy B sandstone. As base-level continued to drop, Tussy A fluvial systems were activated, which unconformably overlie flood plain facies. Another rise in sea-level probably shut down the Tussy A fluvial system.

High-quality reservoir rocks are restricted to channel facies. Facies F2, F3 and F5 have the best reservoir quality, while F4 and F6 have fair reservoir quality. Facies F1 has poor reservoir quality due to abundant cementation by calcite. Facies E, FP, P and M are considered non-reservoir but, form great seals. Primary porosity is abundant, and suggests these rocks were not buried at great depths. Secondary porosity is dominantly from dissolution of feldspars and rock fragments. Pores are intergranular, intragranular, moldic and oversized. Reservoir quality is controlled by grain size, depositional facies and degree of cementation. The best quality reservoir facies are fine to medium grained laminated sandstones with minimal cementation.

CHAPTER V

BOREHOLE-IMAGE ANALYSIS

Introduction

Borehole-image (BHI) logs from three service companies (Schlumberger, Weatherford and Halliburton) were available from eleven wellbores within the study area. All eleven BHI logs were examined in detail to extract stratigraphic and structural information. One of the eleven BHI logs is used as an example: Mid-Con Energy Operating Hembree 3-17 Extended Range Micro Imager (XRMI). Schlumberger, Weatherford and Halliburton designed their tools based on similar principles. Halliburton's EMI is discussed in detail. Wireline-based dipmeter and BHI tools are configured with various arms; four, six, or eight and each arm has a pad. Within each pad are a certain number of sensors, ranging from 4 to 92, depending on the design specifications of the tool (Lagraba et al., 2010). The Halliburton EMI (Figure 41) has six independent arms each with 25 buttons - therefore a total of 150 sensors (Halliburton, 2012). While the sensors are pressed against walls of a borehole they record an alternating electrical current that is induced by an electrode (Lagraba et al., 2010). The tool produces an electrical image by measuring and mapping formation micro resistivity (Halliburton, 2012). The concept behind the BHI tool is to measure resistivity of the flushed zone (Rxo), the zone adjacent to the borehole and saturated with mud filtrate. Mud filtrate displaces formation fluid. Investigation at such short distances from

the borehole and measurement of rock saturated with mud filtrate minimizes the effect of formation fluids on resistivity (Deyhim, 2000).

DeVries (2005) showed that facies can be described by chromatic variation observed from BHI logs. These variations are shown by the range from darker to brighter colors. The brighter colors (white – yellow) are characteristic of resistive rock, whereas the darker colors (orange to black) are indicative conductive rock. Schlumberger, Weatherford and Halliburton use similar presentations for illustrating micro resistivity, all displaying a static image and a dynamic image, side-by-side. The Halliburton Extended Range Micro Imager (Figure 41) uses an additional image display called the Horiz7 Filter, which provides much detail in imagery of sedimentary structures, by use of a high-resolution (3-ft.) sliding window. Static normalization applied throughout the interval of the BHI color-codes a given resistivity value consistently throughout the data set. Alternatively, the dynamic image is normalized dynamically; local normalization of the data is conducted within a sliding window. For high resolution data, size of the sliding window typically is between 2 and 10 ft. The dynamic image provides abundant local detail within a given window. However, relative colors of two equal values of resistivity located in different windows will be eluded (Lagraba et al., 2010). Dynamic images provide excellent local detail, but the static image is the preferred display for use in comparison of resistivity signatures throughout a data set. High-quality BHI data permits accurate interpretation: orientations of strata, composition, texture, degrees of cementation, reservoir quality, faults, fractures, and borehole breakouts.

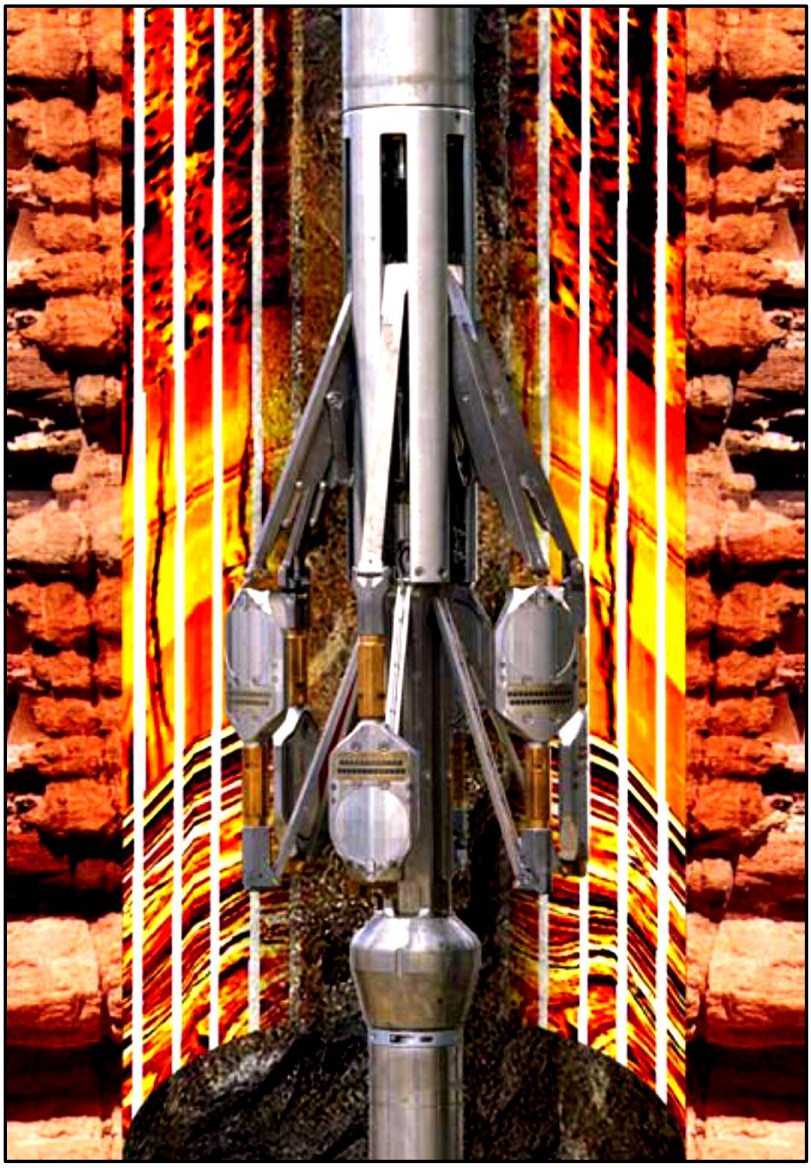

Figure 41: Photograph of Halliburton's XRMI with six arms fully extended (Halliburton, 2012).

Borehole-image Facies Analysis, Illustration of Method

Facies described from core of the Hembree 3-17 were calibrated to borehole-image logs. The working hypothesis was that correlation of a core-calibrated micro image log to other wells with BHI logs but with no cores would allow identification of reservoir facies. Analysis of dip meter data would help define the types of fluvial processes that deposited the Tussy sands. Core-calibrated BHI logs have been effective for interpretation of upper Morrowan sandstone depositional facies and inferring reservoir quality within the Mustang East field in Morton County, Kansas (DeVries, 2005). Pattern recognition of chromatic variation and dip meter orientations of individual core-derived lithofacies in BHI logs were used in combination to interpret depositional facies and reservoir quality and to correlate mappable micro-image log derived facies (DeVries, 2005). Donselaar and Schmidt (2010) showed how BHI logs allow direct interpretation of lithofacies, by comparison with behind-outcrop BHI logs and one behind-outcrop core. Fluvial facies and borehole image facies were interpreted from vertical color successions and dip meter patterns (Donselaar and Schmidt, 2010). Similar methods were employed in this study. Table 2 is an outline of characteristics used to relate micro resistivity signatures to core-derived depositional facies. Figure 42 shows the Tussy B sandstone and Figure 43 shows the Tussy A sandstone from the Hembree 3-17 core. These images are positioned between Halliburton's Static XRMI and Horiz7 dynamic XRMI.

FACIES Terminology	Borehole Image Characteristics Descriptions
F1	Highly resistive (yellow to orange) interbedded, with resistive (dark orange to brown) clay rip-up clasts. Recognizable on the dynamic or Horiz7 images. Dip meter typically shows "random" tadpoles.
F3	Highly resistive (white to orange) with sinusoidal pattern from low-angle planar laminae. Recognizable on the dynamic or Horiz7 image. Dip-meter tadpoles show a unidirectional pattern.
F4	Highly resistive (white to orange to dark orange). Difficult to identify on static and dynamic images due to inconsistency of patterns. (Dipmeter did not record orientations over this interval in the Hembree 3-17.)
F5	Highly resistive (yellow to orange) with slightly less resistive drapes (orange dark orange). Recognizable on dynamic or Horiz7 images; poorly visible on static image. Dip-meter typically shows unidirectional dip pattern.
F6	Highly resistive (yellow to orange) with well-defined stacked, rippled laminae sets. Recognizable on dynamic or Horiz7 images; poorly visible on static image. Dip meter typically shows unidirectional dip pattern.
P-E	Moderately to highly conductive (orange to dark orange). Typically forms the uppermost parts of fining-upward sequences.
M-FP	Highly conductive (dark orange to dark brown).

Table #2: Characteristics of BHI log facies from the Hembree 3-17.

Mid-Con Energy Operating Hembree 3-17 (Sec. 17 T.6S., R.1W)

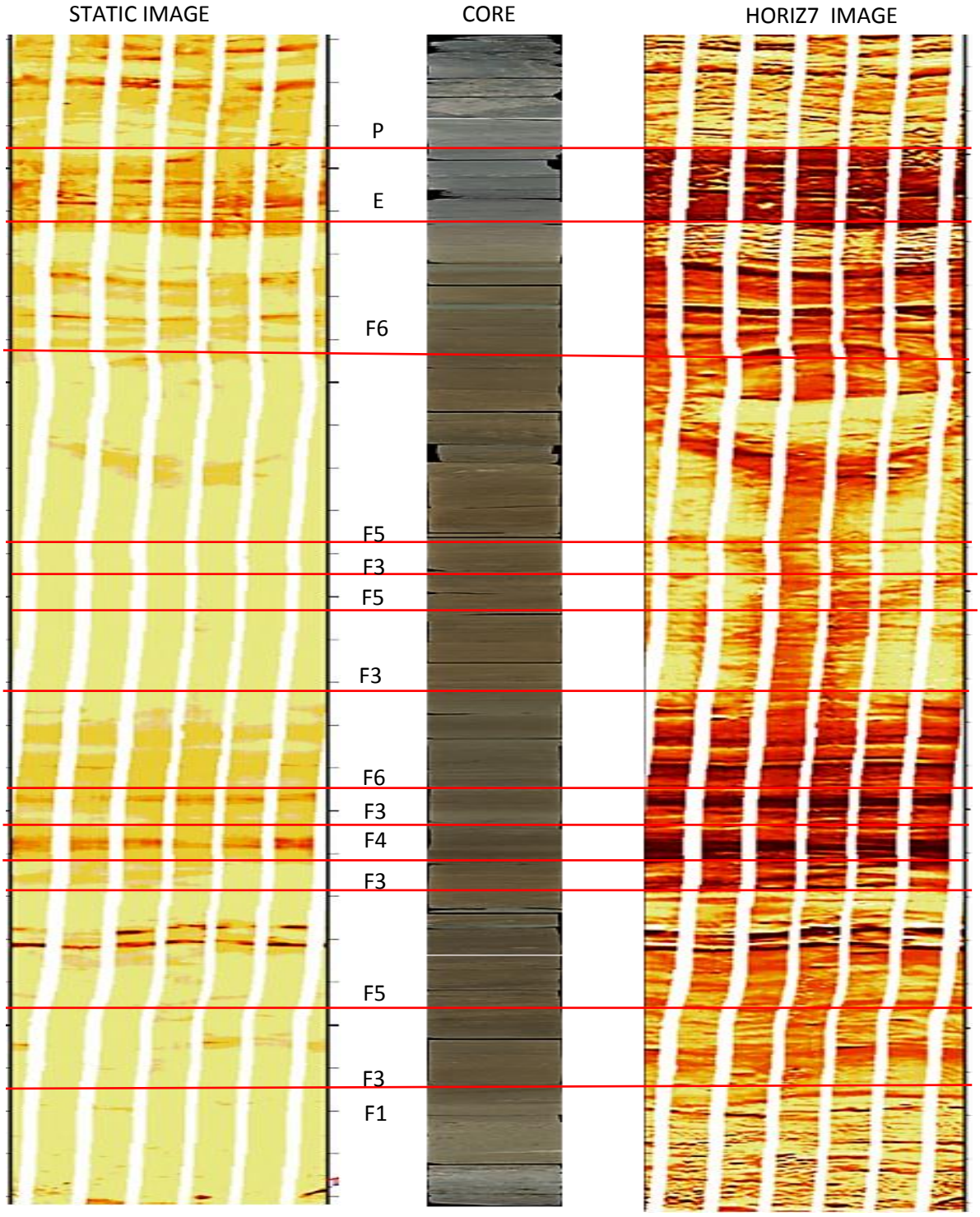

Figure 42: Tussy B sandstone core photograph with static and dynamic XRMI images. Facies designations are shown in table 2. Depth 9009-9035 ft.

Mid-Con Energy Operating Hembree 3-17 (Sec. 17 T.6S., R.1W)

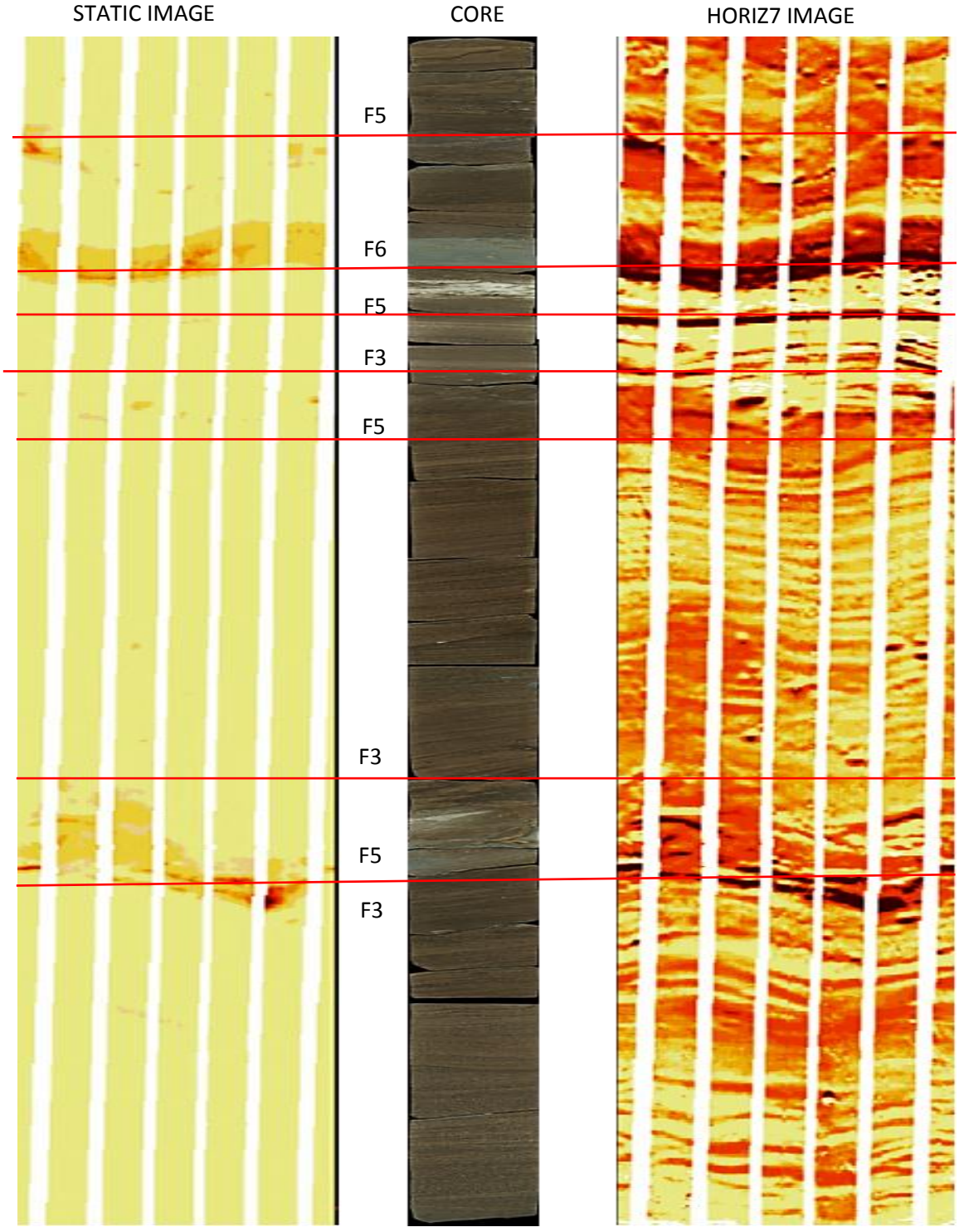

Figure 43: Tussy A sandstone core photograph with static and dynamic XRMI images. Facies designations are shown in table 2. Depth 8980-8990 ft.

(F1) Clay-clast Conglomeratic Sandstone

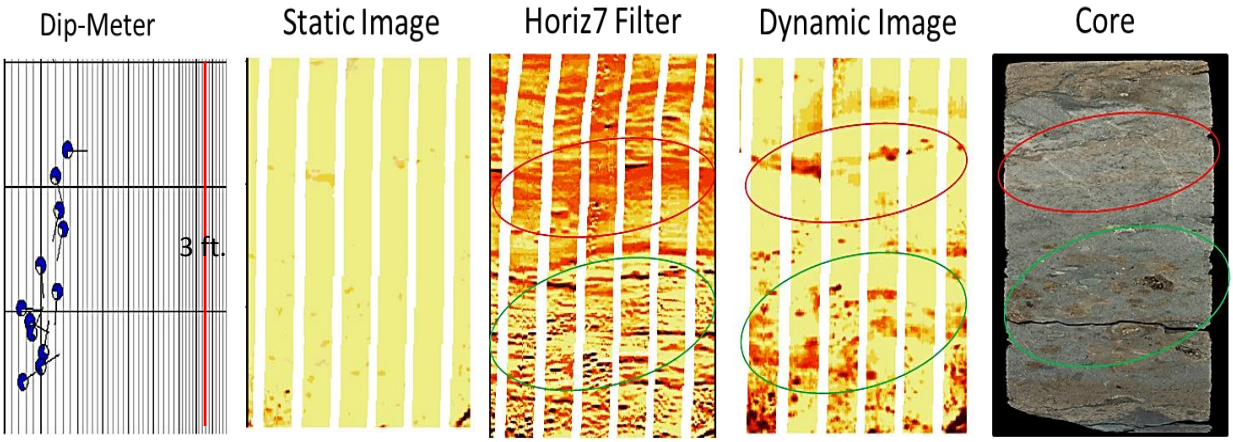

Figure 44: Facies F1. BHI characteristics showing channel-lag clay rip-up clasts and associated "randomly" oriented dipmeter readings.

Facies F1 (Figure 44) is highly resistive (yellow to orange) with resistive (dark orange to brown) rip-up clasts. F1 is easily recognized by use of the dynamic or Horiz7 images. The static image does not highlight clay rip-up clasts. The dynamically normalized image is useful in depicting clay clasts in the conglomeratic sandstone facies, because the sliding window can discriminate among resistivities of the fine-grained sandstone and the less-resistive clay clasts. Dipmeter tadpole orientations are "randomly" oriented within the F1 facies (Figure 41). Thus, analyzing the "random" orientations of dipmeter tadpoles, in combination with inspection of images of resistive clay clasts - as seen in the Dynamic or Horiz7 images - allows reliable interpretation of facies F1.

(F3) Cross-laminated Sandstone

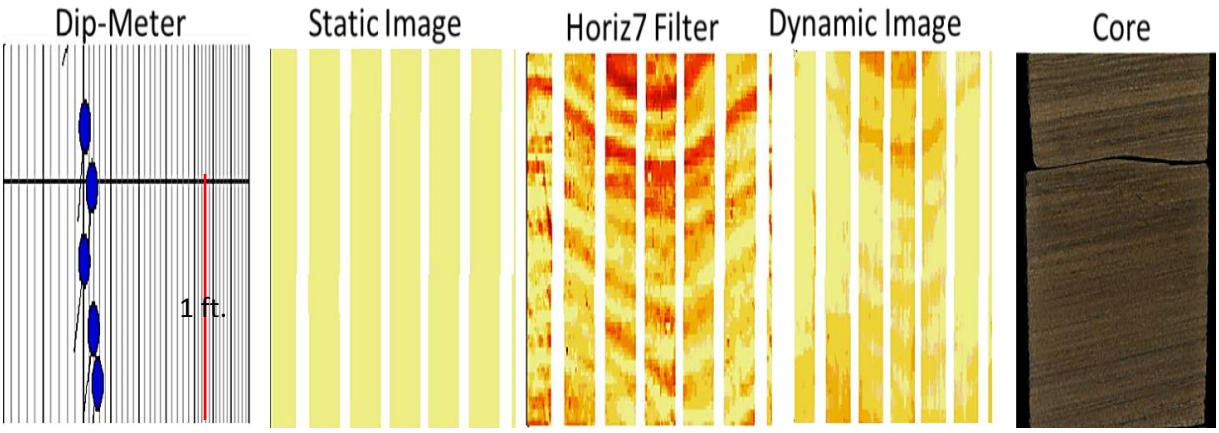

Figure 45: Facies F3 BHI characteristics showing low-angle planar cross-bedding with the characteristic consistent bedding dip direction shown by dip-meter.

Facies F3 is highly resistive (white to orange) on the static image (Figure 45). The statically normalized image shows very little detail regarding cross-laminations, but is indicative of clean (low clay content), reservoir-quality sandstone. The dynamically normalized image reveals more detail, but the Horiz7 Filter depicts the most detailed information about laminar structures. The F3 facies can be deciphered from the dynamic and Horiz7 Filter images by the characteristic sinusoidal pattern, owing to dipping laminae. Laminae are manifest by slight contrast in resistivity, visible in the images. Dipmeter "tadpoles" show almost uniform unidirectional orientation, with very little scatter. This dip pattern is evidence supportive of the interpreted depositional mechanism: dune migration and formation of laterally accreted point bars (Figure 45). The patterns described above are characteristic of this facies; they are useful for inferences about depositional facies in wells that were not cored.

(F4) Trough Cross-laminated Sandstone

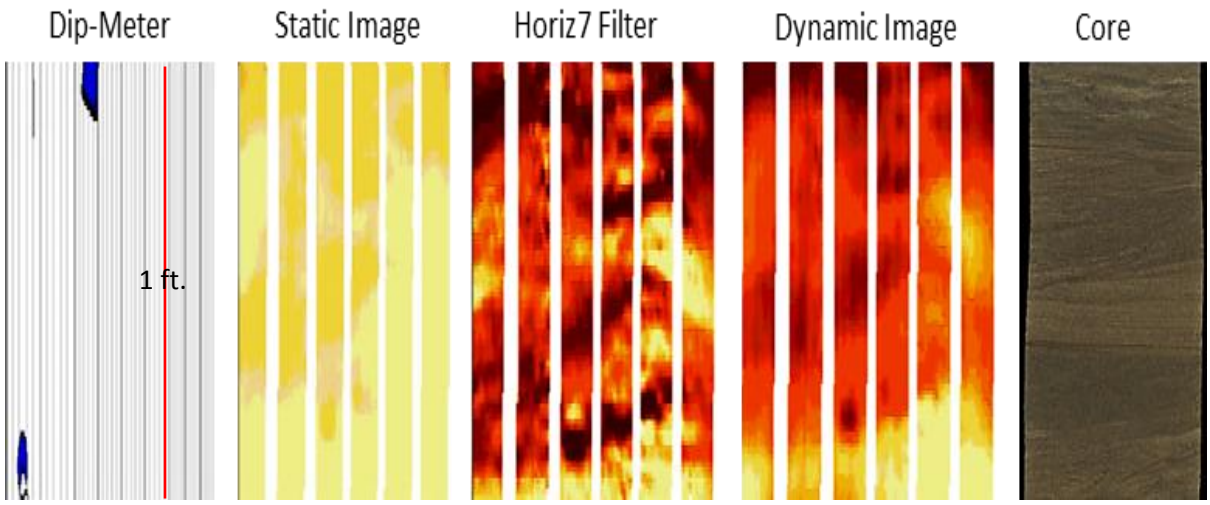

Figure 46: Facies F4. Borehole-images showing suspected trough cross-stratification. Dip-meter shows no tadpoles.

Facies F4 is highly resistive (yellow to orange) on the static image log (Figure 46). The dark yellow to orange hue on the static image is probably indicative of very fine grain size, which reduces the quality of the F4 reservoir facies. (Compare this pattern with solid yellow hue in the F3 facies.) Facies F4 is clearly identifiable on the Horiz7 filter or dynamic image, but overall, its BHI characteristics are not as diagnostic as those of the other facies considered in this paper. In general, the BHI textural characteristics are those of a mottled pattern. (Dipmeter data were not recorded over this stratigraphic interval.)

(F5) Deformed Sandstone

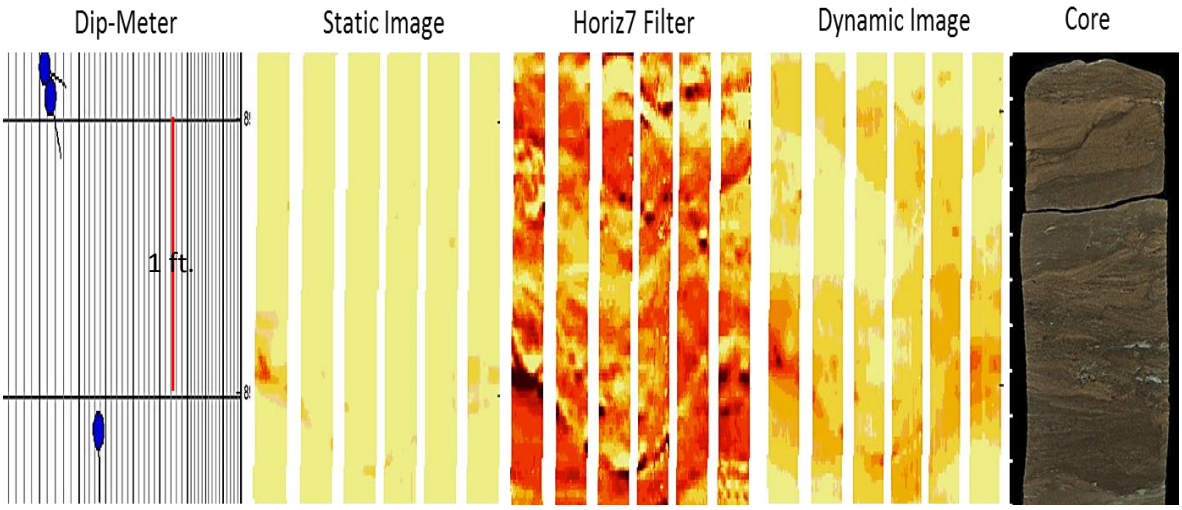

Figure 47: Facies F5. BHI characteristics and dipmeter evidence of facies F5. Clay clasts and traceable deformed laminae are clear images in the Horiz7 filter image. These are diagnostic characteristics of facies F5.

Facies F5 (Figure 47) is shown by a static image indicating high resistivity (yellow). The yellow hue of the static image indicates clay/shale-free sandstone with slight cementation. The Horiz7 filter shows mottled features, indicative of deformed laminae. The F5 facies typically overlies the low-angle cross-laminated sandstone facies F3, and underlies current-rippled sandstones facies F6. Dipmeter data indicate near unidirectional orientation (Figure 47) within this interval. Identification of facies F5 in BHI logs is possible if the textural character of deformed laminae is identifiable in the dynamically normalized window. Dip-meter data alone are not sufficient for identification of the F5 facies.

(F6) Current-rippled Sandstone

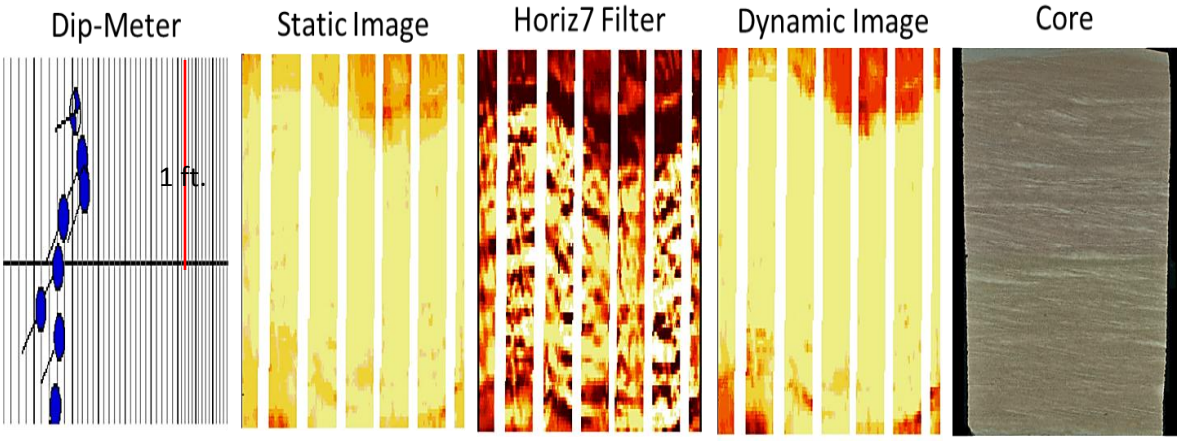

Figure 48: Facies F6. BHI characteristics of stacked asymmetrical ripple cross-laminations with consistent dip directions.

Facies F6 is highly resistive (yellow to orange) on the statically and dynamically normalized images (Figure 48). The Horiz7 Filter in Figure 48 elucidates the asymmetric, current-ripple cross bedding that contains fine-grained sandstone drapes and slightly coarser-grained sandstone. Dipmeter tadpoles show a unidirectional dip direction with minimal scatter. The "uniform" orientation of dipmeter tadpoles (Figure 48) is consistent with the interpreted depositional mechanism of this facies – namely, deposition by unidirectional lower-flow-regime stream flow. This facies can be identified easily in wells without cores, by micro-image logs and conventional wireline logs. The stacked-ripple cross-bed geometries are detectable by orientation of dipmeter tadpoles; moreover, the gamma-ray log signature indicates that grain size tends to fine upwards. This facies is typically positioned near the top of the fining-upward sequence. It is associated with relatively high gamma-ray signatures and low neutron-density porosity, in comparison with coarse-grained sandstone of better reservoir quality.

(P-E) Paleosol-Estuarine

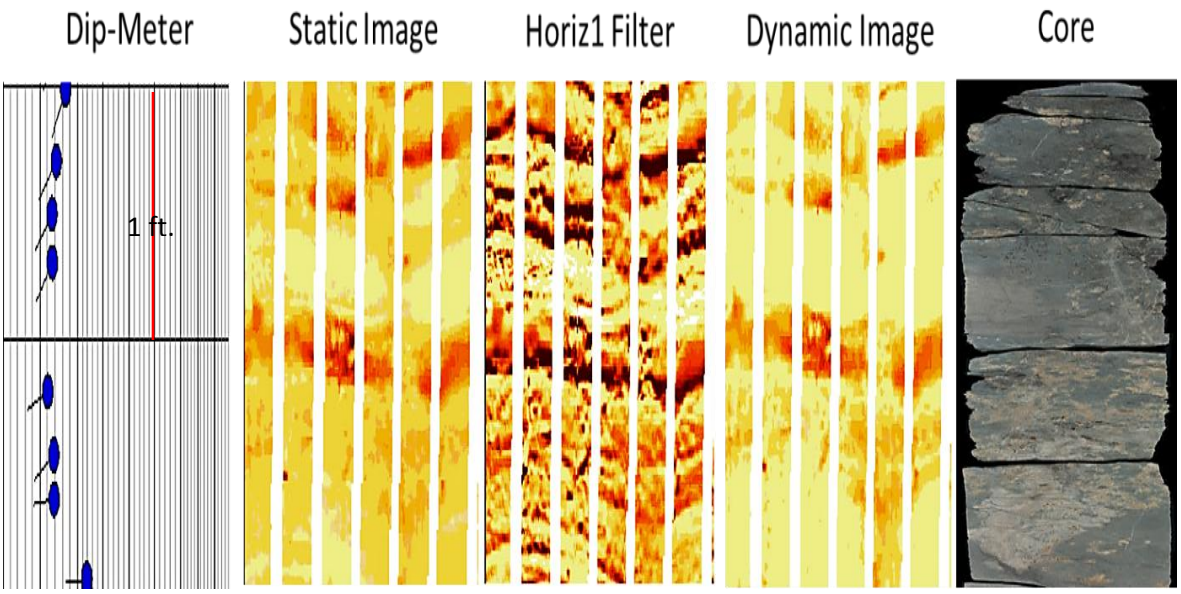

Figure 49: Facies P-E. Characteristic oxidized, conductive material; the product of subaerial exposure and weathering as a result of subaerial exposure and weathering.

BHI facies P-E has a moderately resistive (yellow to dark orange) hue on the static image (Figure 49). The dark yellow to dark orange hue of the static image is indicative of this facies, which is very-fine-grained sandstone to siltstone; the reservoir quality is poor. The P-E facies can be interpreted from borehole imagery by the variegated resistivity pattern. The pattern of colors is derived from resistivity contrasts between the highly oxidized zones (the more resistive) and the moderately oxidized zones. Dipmeter tadpoles show a consistent orientation pattern (Figure 49). The dip pattern may reflect unidirectional low-energy flow of channel abandonment, or of estuarine sediments filling an abandoned-channel belt.

Reservoir Quality Inferred From Chromatic Variation

Reservoir quality can be inferred in borehole image logs by analysis of chromatic variation (Devries, 2005). In the present instance, the rock analyzed was the cored Tussy B interval, in the Mid-Con Energy Operating Hembree 3-17 (Figure 50). Light-yellow-to-white hue indicates clean sandstone that is highly cemented (porosity is occluded); reservoir-quality is poor (less than 10% porosity). Yellow-to-light-orange hue on the static image indicates good reservoir quality and porous-sandstone facies (more than 10% porosity). Light-orange-to-orange hue typically is associated with very-fine-grained silty to shaly sandstone, of fair to poor reservoir quality (less than 8% porosity). Dark-orange-to-brown hue is associated with silt to mudstone; this rock is considered to be of non-reservoir quality. Appendix A shows core-derived porosity and permeability values correlated with core photographs and static BHI logs of the Tussy A and B sandstones in the Hembree 3-17 well.

Borehole-image Facies Associations

The purpose of this section is to group previously defined Tussy lithofacies into borehole-image associations, according to lithology and reservoir quality, and to relate the defined facies associations to wells with borehole-image logs, but no cores. Four borehole-image facies can be correlated on a field-wide scale: (1) fluvial facies, (2) channel abandonment-estuarine facies, (3) floodplain facies and (4) marine facies. The cored Tussy B interval of the Hembree 3-17 is useful for illustration of these four BHI facies associations (Figure 50). The sandstone (reservoir) is underlain by marine mudstones and overlain by abandoned-channel facies and estuarine facies. In Appendix A is a borehole-image cross section. It shows correlations of borehole-image facies at field-wide scale.

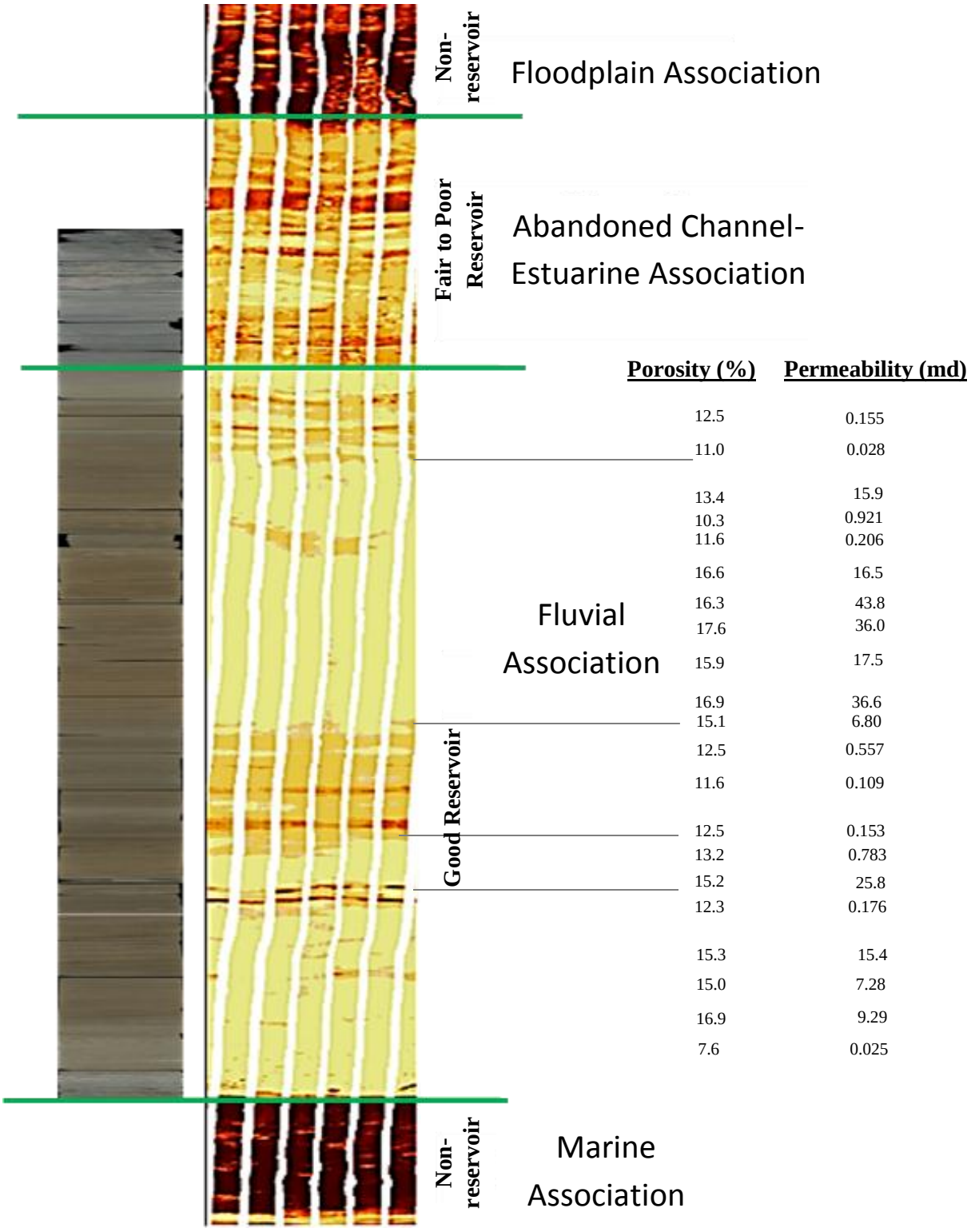

Figure 50: Static image, Tussy B reservoir facies, Mid-Con Energy Operating Hembree 3-17 showing borehole-imagery facies associations, porosity and permeability.

Dipmeter Pattern Analysis and Fluvial Typing

Interpretation of dipmeter data in conjunction with facies analysis is useful in determining the type of fluvial system under investigation: meandering, braided or distributary. Meandering rivers typically are of low gradient; in them are deposited elongated "shoe-string" sand bodies, bordered by floodplain. These shoestring sands are sub-parallel to the sloping depositional profile (Cant, 1982). In comparison to braided streams, meandering rivers are low-energy systems. Meandering systems typically contain sediments with smaller grain size (Slatt, 2006). A typical vertical profile consists of channel-lag conglomerate that fines upward to sand, to mud. Channel-lag deposits grade upward into point-bar deposits, which consist of cross-bedded, plane-bedded, and trough-cross-bedded sands capped by climbing ripples and mud drapes (Cant, 1982). Point bars enlarge by lateral migration of megaripples from the channel floor onto point bars (Allen, 1970; Bridge, 1977; Donselaar and Schmidt, 2010). The deposits of small meandering fluvial systems are manifest in cores as successive fining-upward sequences (Cant, 1982). Similar features were observed from core of the Tussy sandstones.

Figure 51 includes a gamma-ray curve, a statically normalized borehole-image and dip-meter tadpoles of the Tussy A and B intervals in the Mid-Con Energy Operating Hembree 3-17. Dipmeter tadpoles were organized into groups (2-6 ft) of "unidirectional" dip. Each group depicts gradually upward-different dips, which are interpreted as being the record of lateral accretion surfaces of point-bars, an arrangement similar to findings by Donselaar and Schmidt (2010); "The gradual vertical variation in dip angle is the expression of the sigmoidal shape of the accretion surfaces, and the slight upward rotation of the dip direction indicates the (downstream) migration in time of the point bar". (Donselaar and Schmidt, 2010). Small grain size and fluvial-linked sedimentary structures (Figures 33, 34, 35 and 36) support the meandering fluvial environment, in conjunction with dipmeter data described above.

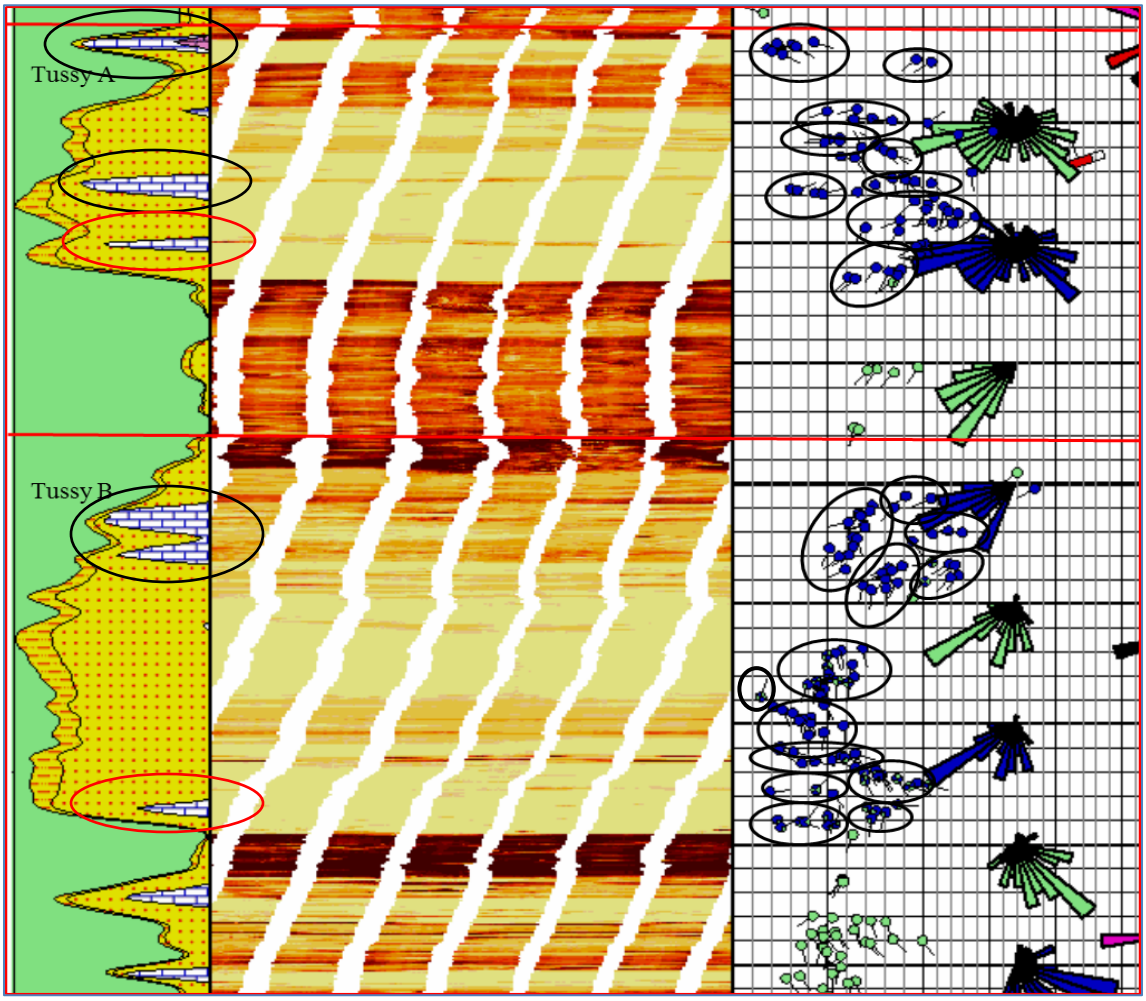

Figure 51: Gamma-ray (left), static image (middle) and sedimentary dip-meter plots (right) from the Mid-Con Energy Operating Hembree 3-17 XRMI. Dip-meter tadpoles are grouped into packages of common "unidirectional" dip orientations, interpreted as lateral accretion of stacked fluvial point bars, within a meandering fluvial system. The carbonate present in the middle-to-upper portions of the channel facies (black ovals) are probably a result of groundwater circulation and/or subaerial exposure, while the carbonate near the base (red ovals) are probably the result of erosion into underlying carbonate-rich mudstone.

Summary

Core-derived lithofacies display distinct textural characteristics on borehole image logs; they allow accurate core-to-borehole-image calibration. The Horiz7 and the dynamic image are most effective for interpretation of sedimentary structures and depositional facies. The static image (Figure 50) is most effective for inferences about diagenetic effects (cementation) and differences in grain-size. Borehole-image facies were grouped into four associations: marine, fluvial, floodplain and abandoned-channel -estuarine (Figure 50). These associations were correlated to records of wells with borehole-image logs, but no cores. Vertical stacking patterns of borehole-image logs provided evidence of this sequence of depositional environments within the Southeast Joiner City oilfield: marine, fluvial channel, channel abandonment, estuarine, floodplain, fluvial channel (from bottom-to-top). This stacking is believed to be evidence of base-level cyclicity that controlled deposition of the Tussy A and B intervals. Sharp contacts between sandstones and underlying mudstones-siltstones, observed on borehole-imagery logs, help solidify the interpretation.

Chromatic variation is effective evidence for inferences about reservoir quality (Figure 50). A yellow hue typically correlates to the best reservoir quality in the Tussy sandstones. Dipmeter data (Figure 51) were available in description of the Tussy fluvial system as a meandering-channel belt, composed of laterally and vertically amalgamated, side-attached point-bars.

CHAPTER VI

SPATIAL CHARACTERISTICS OF THE RESERVOIRS

Net-porous-sandstone Maps

Net-porous-sandstone isopach maps of the Tussy A (Figure 52) and Tussy B (Figure 54) reservoirs were hand contoured and then digitized into Petra Geological software. The maps illustrate distribution of the reservoirs. The net-porous-sandstone cutoffs used to define the Tussy A and B reservoirs are:

(1) Volume of shale less than 40%, and (2) density-porosity is more than 12% (as calculated on the basis of matrix density = 2.71 grams/cm^3)

Storage Capacity (phi*h) Maps

Storage capacity of the Tussy A and B sandstones is shown in Figures 53 and 55, respectively. Storage capacity is the product of average porosity and net pay thickness; it was calculated for the majority of wells in the study area. These maps were constructed using Petra Geological Software. Average porosity (PHIA) was calculated for each well by cross-plotting density porosity (Dphi) and neutron porosity (Nphi), using the following equation:

PHIA = (Dphi + Nphi) / 2.

Storage capacity was calculated for each well by the following equation:

Storage Capacity = Average porosity * Net pay height

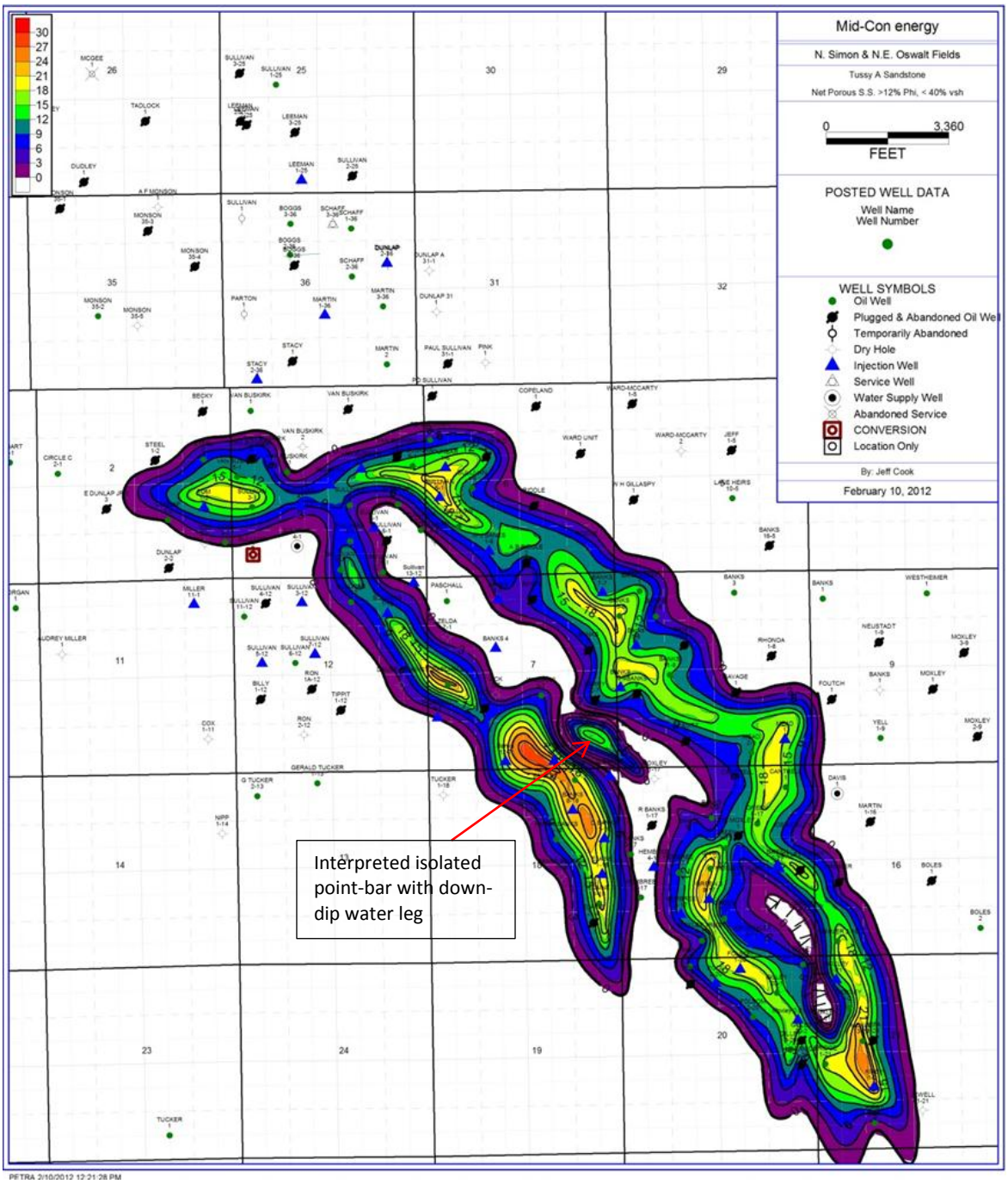

Figure 52: Thickness of net porous Tussy A sandstone (density-neutron porosity > 12%; volume of shale < 40%). Contour interval: 3 ft. Thicknesses shown in color bar, upper left corner of the figure. Actual Range: zero (magenta) to 27 ft (red). Red arrow indicates oil-water contact within an interpreted disconnected sandbody with a down-dip water leg. These abandoned sand bodies were the only observed oil-water contacts in the Tussy A sandstone within the Southeast Joiner City field.

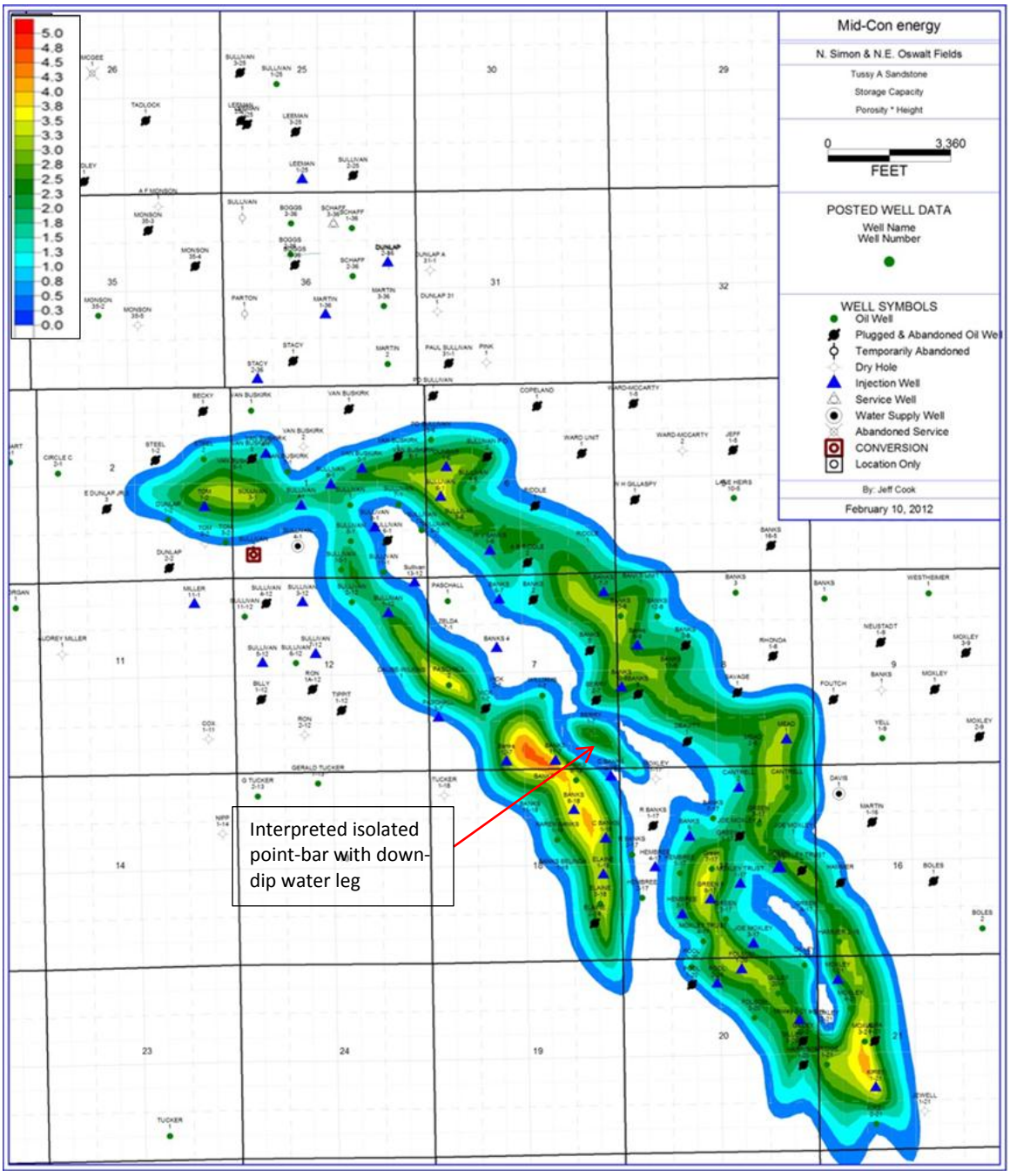

Figure 53: Storage-capacity thickness, Tussy A sandstone. Storage capacity = average porosity * net-pay height. Contour interval and color bar are on left. Red arrow indicates a water leg in an isolated sandstone deposit.

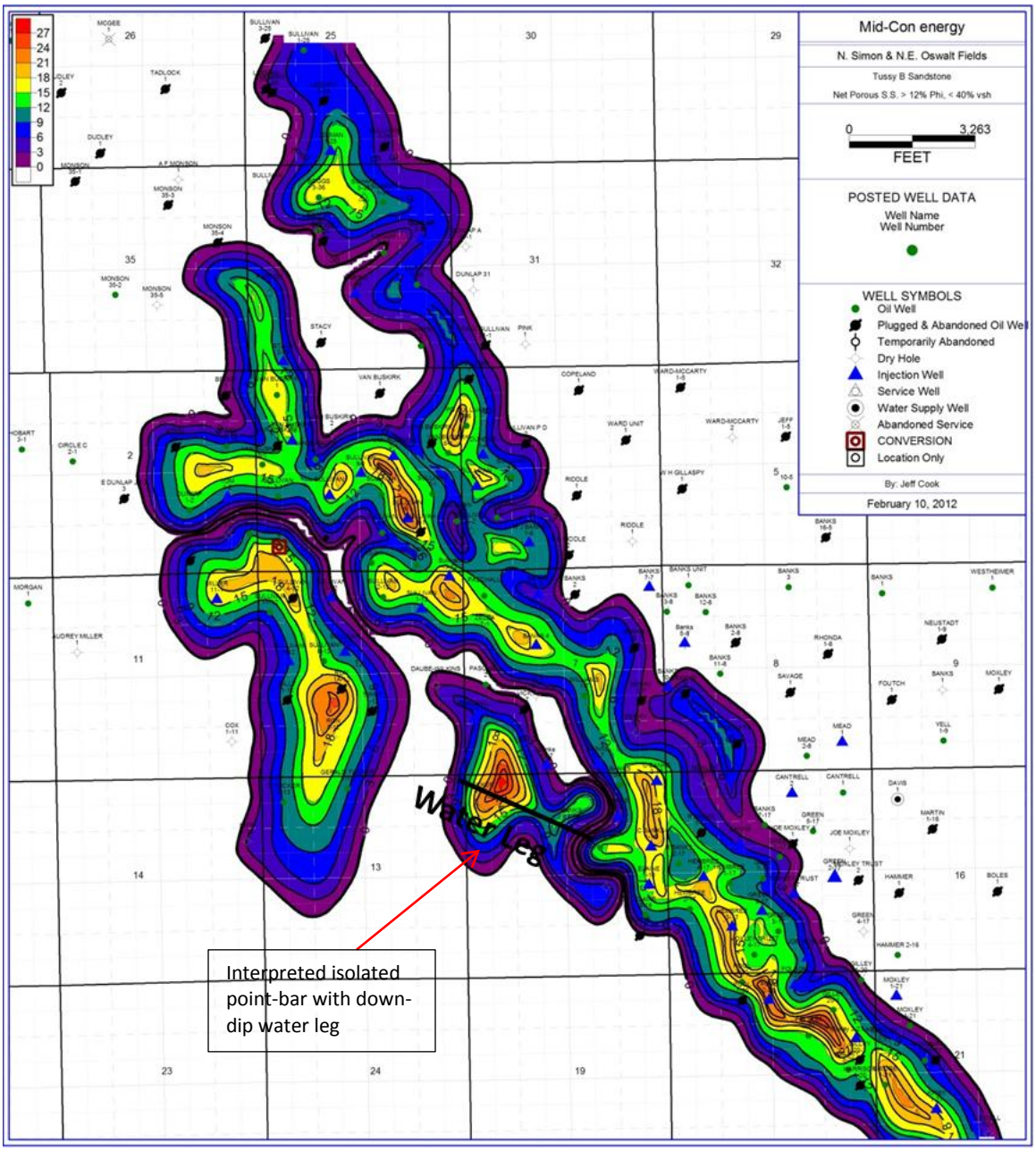

Figure 54: Thickness of net porous Tussy B sandstone (density-neutron porosity > 12%; volume of shale < 40%). Contour interval: 3 ft. Thicknesses shown in color bar, upper left corner of the figure. Actual Range: zero (magenta) to 27 ft (red). Red arrow indicates oil-water contact within an interpreted disconnected sandbody with a down-dip water leg. These abandoned sand bodies were the only observed oil-water contacts in the Tussy B sandstone within the Southeast Joiner City field.

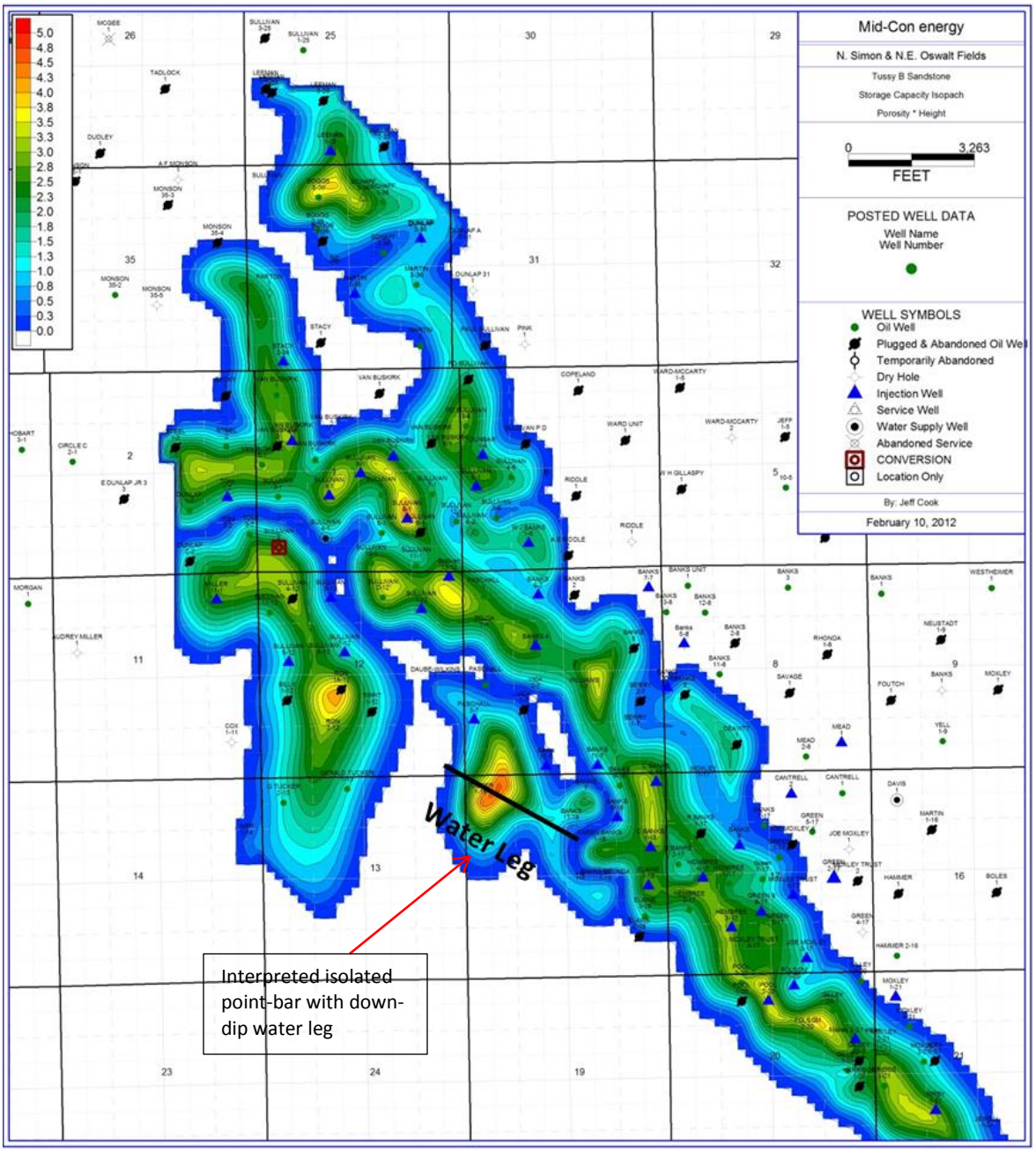

Figure 55: Storage-capacity thickness, Tussy B sandstone. Storage capacity = average porosity * net pay height. Contour interval and color bar are on left. Black line indicates a water leg in an isolated sandstone deposit.

Depositional Model and Meander-belt Analogues

Sedimentary structures and gamma-ray log geometries support the inference of a fluvial origin of the Tussy A and B sandstones. Borehole-imagery and dipmeter data provided patterns consistent with those of point-bar deposits. Sandstone-distribution maps (Figures 52, 53, 54 and 55) depicted patterns indicative of active channel fill. Distribution and geometry of the Tussy sandstones (Figures 52, 53, 54 and 55) resemble analogues of meander-channel belts.

Figure 56 illustrates meander-belt geometry and distribution of sediment in the Mississippi River near Memphis, Tennessee. Figure 57 is a computer simulation of the spatial distributions and geometries of salient features within a meander belt. These two figures were used as conceptual analogues. They were of value in visualizing prominent depositional features and their spatial relationships. Distribution and geometry of the Tussy A and B sandstone, as illustrated by the reservoir isopach maps (Figures 52, 53, 54 and 55) resemble the distribution and geometry of the two meander-belt analogues in Figures 56 and 57. The sandstone bodies form elongated shoestring-like bodies that are oriented generally perpendicular to the depositional profile, which is consistent with meandering fluvial channel geometries described by Cant, 1982. In the meander belt computer simulation in Figure 57, numerous abandoned point-bars are at the sides of the main meander belt; this pattern resembles “pods” of sandstone shown in the Tussy A and Tussy B isopach maps (Figures 52, 53, 54 and 55). The Mississippi River anastomoses and has multiple abandoned channels; numerous meanders are off to the sides of the active channel belt (Figure 56). A similar pattern is interpreted in the Tussy A and B sandstone distribution maps (Figures 52, 53, 54 and 55).

Figure 56: Satellite photograph of Mississippi River meander belt near Memphis, Tennessee, USA (www.eros.usgs.gov).

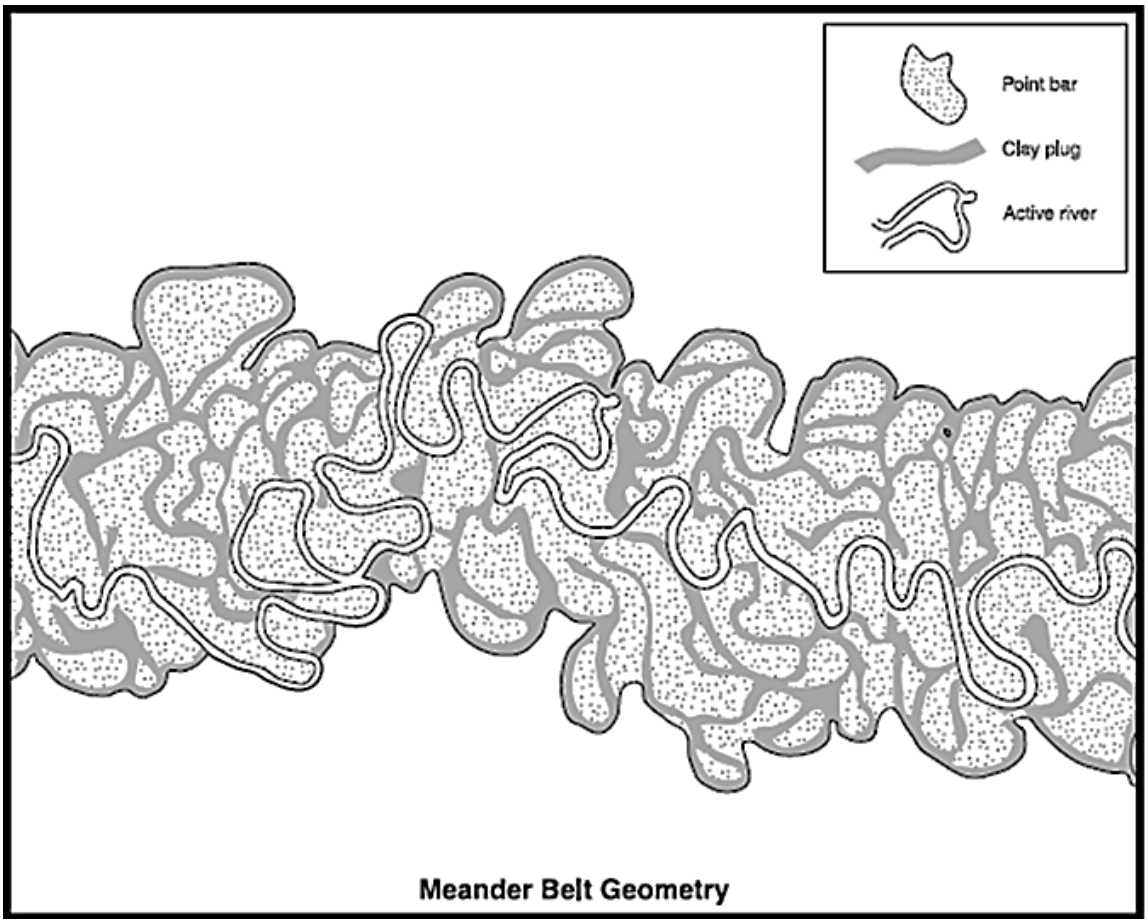

Figure 57: Computer simulation and model of a meander belt, showing prominent point bars and spatial relationships (Sun et al., 1996).

Dimensions of Fluvial Channels

Widths of the Tussy A and Tussy B channels range from approximately 2,000 ft. to 4,500 ft. (Figures 52, 53, 54 and 55). As interpreted from currently available well logs and derived data, the Tussy A and B reservoirs are about 4 to 6 miles long (Figures 52, 53, 54, 55). The reservoirs almost certainly are longer. Analysis of Tussy sandstone production history for the majority of wells in the Southeast Joiner City field has revealed that the more prolific wells (more than 50,000 barrels of oil) are greater than 8 ft. in thickness. Channel thickness ranges from 1 ft. at the edges to 30 ft. near the center.

Channel Connectivity

Figure 58 illustrates two isopach-map scenarios of meandering-point-bar deposits from the Miocene Huesca Fan at Ebro, Spain (Donselaar and Overeem, 2008). The outcrop shown in Figure 59 is interpreted as a sequence of multistoried laterally amalgamated point-bar sandstones – the record of a meander river system. The Miocene Huesca fluvial fan is an outcrop analog of lateral relationships of point-bar deposits. Donselaar and Overeem (2008) described fluvial point-bar connectivity within the Huesca Fan; they showed how point bars can be connected by channel-floor sandstone bodies. This research is important for oil-and-gas operators who develop fields comprised of side-attached (meandering) point-bars, because these types of deposits are well known as being discontinuous – an attribute that is especially problematic waterflooding and other enhanced recovery procedures. When present, reserves of petroleum are larger and productivity is better in meandering-stream deposits that are connected by channel floor sandstones (Donselaar and Overeem, 2008). Point-bar connectivity of similar kind is suspected to be operative in Tussy reservoirs. During enhanced-recovery operations, injection of water has stimulated producing wells that are more than 1 mile from the injection-well. Injector –producer communication is more apparent where both wells are near to the center of the channel belt.

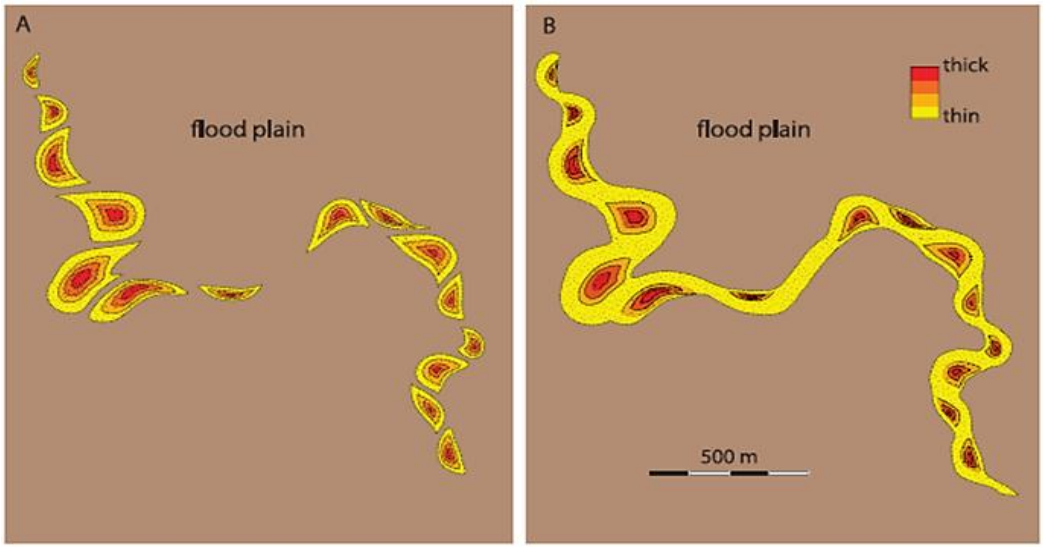

Figure 58: Isopach maps from Miocene Huesca fluvial fan in Ebro, Spain showing two interpretation meander-sandstone distribution and connectivity. (A) Fluvial channel is filled with mud after channel abandonment; point-bars are compartments. (B) Channel floor consists of clean trough-cross-bedded sand. The sand body is connected throughout the trend (Donselaar and Overeem, 2008).

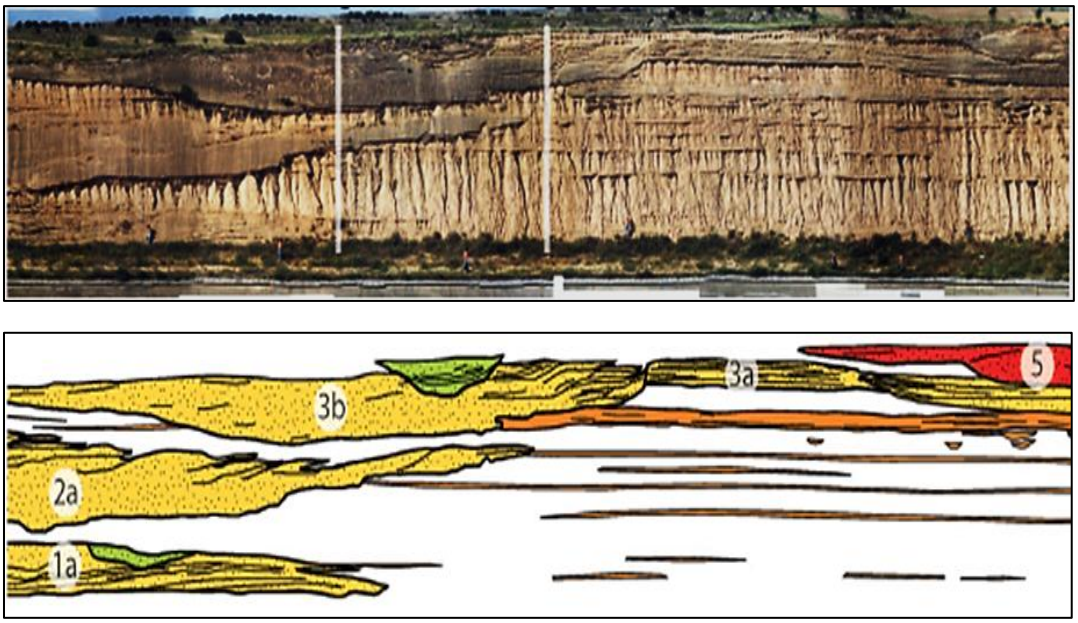

Figure 59: Outcrop photograph and interpretation of multistoried laterally amalgamated point bars in a meandering-river sandstone of the Miocene Huesca fluvial fan. (Donselaar and Overeem, 2008).

Point bars seem to be connected over long distances in most of the study area, particularly where they are in the central part of the channel belt. However, in a few areas injector and producer wells within the same stratigraphic interval are not connected, a fact that is apparent from analysis of injection data and production data. For example, Figure 60 is a well-log cross-section that shows evidence of flow barriers between two wells completed in the Tussy A Sandstone. The large volume of water injected (more than 550,000 bbl) into Tussy sandstone in the Sabre Operating Tom 1-2 has caused no apparent increase in oil or water production in the RDT Tom 3-2, located only 900 feet to the southeast. In November 2011a well test of the Tom 3-2 was 1 barrel of oil and 0 barrels of water (Figure 60). During the month of December 2011, the Sabre Operating Tom 1-2 injection well averaged 355 barrels of water injected per day (Figure 60). Recent injection profiles for the Tom 1-2 show that the injected water enters perforations in the Tussy A sandstones. Thus, the Tom 1-2 is an active injector of water into Tussy sandstones but the nearby Tom 3-2 producer shows no response. The unavoidable conclusion is that at this point, sandstones of the point-bar system are isolated.

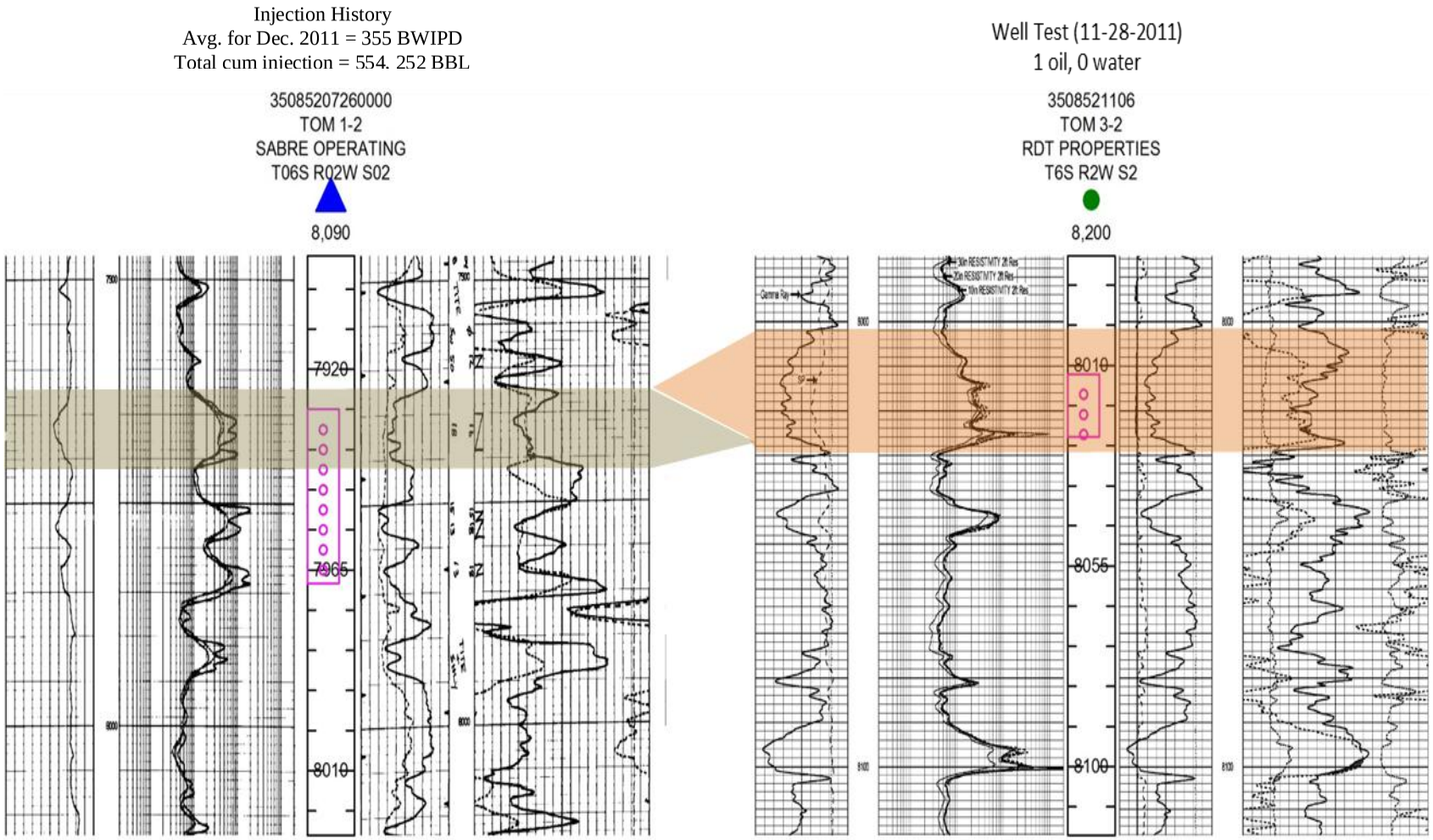

Figure 60: Log cross-section illustrating flow barriers between wells completed in the Tussy Sandstones. The large volume of water injected into the Sabre Operating Tom 1-2 has caused no apparent increase in oil or water production from the RDT Tom 3-2, located only about 900 feet to the southeastward. This flow baffle is consistent with interbar discontinuity in point-bar systems.

Summary

Based on the distribution patterns, sandstone geometry, sedimentary structures, and dipmeter measurements and patterns, the Tussy A and B sandstones of the Southeast Joiner City field are interpreted as having been deposited in fluvial-channel belts. The Tussy reservoirs almost certainly originated as stacked laterally amalgamated point bars, which compose a meander belt. Individual point bars show evidence of a high degree of connection, particularly near the middle of the channel belt. Lateral connection probably is the result of channel-floor sand bodies that extend among individual point-bars within the channel belt. In the study area, some point-bar sandstones contain water, but are up-dip from similar sandstones that contain oil. These point-bars are interpreted to have been abandoned from the main channel, and to be isolated by mudstones. Mapping of the sandstones along with injection and production data showed the locations of connected point bars and abandoned point bars. Mapping the distribution of net porous sandstone with more than 12% porosity delineates reservoir facies. Allowing the depositional model to guide subsurface mapping improves the interpretation of reservoir distribution and connectivity.

CHAPTER VII

CONCLUSIONS

Data collected from two cores, from conventional wireline logs and from borehole-image logs were integrated and interpreted, Conclusions regarding the Lower Desmoinesian Tussy sandstone reservoirs in the Southeast Joiner City field in Love and Carter County, Oklahoma are as follows:

1. Thickness of the stratigraphic interval (175-300 ft) and rose diagrams based on plots of sedimentary bedding-plane dips indicate a dominant north-to-south sediment-transport direction, toward the depocenter, south of the Southeast Joiner City oil field.
2. Lithofacies of the Tussy stratigraphic interval are of marine, estuarine, fluvial and floodplain environments. Vertical stacking patterns reveal cyclic deposition that is suggestive of deposition controlled by variation of base level.
3. The Tussy A and B sandstones are interpreted as amalgamated and laterally connected, side-attached point-bar deposits within a channel belt. This conclusion is based on sedimentary structures, sand-body geometry and sand-body distribution.

4. Apparent variation in base level influenced deposition styles. As interpreted from the stratigraphic sequence the stages were as follows: lowstand, with paraconglomeratic erosive channel base, fluvial sandstones succeeded by estuarine and mixed fluvial-marine deposition during transgression, and subaerial exposure during the subsequent fall in base-level and development of paleosols.
5. Tussy point-bar fluvial facies have the highest porosity (12% - 18%) and permeability (1md - 148 md). These rocks are the best reservoir.
6. Primary porosity is abundant, but secondary porosity is prevalent; it resulted from dissolution of feldspar, rock fragments and detrital clay matrix.
7. Horizontal planar-laminated facies and cross-laminated facies are the best reservoir facies. The deformed sandstone facies also is of good quality, but porosity is high and permeability tends to be low.
8. Core-calibrated borehole-image logs accurately display discrete textural characteristics of core-derived lithofacies. They are the basis for the inferences about depositional facies, grain size and reservoir quality in wells with borehole-image logs, but no cores.
9. Dip-meter data from borehole-image logs provide evidence about migration of dunes. They are useful for interpretation of vertically amalgamated, laterally accreted point-bar deposits.
10. The rather plentiful evidence of fluid transmitted from one point-bar to another could be associated with channel-floor sandstones that connect adjacent point-bars.

REFERENCES

Abbott, B.N., 2006, Pre-Pennsylvanian subcrop map, Love County, Oklahoma, unpublished map

Allen, J.R.L., 1970, Studies in fluviatile sedimentation: A comparison of fining upward cyclothems with special reference to coarse-member composition and interpretation: Journal of Sedimentary Petrology, v. 40, p. 298-323.

Al-Shaieb, Z.F., Thomas, R.G., and Stewart, G.F., 1980, National uranium resource evaluation, Lawton quadrangle, Oklahoma and Texas: U.S. Department of Energy, Open file report.

Asquith, G., Krygowski, 2004, Gamma Ray, *in* G. Asquith and D. Krygowski, Basic Well log analysis: AAPG Methods in Exploration 16, p. 31-35.

Billingsley, P., Banerjee, S., Elmore, R.D., and Sutherland, P.K., 1996, Fluvial-deltaic facies patterns in the lower Deese group (Middle Pennsylvanian), Ardmore Basin, *in* Johnson, K.S. (ed.), Deltaic reservoirs in the southern Midcontinent, 1993 symposium: Oklahoma: Oklahoma Geological Survey Circular 98, p. 240-248.

Boggs, S. Jr., 2006, Principles of sedimentology and stratigraphy 4th ed.

Boyd, D.T., 2002, Map of Oklahoma oil and gas fields, Oklahoma Geological Survey Map GM-37

Bradfield, H.H., 1968, Stratigraphy and structure of the deeper Marietta basin of Oklahoma and Texas: in W.J Stewart, ed., Basins of the southwest, v. 1, p. 54-70: North Texas Geological Society.

Bridge, J.S., 1977, Flow, bed topography and sedimentary structures in open channel bends: A three-dimensional model: Earth surface processes, v. 2, p. 401-416.

Cant, D.J., 1982, Fluvial facies models and their applications, *in* P.A. Scholle and D. Spearing (eds.), Sandstone depositional environments: AAPG Memoir 31, p. 115-138.

Coleman, J.M., Prior, D.B., 1982, Deltaic environments of deposition, *in* Scholle, P.A., Darwin, S., eds., Sandstone depositional environments: AAPG Memoir 31, p. 139-178.

Deyhim, P., 2000, Compartmentalization and overpressuring of the oligocene Vicksburg Sandstone, TCB Field, Kleberg County, Texas: unpublished M.S. thesis, Oklahoma State University, Stillwater, Oklahoma.

DeVries, A. A., 2005, Sequence stratigraphy and micro-image analysis of the Upper Morrow sandstone in the Mustang East Field, Morton County Kansas: unpublished M.S. thesis, Oklahoma State University, Stillwater, Oklahoma.

Donselaar, M.E., and J.M. Schmidt, 2010, The application of borehole image logs to fluvial facies interpretation, *in* M. Poppelreiter, C. Garcia-Carballido, and M. Kraaijveld, eds., Dipmeter and borehole image log technology: AAPG Memoir 92, p. 145-166.

Donselaar, M. E., Overeem, I., 2008, Connectivity of fluvial point-bar deposits: An example from the Miocene Huesca Fluvial Fan, Ebro Basin, Spain, AAPG, Bulletin V. 92, no. 9 p. 1109-1129.

Feinstein, S., 1981, Subsidence and thermal history of southern Oklahoma Aulacogen: Implications for petroleum exploration: AAPG, Bulletin V. 65, no. 12, p. 2521-2533.

Halliburton website, 2012, http://www.halliburton.com/public/lp/contents/Brochures/web/H06462.pdf

Ham, W.E., Denison, R.E., and C.A. Merritt, 1964, Basement rocks and structural evolution of southern Oklahoma: Oklahoma Geological Survey Bulletin 95, 302 p.

Hoard, J.L., 1954, Tussy Sector of the Tatums Field, Carter, and Garvin Counties, Oklahoma: AAPG, Petroleum Geology of Southern Oklahoma: A symposium: Sponsored by the Ardmore Geological Society, V. 1, p. 186-206.

Jorgensen, D.G., 1989, Paleohydrology of the Anadarko Basin, Central United States, Oklahoma Geological Survey Circular 90. p. 176-193.

Keller, G. R. and R. A. Stephenson, 2007, The Southern Oklahoma and Dniepr-Donets aulacogens: a comparative analysis, in Hatcher, R. D., Jr., Carlson, M. P., McBride, J. H., and Martínez Catalán, J. R. (eds.), The 4D Framework of Continental Crust: Geological Society of America, Memoir 200, p. 127-143.

Lagraba, P., J. O., S. M. Hansen, M. Spalburg, and M. Helmy, 2010, Borehole image tool design, value of information, and tool selection, *in* M. Poppelereiter, C. Garcia-Carballido, and M. Kraaijveld, eds., Dipmeter and borehole image log technology: AAPG Memoir 92, p. 15-38.

Mullen, L.M., 1954, The Hewitt Oil Field of Carter County, Oklahoma: AAPG, Petroleum Geology of Southern Oklahoma: A symposium: Sponsored by the Ardmore Geological Society, V. 1, p. 154-161.

Neustadt, W. Jr., 1954, West Hewitt Field, Carter County, Oklahoma: AAPG, Petroleum Geology of Southern Oklahoma: A symposium: sponsored by the Ardmore Geological Society, V. 1, p. 162-173.

Price, C., 2012, Verbal communication.

Rascoe, B. Jr., Adler, F.J., 1983, Permo-Carboniferous hydrocarbon accumulations, Mid-Continent, U.S.A: AAPG Bulletin v. 62, no. 6, p. 979-1001.

Reeves, C.C. Jr., Mount, J.R., 1960, Possibility of hydrocarbon accumulations along northern flank of Marietta Syncline, Love County, Oklahoma, AAPG Bulletin v. 44, no, 1, p. 72-82.

Slatt, R.M., 2006, Stratigraphic reservoirs characterization for petroleum geologists, geophysicists and engineers: Handbook of Petroleum Exploration and Production, v. 12.

Stark, P.H., 1961, Subsurface stratigraphic study of the Pennsylvanian System in the Marietta Basin of south central Oklahoma and north central Texas: unpublished M.S. thesis, University of Wisconsin, Madison, Wisconsin.

Sun, T., P. Meakin, T. Jossang, and K. Schwarz, 1996, A simulation model of meandering rivers: Water Resources Research, v. 32, pt. 9, p. 2937-2954.

Tomlinson, C.W., and McBee W. Jr., 1959, Pennsylvanian sediments and orogenies of Ardmore District, Oklahoma, in Petroleum Geology of Southern Oklahoma, AAPG, v. 2: p. 3-52,

Tomlinson, C.W., and McBee W. Jr., 1962, Pennsylvanian sediments and orogenies of Ardmore District, Oklahoma, in C.C. Branson, ed., Pennsylvanian System in the United States – a symposium: AAPG, p. 461-500. (reprinted with revisions from "Petroleum Geology of southern Oklahoma, v. 2")

United States Geological Survey website, 2012, www.eros.usgs.gov

Waddell, D., E., 1966, Pennsylvanian fusulinids in the Ardmore Basin, Love and Carter Counties, Oklahoma: Oklahoma Geological Survey Bulletin 113.

Westheimer, J M., 1965, Geology and petroleum of Love County, Oklahoma: Part II-Petroleum geology of Love County, OGS Circular 63.

APPPENDIX A

Petrologs, Borehole-images, Core Photos, Thin-section Locations, Core-plug Porosity, Permeabilities, and Borehole-image cross-section

MID-CON ENERGY OPERATING HEMBREE 3-17

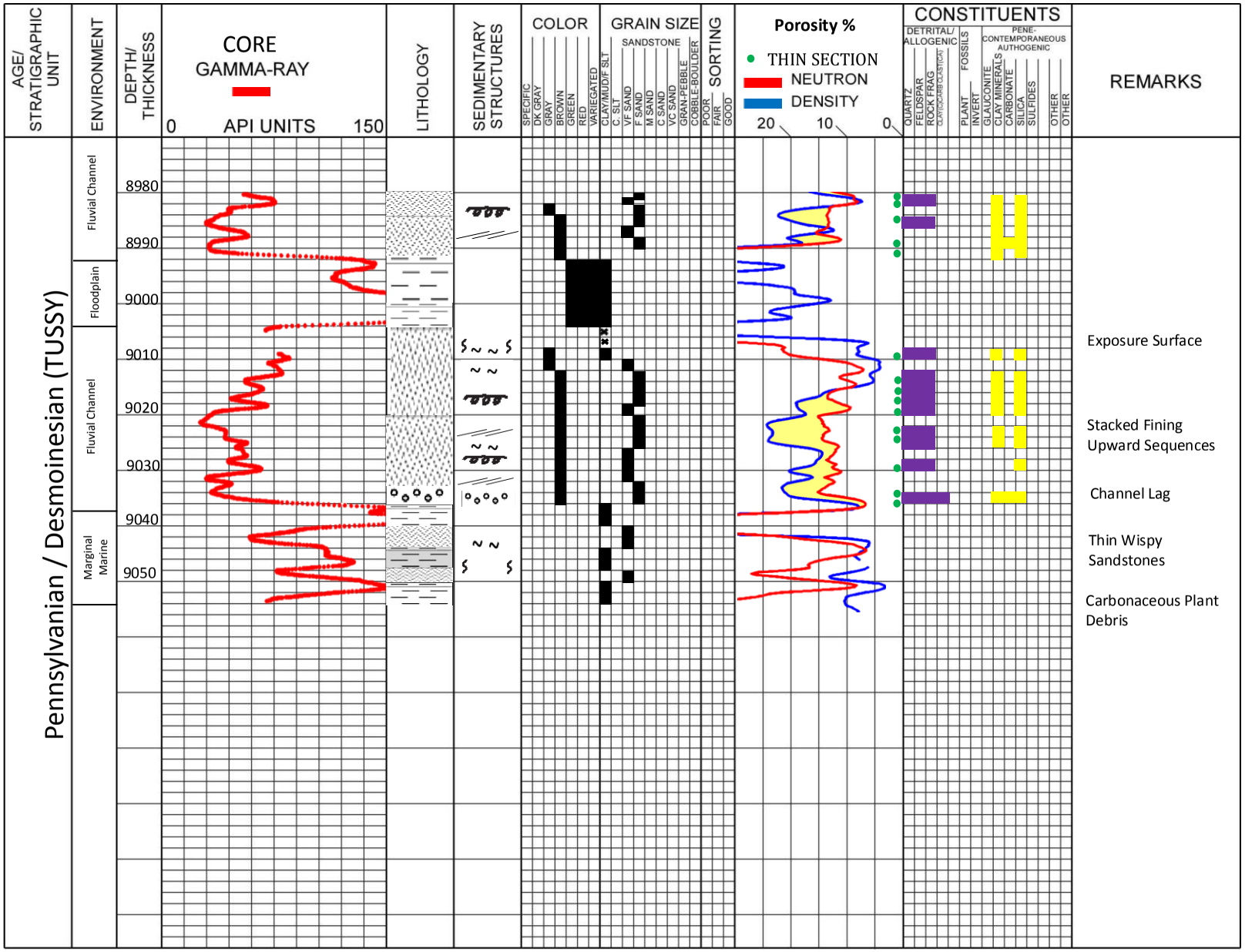

Mid-Con Operating Hembree 3-17
Tussy A Sandstone

Core Plug	Thin Section	Porosity (NCS, 6500 psi)	Permeability (To Air)
●	●	14.2	2.28
●		12.0	0.157
●		3.5	0.0056
●		14.4	2.67
●	●	15.8	131.0
●		16.0	136.0
●		16.0	15.1
●		12.5	3.25
●	●	16.0	58.4
●		12.5	38.6
●	●	9.5	4.59

Mid-Con Operating Hembree 3-17
Tussy B Sandstone

Core Plug	Thin Section	Core Porosity (NCS, 6500 psi)	Core Permeability (To Air)
●		12.5	0.0155
●		11.0	0.028
●		13.4	0.921
●	●	10.3	15.9
●		11.6	0.206
●		16.6	16.5
●	●	16.3	43.8
●		17.6	36.0
●		15.9	17.5
●		16.9	36.6
●		15.1	6.80
●	●	12.5	0.557
●		11.6	0.109
●		12.5	0.153
●	●	13.2	0.783
●		15.2	25.8
●	●	12.3	0.176
●		15.3	15.4
●		15.0	7.28
●		16.9	9.29
●		7.6	0.025

Santa Fe Minerals Gilley 20-2

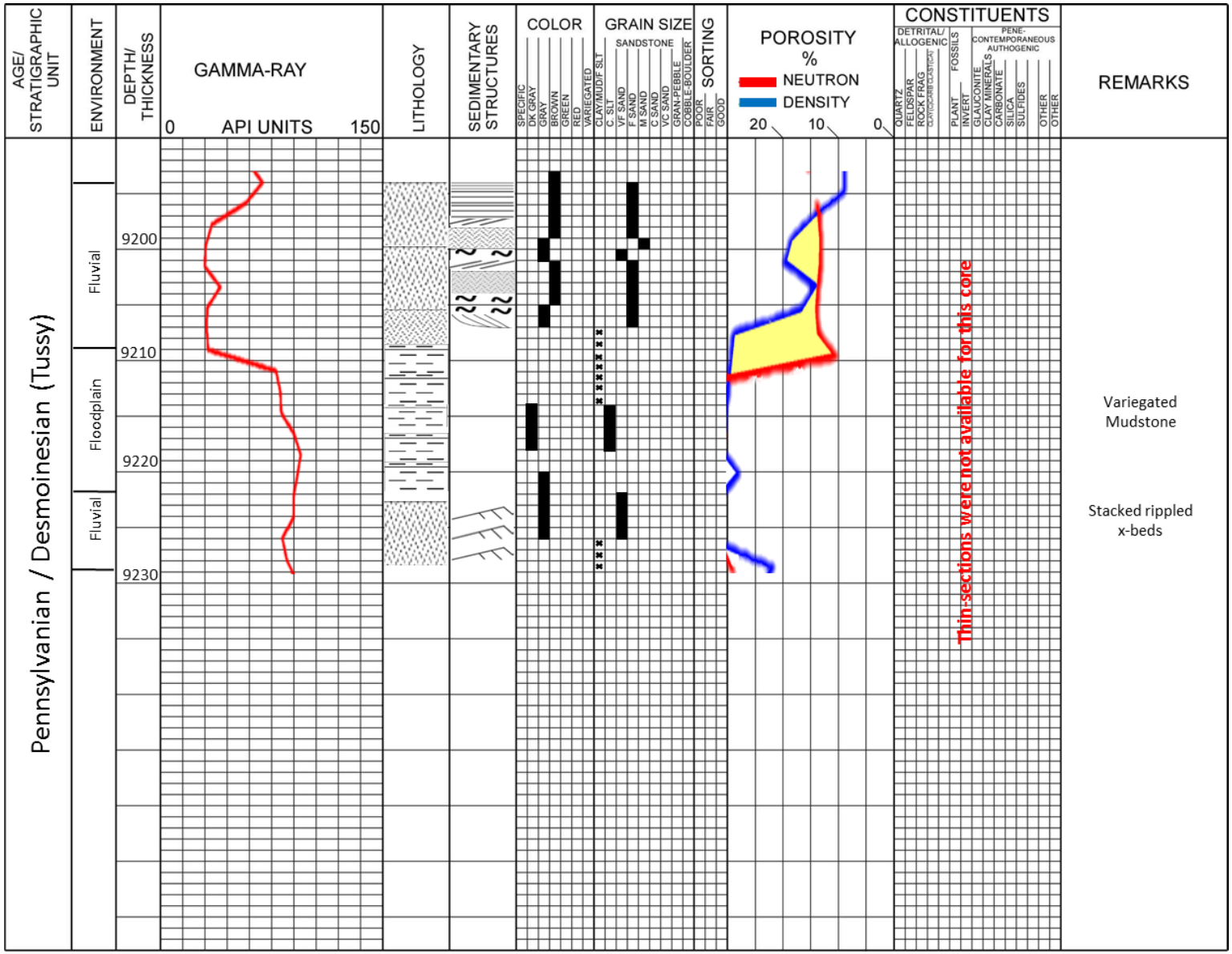

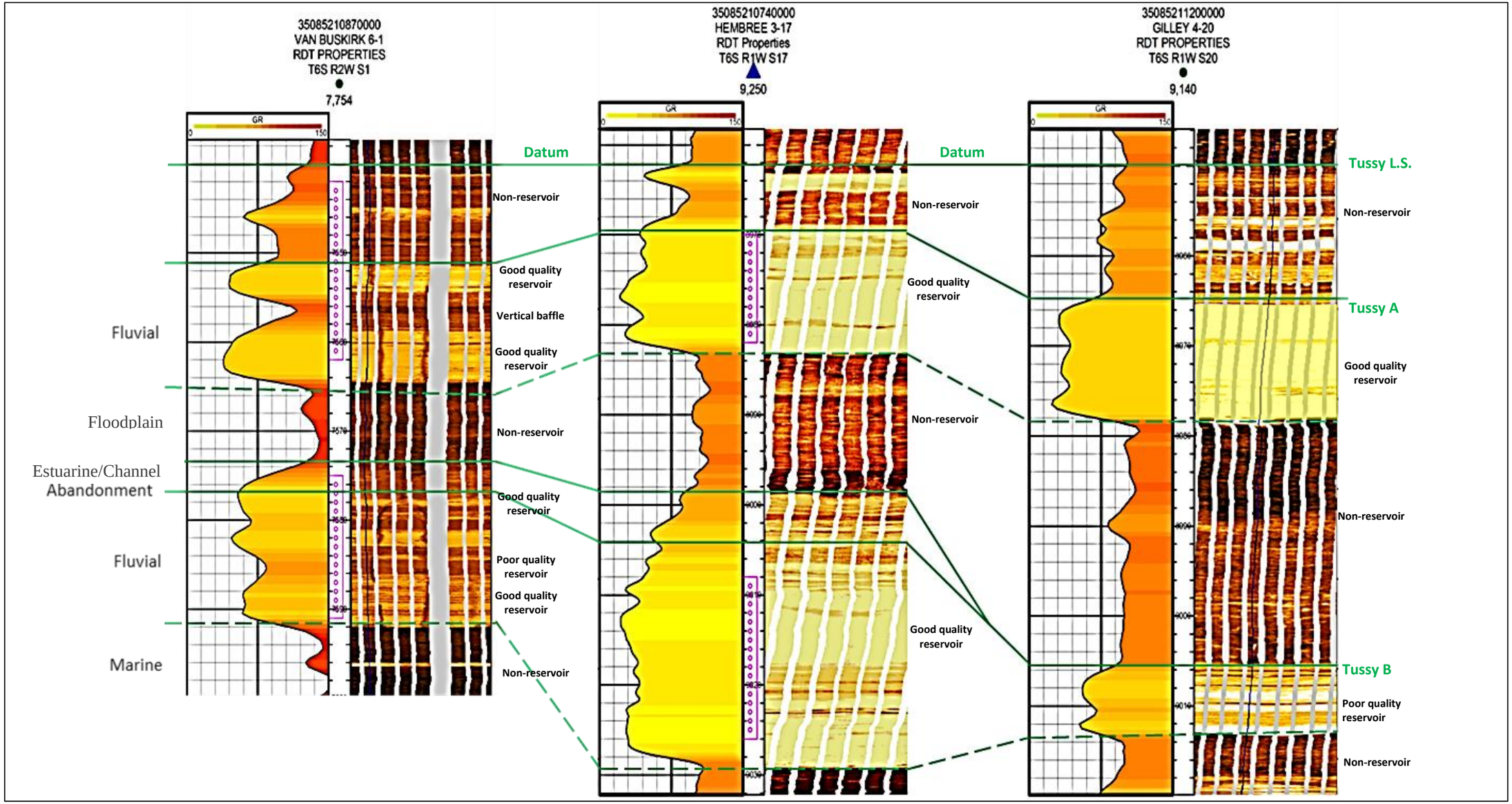
35085210870000
VAN BUSKIRK 6-1
RDT PROPERTIES
T6S R2W S1
7,754
35085210740000
HEMBREE 3-17
RDT Properties
T6S R1W S17
9,250
35085211200000
GILLEY 4-20
RDT PROPERTIES
T6S R1W S20
9,140
GR
0
150
Datum
Datum
Tussy L.S.
Non-reservoir
Good quality reservoir
Vertical baffle
Good quality reservoir
Non-reservoir
Tussy A
Good quality reservoir
Non-reservoir
Poor quality reservoir
Good quality reservoir
Non-reservoir
Tussy B
Poor quality reservoir
Non-reservoir
Fluvial
Floodplain
Estuarine/Channel Abandonment
Fluvial
Marine

VITA

Jeffrey Manning Cook

Candidate for the Degree of

Master of Science

Thesis: STRATIGRAPHY, DEPOSITIONAL ENVIRONMENTS AND RESERVOIR DESCRIPTION OF THE TUSSY (DESMOINESIAN) SANDSTONES, SOUTHEAST JOINER CITY FIELD, LOVE AND CARTER COUNTIES, OKLAHOMA

Major Field: Geology

Biographical:

Personal Data: Born in Oklahoma City, Oklahoma, on October 27, 1985, the son of Greg and Janie Cook.

Education: Graduated from Edmond North High School, Edmond, Oklahoma in May 2004; received Bachelor of Science degree in Geology from University of Oklahoma, Norman, Oklahoma in May 2010. Completed requirements for the Master of Science degree with a major in Geology in May 2012.

Experience: Employed by Mid-Con energy as an intern geologist from May 2010 to August 2010. Employed by Mid-Con Energy as a full-time staff geologist from September 2010 to May 2012. Employed by Texland Petroleum as a geologist from May 2012 to present.

Professional Memberships: American Association of Petroleum Geologists, Oklahoma City Geological Society, Tulsa Geological Society

Name: Jeffrey M. Cook Date of Degree: May, 2012

Institution: Oklahoma State University Location: Stillwater, Oklahoma

Title of Study: STRATIGRAPHY, DEPOSITIONAL ENVIRONMENTS AND RESERVOIR DESCRIPTION OF THE TUSSY (DESMOINESIAN) SANDSTONES, SOUTHEAST JOINER CITY FIELD, LOVE AND CARTER COUNTIES, OKLAHOMA

Pages in Study: 95 Candidate for the Degree of Master of Science

Major Field: Geology

Scope and Method of Study: The Pennsylvanian (Desmoinesian) Tussy sandstones were studied in the Southeast Joiner City field of Love and Carter Counties, Oklahoma. Data collected from two cores, conventional wireline logs and borehole-image logs were analyzed and interpreted. This set of data permitted interpretations of the stratigraphic framework, depositional environments, and reservoir quality, geometry and distribution for the Tussy sandstones within the Southeast Joiner City Field.

Findings and Conclusions: The Tussy interval is defined as the set of strata between the Tussy Limestone at the top and the Upper Dornick Hills Group at the base. Analysis of cross-sections revealed a southerly thickening of the Tussy interval, and rose plots of bedding dips show a dominant north-to-south sediment transport direction. Thus, the basin depocenter was south of the Southeast Joiner City field during Tussy deposition.

The Tussy A and B cored intervals are rocks that were deposited in marine, fluvial, floodplain and estuarine environments; they show evidence of sea-level cyclicity. Eleven core-derived facies were interpreted, each with distinct sedimentary structures and reservoir quality. Characteristics of the lithotypes from analyses of core, thin-sections and core-derived porosity and permeability data reveal that grain-size, degree of cementation and clay content are the major controls on reservoir quality. The best reservoir facies are of coarse grain-size, are poorly cemented, and have small amounts of pore-clogging clays.

The Tussy A and B sandstones were interpreted as meandering stream deposits, composed of amalgamated and laterally connected, side-attached point-bar deposits within a channel belt. This conclusion is based on sedimentary structures, sand-body geometry and sand-body distribution patterns which resemble modern analogues of meander belts.

ADVISER'S APPROVAL: Dr. James Puckette